

UC Berkeley

UC Berkeley Electronic Theses and Dissertations

Title

Genetic, Biochemical, and Structural Studies of the *Hyaloperonospora arabidopsidis* Effector ATR13 and its Cognate *Arabidopsis thaliana* R-gene, RPP13

Permalink

<https://escholarship.org/uc/item/649803bw>

Author

Leonelli, Lauriebeth

Publication Date

2011

Peer reviewed|Thesis/dissertation

Genetic, Biochemical, and Structural Studies of the *Hyaloperonospora arabidopsidis*
Effector ATR13 and its Cognate *Arabidopsis thaliana* R-gene, RPP13.

By

Lauriebeth Leonelli

A dissertation submitted in partial satisfaction of the
requirements for the degree of
Doctor of Philosophy
in
Plant Biology
in the
Graduate Division
of the
University of California, Berkeley

Committee in charge:

Professor Brian Staskawicz, Chair
Professor James Berger
Professor Steve Lindow
Professor Sheila McCormick

Spring 2011

Abstract

Genetic, Biochemical, and Structural Studies of the *Hyaloperonospora arabidopsidis* Effector ATR13 and its Cognate *Arabidopsis thaliana* R-gene, RPP13

By

Lauriebeth Leonelli

Doctor of Philosophy in Plant Biology

University of California, Berkeley

Professor Brian Staskawicz, Chair

The oomycete *Hyaloperonospora arabidopsidis* (Hpa) is the causal agent of downy mildew on the model plant *Arabidopsis thaliana*. Since oomycetes are a particularly important agricultural pest, this pathosystem is an ideal setting for exploration of interactions between host and microbe, as genome sequences for both are available and possess a high level of genetic diversity between naturally occurring populations. Plant recognition of Hpa infection occurs when resistance proteins (R-genes) in the plant host recognize pathogen-derived effectors, which are proteins delivered to the host. One such protein, the Hpa effector ATR13 Emco5, is examined in this study.

Herein, we use NMR to solve the backbone structure of a highly disordered protein, ATR13 Emco5, revealing a loosely packed protein possessing a great deal of flexibility. In addition to solving this structure, we use site-directed and random mutagenesis to expose several amino acid residues involved in the recognition response conferred by RPP13-Nd, the cognate R-gene that triggers programmed cell death (HR) in the presence of recognized ATR13 variants. Using our structure as a scaffold, we map these residues to one of two surface-exposed patches composed of residues that are under diversifying selection. Exploring possible roles of the disordered region within the ATR13 structure, we perform domain swapping experiments and identify a peptide sequence involved in nucleolar localization. We conclude that ATR13 is a highly dynamic protein with weak structural similarities to RAN-GTP that contains two surface-exposed patches, only one of which is involved in RPP13 recognition specificity. Furthermore, we have identified two potential protein targets of ATR13 (the RCC1 and PRP39 families). Finally, and we have performed several different EMS mutagenesis screens leading to the isolation of three lines of *A. thaliana* plants disrupted in RPP13 signaling.

Table of Contents

List of Figures.....	ii
List of Tables.....	iv
Acknowledgements.....	v
Chapter 1. An Introduction to Plant-Microbe Interactions.....	1
Chapter 2. Features of the ATR13 three dimensional structure.....	4
Introduction.....	4
Materials and Methods.....	6
Results.....	10
Discussion.....	23
Summary and Future Directions.....	25
Chapter 3. ATR13 interactors and Co-immunoprecipitation experiments.....	29
Introduction.....	29
Materials and Methods.....	31
Results/Discussion.....	36
Summary and Future Directions.....	47
Chapter 4. The Search for Members of the RPP13 Signaling Pathway.....	50
Introduction.....	50
Materials and Methods.....	52
Results/Discussion.....	54
Summary and Future Directions.....	64
References.....	65

List of Figures

Figure 2-1. Growth assay of <i>Pseudomonas syringae</i> DC3000 on <i>Arabidopsis thaliana</i>	10
Figure 2-2. Virulence effect of ATR13 Emco5 expressed <i>in planta</i>	11
Figure 2-3. ATR13 suppression of basal resistance.....	12
Figure 2-4. Determining active truncations of ATR13 Emco5.	13
Figure 2-5. Crystals of ATR13 Emco5.....	14
Figure 2-6. NMR analysis of ATR13 Emco5.....	15
Figure 2-7. Naturally occurring polymorphisms of ATR13.....	16
Figure 2-8. Site-directed loss-of-recognition and random gain-of-recognition mutagenesis of ATR13 scored for HR in RPP13Nd transgenic <i>N. benthamiana</i>	19
Figure 2-9. Random loss-of-recognition mutagenesis of ATR13 Emco5 scored for HR in RPP13Nd transgenic <i>N. benthamiana</i> plants.....	20
Figure 2-10. Nucleolar targeting signal of ATR13.....	21
Figure 2-11. Structural overlay of ATR13 Emco5 with the first 200 amino acids of nuclear Ran-GTP subunit D.....	22
Figure 3-1. Pulldowns with GST-ATR13 Emco5 and plant lysates from <i>Arabidopsis thaliana</i> ecotypes Col5 and Col5 :RPP13Nd.	36
Figure 3-2. Stable transgenic Col5 plants containing an HA-tagged version of RPP13Nd.....	37
Figure 3-3. ATR13 and RIN4 CNBr-activated sepharose pulldowns of Col5:RPP13Nd-HA and Col0:Rps2-HA.....	38
Figure 3-4. Stable transgenic <i>Arabidopsis</i> lines expressing dexamethasone inducible ATR13 Emco5, Emoy2, or CFP.....	39
Figure 3-5. Dexamethasone toleration of stable transgenics grown on MS medium.....	40
Figure 3-6. Immunoprecipitation of ATR13 and interacting proteins.....	41
Figure 3-7. Pulldown of dex-induced ATR13 Emco5+CFP expressed in stable transgenic <i>Arabidopsis</i> using α -GFP dynabeads.	41
Figure 3-8. Methanol-soluble organic compounds isolated from <i>A. thaliana</i>	42
Figure 3-9. ATR13 and RPP13 association in <i>N. benthamiana</i>	43
Figure 3-10. Pulldowns of ATR13-associated proteins from <i>N. benthamiana</i>	44

Figure 3-11. Alignments generated from BLAST hits of contigs associated with peptides pulled down with flag-ATR13 protein expressed in <i>N. benthamiana</i>	45
Figure 4-1. Mutant Col5:RPP13 plants screened with <i>Pseudomonas syringae</i> DC3000 delivering ATR13 Emco5.	54
Figure 4-2. Disease assay on potential Col5:RPP13 mutants.....	55
Figure 4-3. Selection for Col5:RPP13Nd+dexATR13 Emco5 mutants unable to mount a defense response after dex induction.....	56
Figure 4-4. HR assay using <i>P. fluorescens</i> delivering various effectors on Col5:RPP13+dex ATR13 Emco5 mutant plants.....	56
Figure 4-5. Growth assay of <i>P. syringae</i> DC3000 on mutant Col5:RPP13Nd+dexATR13 Emco5 plants showing individuals compromised in ATR13 recognition.....	57
Figure 4-6. EMS mutants of Col5:RPP13Nd +dexATR13 Emco5 plants no longer producing HR.....	58
Figure 4-7. Hpa inoculations on Col5:RPP13Nd +dexATR13 Emco5 mutant plants.....	59
Figure 4-8. Lactophenol trypan blue staining of Hpa on potential mutant plants.....	59
Figure 4-9. EMS Col5:RPP13Nd mutants no longer able to restrict Hpa Maks9 growth.....	60
Figure 4-10. Punnett square illustrating expected segregation ratios for various scenarios of mutant phenotype.....	61
Figure 4-11. Subcellular fractionation of RPP13Nd:HA.....	63

List of Tables

Table 1-1. Ecotypes of <i>A. thaliana</i> and resistance phenotypes corresponding to different isolates of <i>H. arabidopsidis</i>	3
Table 2-1. NMR parameters, restraints, and statistics regarding the ATR13 structure.....	26
Table 2-2. Proteins with structural homology to ATR13 Emco5 identified by the DALI server.....	27
Table 2-3. Various amino acid changes in ATR13 Emco5 that disrupt RPP13 recognition.....	28
Table 3-1. List of stable transgenic <i>Arabidopsis thaliana</i> plants generated during my dissertation work.....	48
Table 3-2. List of peptides identified in <i>N. benthamiana</i> flag-ATR13 pulldown sample and the <i>Nicotiana</i> contigs associated with them.....	48
Table 3-3. Best BLAST hit alignments with contigs identified from peptides found in samples A1 and A2 from <i>N. benthamiana</i>	49

Acknowledgements

Thank you to all the members of the Staskawicz Lab, past and present, who have helped me along the way, including but not limited to: Brian for taking me on in the first place and granting me the freedom to follow my own whims and follies, Maiké for helping me transition from totally clueless to only somewhat lost, Ann-Maree for being such a stellar bay-mate and sounding board, Doug Dahlbeck for his unerring knowledge of pretty much everything, and his perpetual smile in the face of all my questions, Sandra for her cheerful demeanor, and of course my lab twin, KVK, for her general awesomeness.

I would also like to acknowledge all of the people who have contributed to this research by serving on my qualifying exam committee and/or thesis committee. Dr. Steve Lindow, Dr. Pat Zambryski, Dr. Bob Fischer, Dr. Tom Alber, Dr. James Berger, and Dr. Sheila McCormick, thank you for all of your time and efforts in making the completion of this thesis work possible. So many big brains working on my tiny slice of science, it's hard to believe how lucky I am.

Dr. Allyn Schoeffler, you are an amazing teacher and friend and I would have gone crazy long ago if it weren't for you. Truly wonderful collaborating with you; I can't thank you enough. Thank you to Dr. Jeffery Pelton for working with me to solve our structure and for never giving up, despite the challenges of our protein. Thank you also to the PMB support staff, especially Jason Trout who has rescued my computer innumerable times, and Nikki Groen who has facilitated many a speedy reimbursement.

Friends, some of you have been thanked above, but I also want to acknowledge the ladies of my cohort for being so wonderful and supportive along the way. Coffee breaks, cookies, and martinis are the perfect antidote to stress-induced panic attacks. Anna Park deserves a special mention since she's not in the program, but mostly because she's such a special person.

Mom, Dad, Sean, and Brian, words fail me. "Thank you" is pretty insufficient for all the love, support, and in the case of my brothers, torment, of the last thirty years. Strong, smart, and stubborn—I blame you.

Matthew Brooks: culinary genius, external hard drive, navigational system, therapist, dishwasher, technical advisor, friend and hero. Thank you, for everything. Lastly, I would like to acknowledge the pups: Tarbaby and the Ham. Woodland walks and wet noses brought me back from the edge more times than I can count. You guys wagged away most of my worries over the last few years. Thanks.

Chapter 1. An Introduction to Plant-Microbe Interactions

Plant disease is caused by an array of diverse agents: from mollicutes, viruses, and bacteria, to fungi, protozoa, and even other plants. One particularly devastating class of plant pathogens are the oomycetes, literally translated “egg fungi,” that include the white rusts and downy mildews that sap nutrients and resources from valuable crop species. Oomycetes are unicellular protists that share the Stramenopila clade with brown algae and diatoms. Previously these organisms had been classified as fungi, but a sequence comparison of small subunit rRNA of several genera of oomycetes, fungi, and algae resulted in their reclassification to the kingdom Chromista [1]. Biochemically, fungal cell walls consist primarily of chitin, while oomycete cell walls are made predominantly of cellulose; however, both share a convergent evolutionary trait: the production of specialized feeding structures known as haustoria. During fungal and oomycete infection, these parasites penetrate the plant cell through the junction between epidermal cells and create a sac-like protrusion, the haustorium, which presses up against the plant cell’s plasma membrane [2]. Within this specialized structure, proteins known as effectors are made by the oomycete and secreted across the haustorial membrane and cell wall into the extra-haustorial matrix [3]. Then, by a mechanism yet to be described, these proteins are taken up into the host cytoplasm through the extra-haustorial membrane (formerly the plant plasma membrane) where they presumably suppress host-defense and hijack machinery for exporting nutrients and metabolites back to the invading pathogen.

In recent years, the genomes of several *Phytophthora* species and *Hyaloperonospora arabidopsidis* (Hpa) have been published [4], [5],[6], resulting in a resurgence of oomycete-related research. As an obligate biotroph, Hpa is especially interesting, in that it lacks components necessary for survival independent of a host, but also possesses means to manipulate their hosts’ defense response and nutrient trafficking for their own continued existence. Genomes from these oomycetes have been compared, and Hpa was found to lack several genes essential in nitrogen and sulfur assimilation, hinting at what genes are necessary for an independent lifestyle and which nutrients it might acquire from its host [4]. These genomes have also been mined for predicted effectors that might help accomplish these goals using programs trained on motifs and patterns of known effectors [7], [8]. Having been implicated in the translocation of secreted effectors into the host cytoplasm, the RxLR motif is one of the best characterized patterns associated with these oomycete effectors [9]. ATR13, one of these known effectors, falls into the RxLR class of effector proteins and will be the focus of this study.

Concurrent to the evolution of oomycete stealth and nutrient acquisition equipment, plants evolved elaborate sensory mechanisms to detect the presence of an invading pathogen and its secreted effector molecules. Plant cell surface receptors recognize molecular patterns associated with pathogen surface proteins such as bacterial flagellin and elongation factor Tu, and pathogen polysaccharides like fungal chitin and oomycete beta-glucans [10]. Once detected by the plant’s pathogen recognition receptors (PRRs) or receptor-like kinases (RLKs), a signaling pathway is activated that results in transcriptional induction of pathogen-responsive (PR) genes, the production of reactive oxygen species, and callose deposition to reinforce the plant

cell wall at infection sites [11]. These defense responses are collectively referred to as pathogen triggered immunity or PTI. In the face of this adversity, pathogens have evolved effectors capable of interfering or disrupting PTI signaling, allowing pathogens to evade recognition and incite disease [12]. For instance, the *P. syringae* effector AvrRpm1 acts on the plant protein RIN4, subsequently preventing PTI by suppressing programmed cell death and PR expression [13]. Another *P. syringae* effector, AvrPphB, cleaves the plant protein PBS1, resulting in manipulation of a known defense related pathway, the JA signaling pathway [14], [15]. Regarding oomycetes, little is known about the function of known or predicted effectors, though their general role in host manipulation is most likely conserved. In general, oomycete effectors share little sequence similarity with known proteins, therefore speculations on functionality are difficult without first describing tertiary protein folds and identifying *in vivo* plant targets [16].

Despite the complex array of oomycete effectors manipulating PTI and host plant defense, plants have evolved additional means of detecting pathogen invasion. A second layer of immunity known as effector-triggered immunity (ETI) is initiated upon the detection of pathogen effectors in the plant cytoplasm by resistance proteins, the product of resistance genes (R-genes). R-gene recognition of effector presence or activity is the first step in the activation of a resistance signaling cascade that results in localized cell death (HR), system acquired resistance (SAR), and containment of pathogen spread ([17], [18]. In 1942, based on his studies with flax and its rust fungus, H.H. Flor was the first scientist to show a race-specific gene-for-gene relationship between pathogen and host recognition [19]. Resistance appeared to segregate following a Mendelian inheritance pattern, yet identifying the factor responsible for this resistance was unfeasible at the time. It was not until the early 1990s that an R-gene was identified and cloned [20]. The completion of the *Arabidopsis thaliana* sequencing project (1990) and the identification of native pathogens of this model organism have lead to the identification of a number of resistance genes. One such pathogen identified by Koch and Slusarenko in 1990 is the downy mildew oomycete *Hyaloperonospora arabidopsidis* [21].

As described briefly above, certain ecotypes of *A. thaliana* possess specific alleles of R-genes that can recognize effectors delivered by particular strains of *H. arabidopsidis* and trigger the HR response. The resistance gene of interest in this study is RPP13, first described by Bittner-Eddy et al (1999), that has been shown to recognize specific isolates of ATR13, an effector delivered by *H. arabidopsidis* during the course of infection [22], [23]. Both *ATR13* and *RPP13* are highly polymorphic genes, implying that the alleles have undergone diversifying selection at their respective loci [24]. Oomycete recognition only occurs if the cognate allele of RPP13 in *Arabidopsis* recognizes the form of ATR13 delivered by the pathogen [23]. For instance, the RPP13 allele present in the Columbia ecotype of *A. thaliana* fails to recognize either the Emco5 or Emoy2 alleles of ATR13, while the Neiderzenz ecotype is able to recognize ATR13 Emco5, but not Emoy2 [25]. Interestingly, despite the highly polymorphic nature of RPP13, only a few of the many alleles that have been sequenced actually recognize ATR13, those that do differing by five amino acid changes at most [26]. Below is a list of these recognition specificities that will be useful for reference throughout the following chapters (Table 1).

Transgenic *A. thaliana* Columbia plants containing the Neiderzenz allele of RPP13 (Col5:RPP13Nd) are resistant to *H. arabidopsidis* strains containing the Emco5 allele of ATR13, suggesting that all the machinery necessary for disease resistance is present in the susceptible Col5 ecotype, but that the recognition event only takes place in the presence of the Neiderzenz allele of RPP13. Interestingly, the resistance conferred by RPP13 recognition has been shown to be functional against a wide array of pathogens in addition to Hpa, including bacterial and viral pathogens [27]. RPP13 signaling also appears to function independently of the two major resistance pathways described to date in *A. thaliana*: the NDR1 and EDS1 pathways [28]. When plants containing RPP13 in an *eds1/ndr1* mutant background are challenged with Hpa isolate Emco5 or *P. syringae* delivering ATR13 Emco5, pathogen spread is restricted and plants remain healthy and viable [28]. This is exciting news, as it suggests that there remains a completely uncharacterized and conserved resistance pathway to be discovered and described in *Arabidopsis*.

The goal of the following work was to address several gaps in knowledge regarding the ATR13 and RPP13 cognate pair. We sought to solve the structure of ATR13 by various means to glean functional information based on structural homologs, to identify targets of ATR13 activity, and finally, to elucidate the seemingly novel RPP13 recognition pathway.

Table 1-1. Ecotypes of *A. thaliana* and resistance phenotypes corresponding to different isolates of *H. arabidopsidis*. Plant ecotypes are listed to the left, and Hpa isolates are listed across the top. “S”, or susceptible, denotes a compatible interaction between host and pathogen and “R”, or resistant, denotes an incompatible interaction. For a more complete list, please refer to reference [26].

	Emoy2	Emco5	Maks9	Aswa1	Wela3	Bico1	Goco1
Col5	S	S	S	S	S	S	S
Nd-1	S	R	R	R	S	R	R

Chapter 2. Features of the ATR13 three dimensional structure

Introduction:

Oomycetes are a devastating class of filamentous eukaryotic pathogens that afflict both plants and animals alike [3], [29]. Notorious for their role in the Irish Potato Famine and more recently for their decimation of live oak species throughout California, oomycetes have run rampant—quickly overcoming chemical control methods and costing billions of dollars annually in crop losses [30], [31]. Despite the enormous impact of these pathogens, our knowledge of how they manipulate plant resources and overcome host defenses resulting in disease is still extremely limited. Many oomycetes are obligate biotrophs, making them difficult, if not impossible, to culture and genetically transform. Phytopathogenic oomycetes grow intercellularly forming parasitic structures called haustoria (a common feature to fungi), which presumably play a role in feeding and suppression of host defense systems. A cohort of pathogen proteins known as effectors are secreted across this haustorial membrane, a subset of which are further translocated across the plant plasma membrane by an unknown mechanism that is functional in both plants and animals [32], [33]. The role of most of these oomycete effectors in pathogen virulence has remained elusive, as many of their protein sequences lack similarity to sequences currently in the databases [16], [34].

Several effector molecules from other classes of pathogens have been structurally elucidated providing insight into their mode of action and virulence. The fungal effector AvrL567 from *Melampsora lini*, a flax rust, has similarity to ToxA [35], a protein involved in cell death induction from the necrotrophic wheat pathogen *Pyrenophora tritici-repentis* [36]. The NEP1-like effector, NLP_{pya}, from the oomycete *Pythium aphanidermatum* has structural similarity to actinoporins, proteins derived from various marine invertebrates that form transmembrane pores facilitating membrane disintegration [37]. Additionally, crystal structures of bacterial effectors like AvrPto from *Pseudomonas syringae* in complex with their targets have provided a structural basis for the activation of plant immunity, showing how an effector interacts with its target and derepresses host defenses [38].

ATR13 is an RxLR effector from the downy mildew oomycete *Hyaloperonospora arabidopsidis* (Hpa) that is recognized in a race-specific manner by its cognate R-gene, RPP13, in *Arabidopsis thaliana* [39]. This class of proteins contains an RxLR motif that is implicated in host translocation. The Hpa/*Arabidopsis* pathosystem is an ideal model for studying oomycete-host interactions, as genome sequences for both are publically available, allowing for genetic exploration and dissection of each species (www.arabidopsis.org, <http://oomycetes.genomeprojectsolutions-databases.com/>). Both *ATR13* and *RPP13* are highly polymorphic genes, implying that the alleles have undergone diversifying selection at their respective loci [24], [39]. The maintenance of *ATR13* in all isolates of Hpa, together with the evidence of diversifying selection at this locus [40] implies that this effector confers a benefit to the invading oomycete. However, the function of *ATR13* has been difficult to extrapolate as no known proteins share sequence similarity to this effector. Although recognized alleles of *ATR13* delivered to *Arabidopsis* by the surrogate bacterial pathogen *Pseudomonas syringae* pathovar

DC3000 show a clear restriction of bacterial growth, in our hands we did not see enhanced bacterial virulence conferred by ATR13 on susceptible ecotypes [27].

To obtain more information on the virulence function and recognition domains of ATR13, we take both crystallographic and Nuclear Magnetic Resonance (NMR) approaches to solve its backbone structure. Further, we map loss-of-recognition and gain-of-recognition mutants generated through both site-directed and random mutagenesis. Additionally, we describe a region of ATR13 required for nucleolar localization but show that ATR13 subcellular localization has no effect on recognition by RPP13. Mutational effects of ATR13 Emco5 (recognized by RPP13) and ATR13 Emoy2 (not recognized by RPP13) are assayed using the *Agrobacterium tumefaciens*/*Nicotiana benthamiana* surrogate system [41], where ATR13 recognition by RPP13, in this case the Neiderzenz allele (RPP13-Nd), results in the hypersensitive response (HR), a plant-specific form of programmed cell death purported to limit pathogen spread.

Material /Methods:

2.1 ATR13 suppression of basal immunity

Other labs have shown that ATR13 expressed in planta can suppress the oxidative burst associated with PAMPs detection, in this case flg22. Eight to twelve leaves from transgenic Col5 *Arabidopsis* lines containing ATR13 Emco5, ATR13 Maks9, ATR13 Emoy2, ATR13 Emco5+CFP, or CFP were cut into 1mm leaf slices from the center of every 3rd leaf to control for developmental differences. These slices were placed in an opaque 96-well plate containing 100ul of 30uM dexamethasone and incubated at room temperature for 24 hours. The following day 100ul of elicitor (100nM flg22, 10ug/mL HRP, 17ug/mL luminol) was added to each well and light readings were measured immediately with the EnVision plate reader. Values and trends are plotted using Microsoft Excel. After three repeats of eight to twelve replicates, the trends observed in Sohn et al.'s paper [42] were not reproducible in our hands.

2.2 Native protein expression

pET-DUET1 constructs were transformed into chemically competent Rosetta(DE3)pLysS *E. coli* (Novagen), and selected on LA plates containing 50ug/ml carbenicillin. Single colonies were used for overnight starter cultures and diluted to an OD of 0.1 in LB +carb the following morning. These cultures were incubated at 37°C, 250rpm until reaching an OD of 0.55 when IPTG was added to a final concentration of 500uM for induction. Cultures were induced for 16h at 28°C, 250rpm and cells were harvested by centrifugation at 3,000rpm. Cells were resuspended in a small volume of buffer A (20mM phosphate buffer pH 7.2, 20mM imidazole, 0.5M NaCl, 10% glycerol), snap frozen in liquid nitrogen, and stored at -80°C.

2.3 Labeled protein expression

Overnight starter cultures were prepared as described above, spun down at 3,000 rpm for 15 minutes and washed once in M9 minimal media. For NMR experiments, uniformly ¹⁵N-labeled and uniformly-¹⁵N/¹³C – labeled ATR13 were expressed in *E. coli* using M9 minimal medium containing either one gram of ¹⁵N – labeled ammonium chloride, or one gram of ¹⁵N – labeled ammonium chloride and two grams of ¹³C-labeled glucose per liter of medium (Cambridge Isotopes Laboratories). A 10% fractionally ¹³C-labeled sample was prepared by growing the bacteria in medium containing 10% ¹³C-labeled glucose. Yields ranged from 20 to 25 mg per liter. The labeled protein was purified as described above. Protein samples were prepared for NMR experiments by dissolving lyophilized protein in buffer containing 20mM sodium phosphate pH 7.1, 150 mM sodium chloride, and 5% D₂O. The final protein concentration for each sample was approximately 1 mM.

2.4 Protein purification

Frozen cell suspensions were thawed and incubated with 10ug/ml lysozyme on ice for 30 minutes. Cells were sonicated at 30% duty cycle, 30% output for three 30 second bursts, and cell debris was spun down at 19,000xg for 20 minutes. Lysate was filtered and loaded onto an equilibrated 5ml Nickel column (GE Healthcare), washed

with 100ml of buffer A, and eluted in 2ml fractions from the column using an imidazole gradient (final concentration 200mM in buffer A). Fractions were run on SDS-PAGE gels and visualized using coomassie stain. Those containing ATR13 were pooled and incubated with 6His-TEV protease overnight at 4C while dialyzing against buffer A to remove imidazole added during elution. The TEV digest was then loaded onto an equilibrated nickel column and flow through containing cleaved ATR13 was collected; other contaminants and uncleaved 6His-ATR13 remained bound to the column. The flow through was then concentrated to 500ul of 1-3mM using a Millipore spin column (3,000MW) and dialyzed against 20mM phosphate buffer pH 7.1, 150mM NaCl.

2.5 Making antibody and affinity purification

Four aliquots of 500ul 1mg/ml 6His-ATR13 Emco5 protein were sent to Covance for custom antibody production. Two New Zealand white rabbits were used in the standard 118-day protocol and bleeds were checked against purified ATR13 protein on a dot blot. Antibody was enriched by affinity purification using ATR13 conjugated to CnBr-Sepharose 4B according to manufacturer's instructions (GE Healthcare).

2.6 Crystallography experiments

To generate crystals, we purified protein truncations including $\Delta 19$, $\Delta 41$, and $\Delta 53$ Emco5 with various TEV cleavable tags (MBP, GST, 6HIS both with and without tag) and ATR13 at concentrations ranging from 10mg/ml to 46mg/ml. We set up the following sparse matrix screens in both hanging and sitting drop trays: JCSG (Qiagen), Wizard I&II (Jena Biosciences), pH Clear (Qiagen), Nextal Classics Lite (Qiagen), PEG Ion/Natrix (Hampton), Hampton Index I&II (Hampton), Hampton detergent screen I, II, III (Hampton), and MB Class. For conditions that produced crystals, we designed focused screens around these hits to optimize crystal size and morphology in hopes of producing high quality diffraction. We also used the Hampton additive screen to try to improve crystal quality, but to no avail.

Crystals were harvested using various schemes including stepwise addition of cryoprotectant (glycerol, ethylene glycol, various PEGs, MPD, xylitol, hexanediol, and butanediol), quick dunks in cryoprotectant (cryo), no cryo, dragging crystals through paratone N, dehydrating crystals, gluteraldehyde crosslinking of crystals (with and without cryo), and growing and collecting crystals at 4°C as well as the typical 19°C condition. We also collected data sets from crystals at room temperature and 90°K.

Labeled protein crystals for obtaining phasing information were grown from selenomethionine-labeled protein, or generated from native protein grown in drops containing platinum, or from native protein crystals in soaked in platinum drops. Ideal metal soaks were determined by addition of various platinum and lanthanide metals to unlabeled ATR13 protein, followed by running a native PAGE gel and looking shifts in protein migration due to association with metal compounds.

2.7 NMR experiments

All spectra were recorded at 25°C on a Bruker Avance 500 MHz instrument equipped with a room temperature probe, unless stated otherwise. NMR data were processed with NMRPipe [43] and were analyzed using CARRA [44]. Backbone

assignments were made with standard 3D heteronuclear NMR experiments including HNCACB, CBCA(CO)NH, HNCO, HN(CA)CO, as well as a 3D ^{15}N NOESY-HSQC (100 ms mixing time) [45], [46]. The latter experiment was acquired on a Bruker 800 MHz instrument equipped with a room temperature probe. Sidechain $^1\text{H}/^{13}\text{C}$ signals were assigned with HCCH-TOCSY, (H)CCH-TOCSY, and (H)CCH-COSY experiments and a $^1\text{H}-^{15}\text{N}$ TOCSY-HSQC spectrum (60 ms mixing time), and were confirmed with (H)C(CO)NH, and H(CCO)NH experiments, as well as a HCCH-COSY recorded at 800 MHz [45], [46]. Magnetization transfer in (H)C(CO)NH, H(CCO)NH and $^1\text{H}-^{15}\text{N}$ TOCSY-HSQC spectra was poorer than would be expected for a 12 kDa protein, indicating some dynamics or transient protein-protein interactions. Phi torsion angle restraints were derived from $^3J_{\text{HNHA}}$ couplings obtained from an HNHA spectrum [47]. Stereospecific assignments for the methyl groups of 2 of 4 valine and 5 of 8 leucine residues were obtained by comparison of $^1\text{H}-^{13}\text{C}$ HSQC spectra of 10% and fully ^{13}C -labeled samples [48]. NOEs were identified in the 3D $^1\text{H}-^{15}\text{N}$ NOESY-HSQC spectrum and a $^1\text{H}-^{13}\text{C}$ NOESY-HSQC spectrum (85 ms mixing time) recorded on a Bruker Avance II 900 MHz instrument equipped with a cryoprobe. Residual dipolar couplings were measured from IPAP spectra [49] recorded on a ^{15}N -labeled sample dissolved in buffer containing 12 mg/ml of Pf1 phage (Asla Biotech Ltd, Riga, Latvia).. Tensor parameters were determined from a histogram of the couplings and values based on intermediate structures [50]. The magnitude of the alignment tensor and rhombicity were set to -11 Hz and 0.3, respectively. Qualitative backbone dynamics information was obtained from a $^1\text{H}-^{15}\text{N}$ heteronuclear NOE experiment [51].

2.8 Structure Generation

Initial structures were calculated with Cyana (version 2.1) [52]. Residual dipolar coupling data was included in the final rounds of refinement using CNS (version 1.3) [53]. Structures were viewed and analyzed using MOLMOL [54]. In the calculations, NOEs were classified qualitatively as strong (1.8 – 2.7 Å), medium, (1.8 – 3.5 Å) or weak (1.8 – 5.0 Å), and Phi torsion angles were constrained to -60 ± 30 deg for $^3J_{\text{HNHA}}$ values less than 6 Hz. Hydrogen bonds were identified on the basis on NOEs and slow amide proton exchange rates (protection factors greater than 100 [55]). Constraints were applied between HN and O atoms (2.8 – 3.3 Å) and between N and O atoms (1.8 – 2.3 Å). Force constants for NOEs, dihedral angles, and hydrogen bonds were set to default values. Force constants for HN residual dipolar couplings were set to 0.7 Kcal mole $^{-1}$ Hz $^{-1}$ to yield r.m.s.d.s equal to the uncertainties in the measurements (~ 1 Hz). Assignments have been submitted to the BioMagResBank under accession number RCSB10216 and the 20 of 200 structures with the lowest energies have been deposited in the Protein Data Bank under accession number 2LAI.

2.9 Site directed mutagenesis

Site-directed mutants were generated using the Quickchange Lightning Site-Directed Mutagenesis kit (Stratagene) as per the manufacturer's instructions.

2.10 Loss/Gain of function mutagenesis screens

For loss of function mutant screen, pENTR/D-d41 ATR13 Emco5 was subjected to random PCR mutagenesis using M13 primers and the Diversify Mutagenesis kit from

Clontech, buffer condition 4, as described in the product manual. For gain of function mutagenesis, pENTR/D-d41 ATR13 Emoy2 was used as template. PCR product from both reactions was gel purified and cloned into the pEarleygate 202 vector using LR clonase, transformed into maximum efficiency DH5a (Invitrogen), and plated out on LA with kanamycin selection 25ug/ml. The following day, colonies were harvested, minipreped, and transformed into electrocompetent *Agrobacterium tumefaciens* GV3101. 1,200 loss of function GV3101 colonies were resuspended in induction medium (0.1mM MES pH5.6, 0.1mM MgCl₂, 0.1mM Acetosyringone) to an OD between 0.3-0.7. After 3 hours at room temperature, suspensions were inoculated onto transgenic *Nicotiana benthamiana* containing RPP13Nd. Plants were scored for altered hypersensitive response at 24h, 48h, and 72h post inoculation. 800 gain of function GV3101 colonies derived from the ATR13 Emoy2 allele were screened in an identical fashion as described above.

2.11 Emco5 and Emoy2 NoLS chimeras

Emco and Emoy NoLS chimeras were generated using two-step PCR fusions. For the Emco + NoLS construct, 5' and 3' portions of Emco were amplified from pENTR-d41ATR13 Emco using the following primers: 5' caccatggcagccgagcagcga 3', 5' ctctataatcttctcgtggatgccttagc 3' and 5' gcacacgatcttcatgtctcctcaaatctaa 3', 5' ctgtctgtcaagagca 3'. The NoLS insert was amplified using pENTR-d41ATR13 Emoy as template with the following primers: 5'cgagaagattatagaggcatagcagcagcga 3' and 5'catgaagatcgtgtgccatcttagattgg 3'. Products from these three reactions were run on a high percentage agarose gel and purified by expected size using the Qiaquick Gel Extraction kit from Qiagen. The purified PCR products were pooled and used as template with the following primers: 5' caccatggcagccgagcagcga 3' and 5' ctgtctgtcaagagca 3'. Product was gel purified and cloned into pENTR via the TOPO reaction (Invitrogen). The Emco+NoLS fusion was then cloned into pEG103 using LR clonase (Invitrogen). For the Emoy –NoLS construct, 5' and 3' regions of ATR13 Emoy were amplified using pENTR-d41ATR13 Emoy with the following primer sets: 5' caccatggcag cgcagcagcga 3', 5'catgacgatcgtgtgcct ttataatcttctcgtggatgcc 3', and 5'cgagaagattataaaggcacacgatcgtcatg tctccaaa 3', 5'ctgactggcaacggc 3'. Product from these reactions was pooled and amplified using the following primer pair: 5'caccatggcagccgagcagcga 3', 5'ctgactggcaacggc 3'. pEG103-ATR13Emoy –NoLS was obtained by following the procedure described above.

2.12 Microscopy and Image processing

Images were obtained using an LSM 710 Confocal microscope from Carl Zeiss, Inc. Pictures were taken with 40x or 60x objectives using whole leaf mounts of *N. benthamiana* expressing ATR13. Images were processed with ImageJ [56].

Results:

ATR13 does not enhance virulence of DC3000 or Hpa Maks9

The Jones lab suggested that ATR13 has a virulence effect on the growth of DC3000 on *A. thaliana* [42], claiming that callose deposition was suppressed and that

A

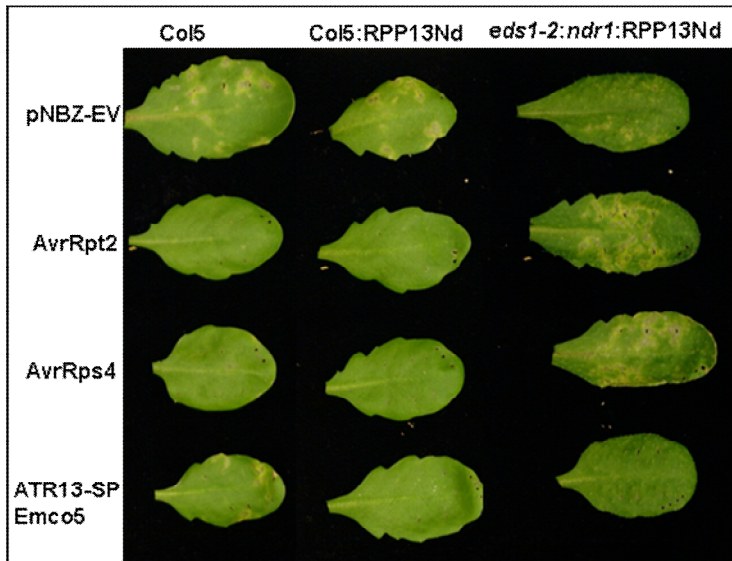
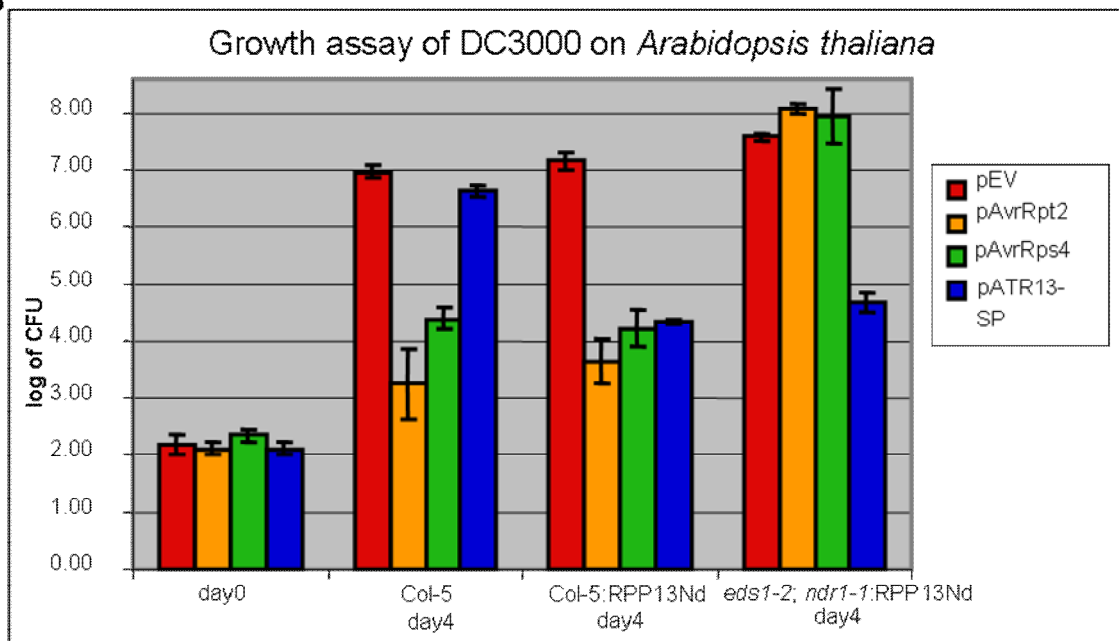


Figure 2-1. Growth assay of *Pseudomonas syringae* DC3000 on *Arabidopsis thaliana*.

A. *A. thaliana* leaves inoculated with DC3000 delivering various effectors. Unrecognized effectors promote disease on susceptible ecotypes.

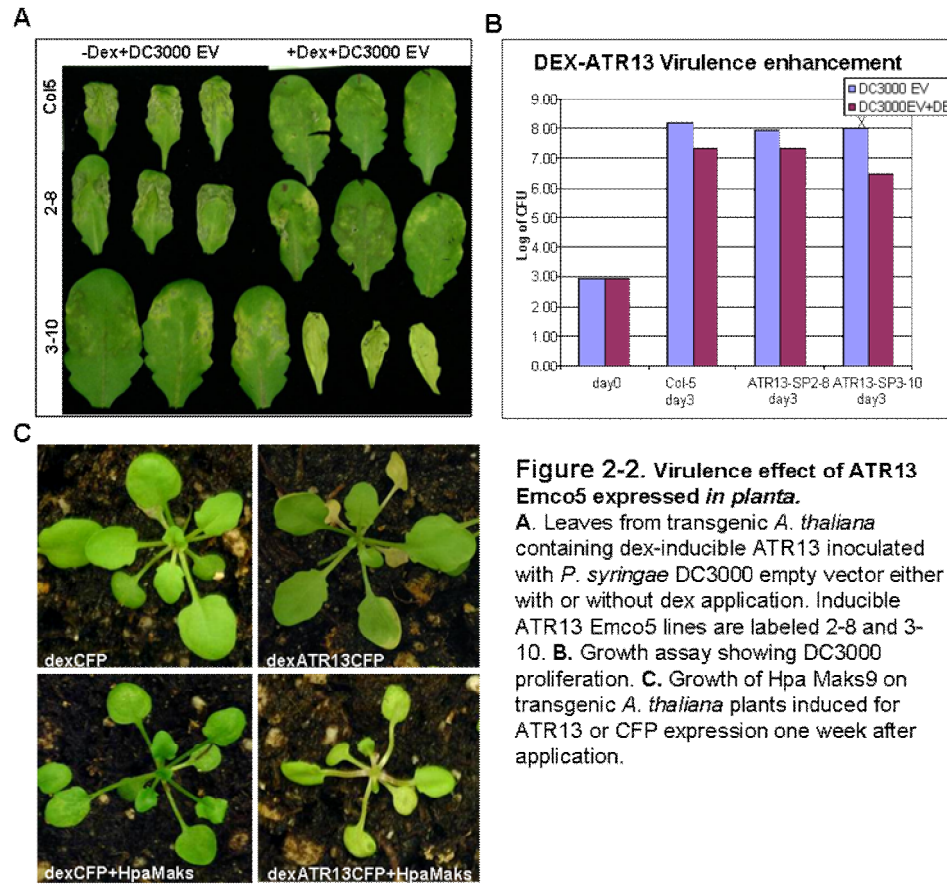
B. Corresponding growth assay of leaves from panel A showing recognition and restriction of various effectors on different ecotypes, including ATR13Emco5-SP.

B



generation of reactive oxygen species was dampened in transgenic lines presented with flg22. However, my results using either the pNBZ vector (with the type three secretion signal (TTSS) from AvrRpm1) or their vector pEDV3 (TTSS from AvrRps4), suggest that ATR13 does not affect the growth of *Pseudomonas syringae* DC3000 (Figure 2-1A, B). While we saw that RPP13Nd recognition machinery was functional and mounts a

defense response against *P. syringae* DC3000 delivering ATR13 Emco5 –SP, restricting bacterial growth relative to empty vector, we did not see enhanced growth of DC3000 strains containing ATR13 Emco5 –SP relative to growth of empty vector on susceptible ecotypes. In addition, when I induced ATR13 Emco5

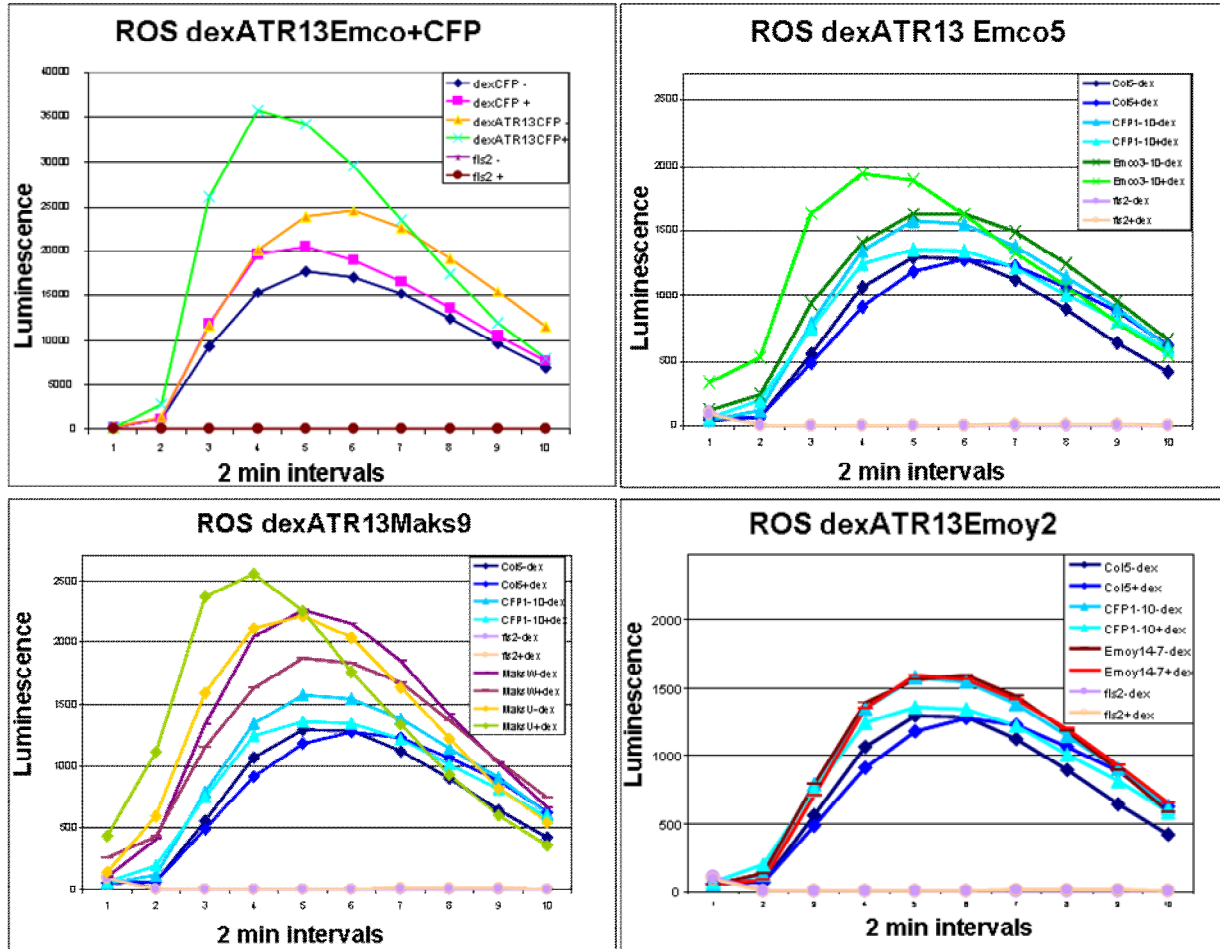


expression in stable transgenic *A. thaliana* plants by adding dexamethasone and inoculated these plants with either DC3000 carrying empty vector (Figure 2-3A) or Hpa Maks9 (Figure 2-3B), I still did not see enhanced susceptibility to respective pathogens. There is some yellowing and shriveling of leaves associated with certain transgenic lines expressing ATR13, however this appears to be independent of the presence of pathogen. In fact, plants that appear chlorotic support less pathogen growth than healthy plants.

ATR13 does not suppress Reactive Oxygen Species (ROS) production

While the Jones laboratory showed reduced ROS production upon detection of flg22 (a PAMP from bacteria) in stable transgenic lines expressing ATR13 alleles [42], we were unable to reproduce these results. As illustrated in figure 2-3A, we saw an opposite trend of ROS production in our transgenic lines (creation described in subsequent chapters). In the two *A. thaliana* lines containing ATR13 Maks9 obtained from the Jones lab [42], two different trends emerged: their line “W” showed trends consistent with their published data, however their “U” line showed trends consistent with the observed trends of our ATR13 Emco5 lines. In our ATR13 Emco5 lines, as well as the ATR13 Maks9 “U” line, we saw a more rapid and enhanced production of ROS in plants that had been induced for ATR13 with dexamethasone (dex) for 24 hours, followed by a sharp drop that eventually dropped below uninduced levels. ATR13 protein accumulation of assayed tissues is shown in figure 2-3B. From panel B we see

A



B

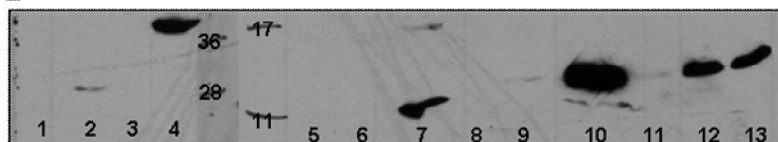


Figure 2-3. ATR13 suppression of basal resistance.

A. ROS production measured by luminescence after addition of flg22 to *A. thaliana* lines induced or uninduced for expression of ATR13 or CFP. **B.** Western blots of these leaf slices probed with anti-GFP (lanes 1-4) or anti-ATR13 antibody (lanes 5-13). Please note the negative control for MaksU -dex is out of sequence with its induced sample.

1. CFP1-10 -dex
2. CFP1-10 +dex
3. ATR13Emco3-10 -dex
4. ATR13Emco3-10 +dex
5. Col5 +dex
6. ATR13Emco3-10 -dex
7. ATR13Emco3-10 +dex
8. ATR13Emoy14-7 -dex
9. ATR13Emoy14-7 +dex
10. ATR13MaksU +dex
11. ATR13MaksW -dex
12. ATR13MaksW +dex
13. ATR13MaksU -dex

that the ATR13 Emoy2 line did not induce, and therefore shows a trend similar to dex-induced CFP or Col5 controls. These experiments were repeated four times with similar results.

ATR13 protein expression and deletion analysis

To obtain soluble protein for structural studies, we expressed truncations of three different alleles of ATR13: Emco5, Maks9, and Emoy2, minus the signal peptide and RxLR domains (Δ 41 truncations) (Figure 2-4A). Of the three alleles, ATR13 Emco5

produced the most soluble protein and was therefore selected to pursue for generation of crystals for structural determination. Unfortunately, initial crystal hits took more than two months to grow, leading us to believe that some kind of natural proteolysis was

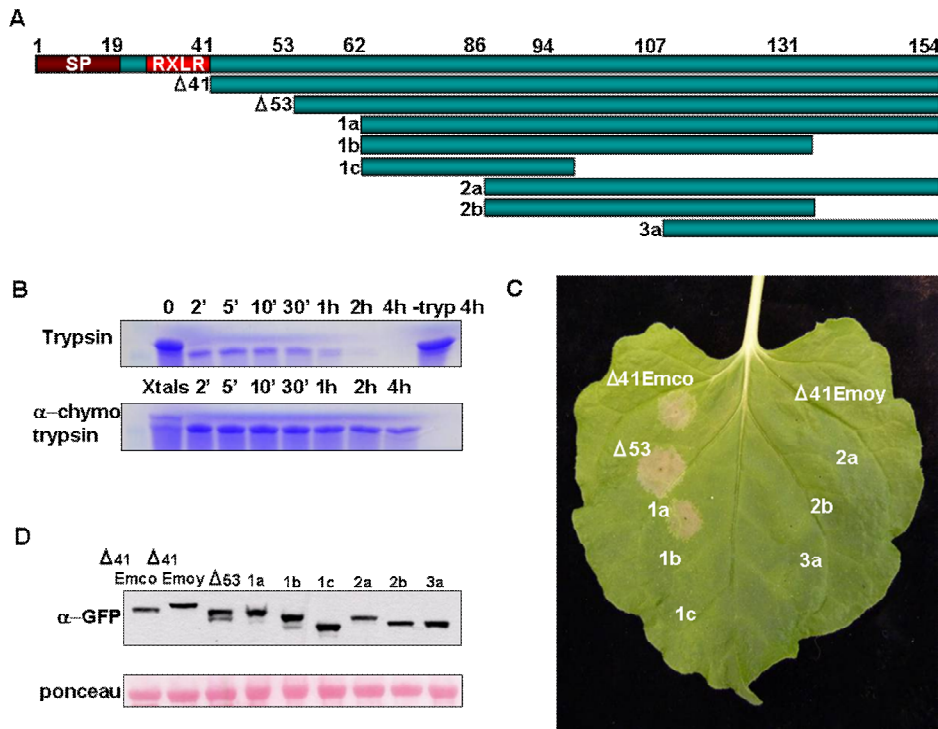


Figure 2-4. Determining Active Truncations of ATR13 Emco5.

A. Cartoon figure of ATR13 Emco5 truncations cloned into pEarleygate101 and assayed for activity. Features include a signal peptide involved in effector secretion and an RxLR motif implicated in host-translocation. **B.** Coomassie-stained SDS-PAGE gel showing limited proteolysis of purified $\Delta 41$ ATR13 Emco5 using trypsin and α -chymotrypsin. Twenty crystals were harvested, dissolved, and run with the α -chymotrypsin samples. **C.** *Nicotiana benthamiana* RPP13-Nd transgenic recognizing various transiently expressed ATR13 Emco5 truncations. **D.** Western blots probed with GFP antibody and loading-control ponceau of protein extracted from *N. benthamiana* transiently expressing ATR13 Emco5 truncations.

taking place in the droplet before the protein could crystallize. To address this, we performed limited proteolysis [57] using both trypsin and chymotrypsin on ATR13 Emco5 samples to generate the most stable version of the protein (Figure 2-4B). Additionally, we determined that the protein in the crystals existed in two forms: the original $\Delta 41$ version and a cleaved version we later learned by mass spectrometry to be a $\Delta 53$ truncation (data not shown).

To verify the biological relevance of our $\Delta 53$ ATR13 Emco5 truncation, we cloned $\Delta 53$ ATR13 Emco5 into pEarleygate 101 and transiently expressed this truncation in *N. benthamiana* containing the RPP13-Nd transgene, demonstrating a functional HR. Furthermore, to determine the minimal region necessary for RPP13-Nd recognition, truncations from both the N-terminus and C-terminus of ATR13 Emco5 were cloned into pEarleygate 101 [58] and transiently expressed in *N. benthamiana* via *Agrobacterium* inoculations. While RPP13-Nd was able to recognize ATR13 Emco5 N-terminal truncations up to 62 amino acids, once 86 amino acids are removed, RPP13-Nd recognition was compromised (Figure 2-4C). C-terminal deletions resulted in compromised recognition, as even removing eight amino acids from the end of the protein results in loss of recognition (as determined from early stop codons generated in the random mutagenesis assay described below).

Crystallography with ATR13

Eventually we generated crystals of $\Delta 53$ Atr13 Emco5 (Figure 2-5A, B) in several conditions and collected a number of data sets from these crystals, typically diffracting in the 3.5-4 Ångstrom range (Figure 2-5C). The most common space group associated with our crystals was the I4 space group with dimensions of $a=87$, $b=87$,

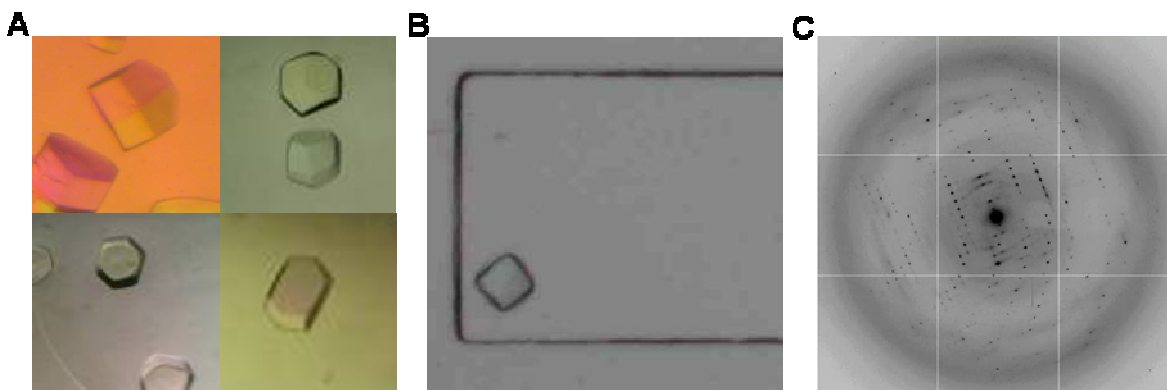


Figure 2-5. Crystals of ATR13. A. $\Delta 53$ ATR13 Emco5 crystals grown in various conditions in sitting drop trays. B. ATR13 crystal grown in chip format. C. Typical diffraction pattern associated with ATR13 crystals, regardless of handling and cryo schemes.

and $c=65$ Ångstroms with alpha, beta, and gamma angles at 90 degrees. Attempts to phase our data using selenomethionine-derivatized crystals and heavy metal soaking were unsuccessful. We consistently observed highly mosaic diffraction, which despite our best efforts, could not be improved. The absence of phasing information or an obvious structural homolog made the generation of electron density maps impossible.

ATR13 structures by NMR

After attempts to solve the structure using crystallography stalled, we turned to NMR to solve the structure of ATR13. Our first ^1H - ^{15}N HSQC spectrum provided insight as to why crystallography was proving so difficult; only three-fourths of the protein truncation we were using was actually ordered (Figure 2-6A). Worried that this region of internal disorder was due to several missing direct repeats in the Emco5 allele relative to other alleles of ATR13 (Figure 2-7A), we purified ATR13 Maks9 and collected its ^1H - ^{15}N HSQC spectrum. The Maks9 allele of ATR13 has an equal number of ordered residues to the Emco5 allele, suggesting that the insertion present in the longer alleles does little to stabilize the disordered loop. Overlays of the Maks9 and Emco5 spectra also reveal significant overlap between ordered peaks present in both samples, indicating that the additional missing peaks in Maks9 are most likely part of the direct repeat region not found in Emco5.

Backbone amide proton assignments were obtained using standard 3D triple resonance heteronuclear experiments (see materials and methods) for 81 residues including those in segments G56 through D96, N104 and A105, and L116 through Q154 with the exception of I92. Only one sharp peak and two broad peaks remain unassigned in the HSQC spectrum, indicating that approximately 16 of the 95 expected HN signals

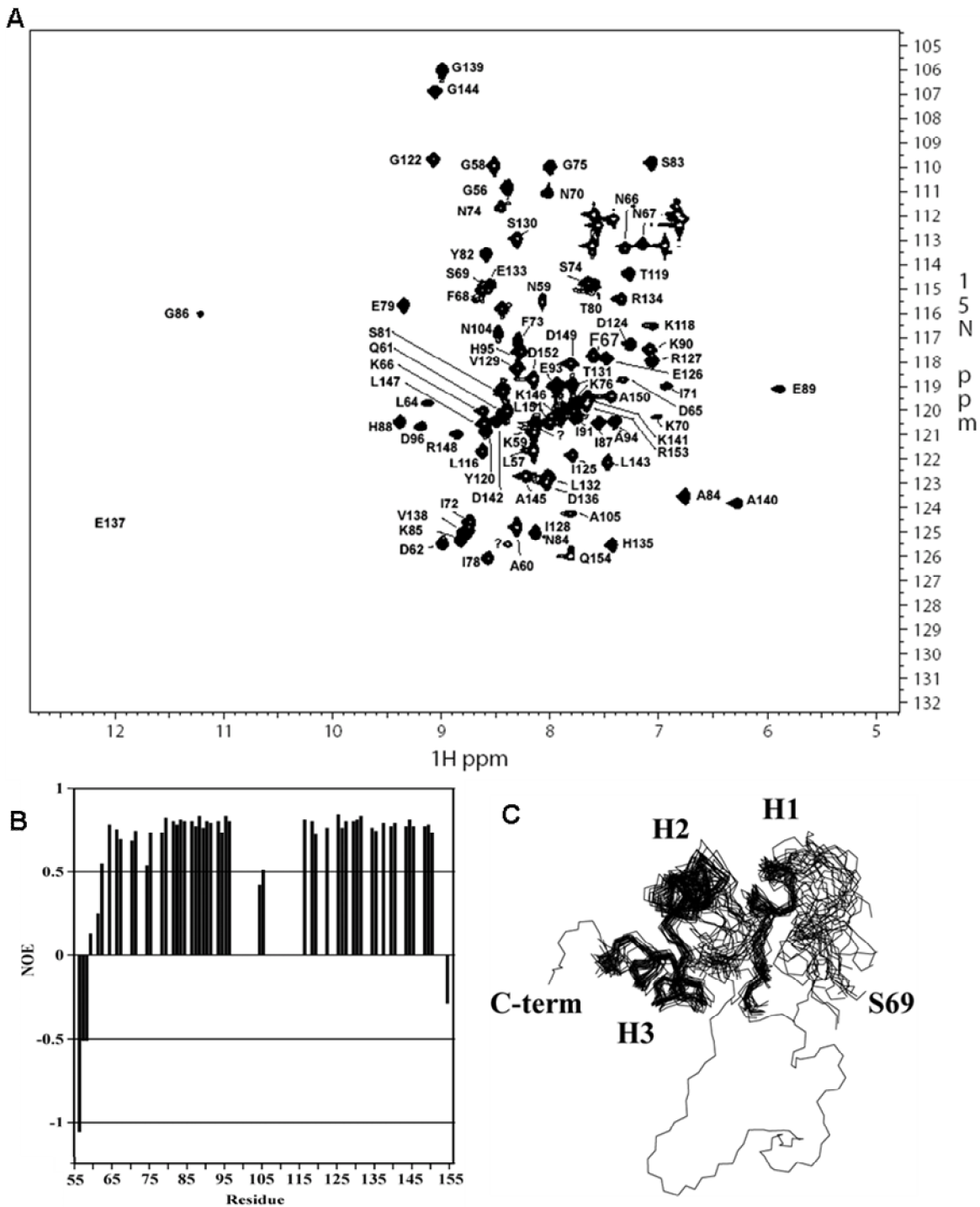


Figure 2-6. NMR analysis of ATR13 Emco5. A. ^{15}N -HSQC of $\Delta 53$ ATR13 Emco5 showing ordered residues. **B.** Heteronuclear NOE diagram of ATR13 Emco5 showing dynamics of ATR13 Emco5 residues. Flexible residues have values below 0.5. **C.** An overlay of the twenty lowest energy structures forming a consensus at the C-terminus and part of the N-terminal region shown here connected by a representative loop from one of the twenty structures. Alpha helices are denoted as H1: residues 77-85, H2: residues 122-135, and H3: residues 140-150.

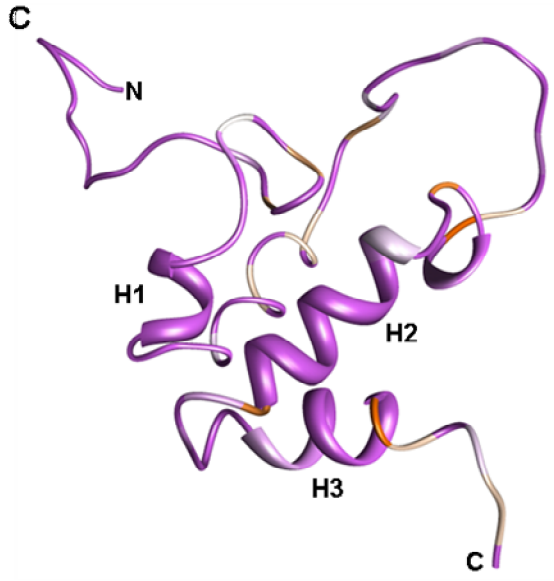
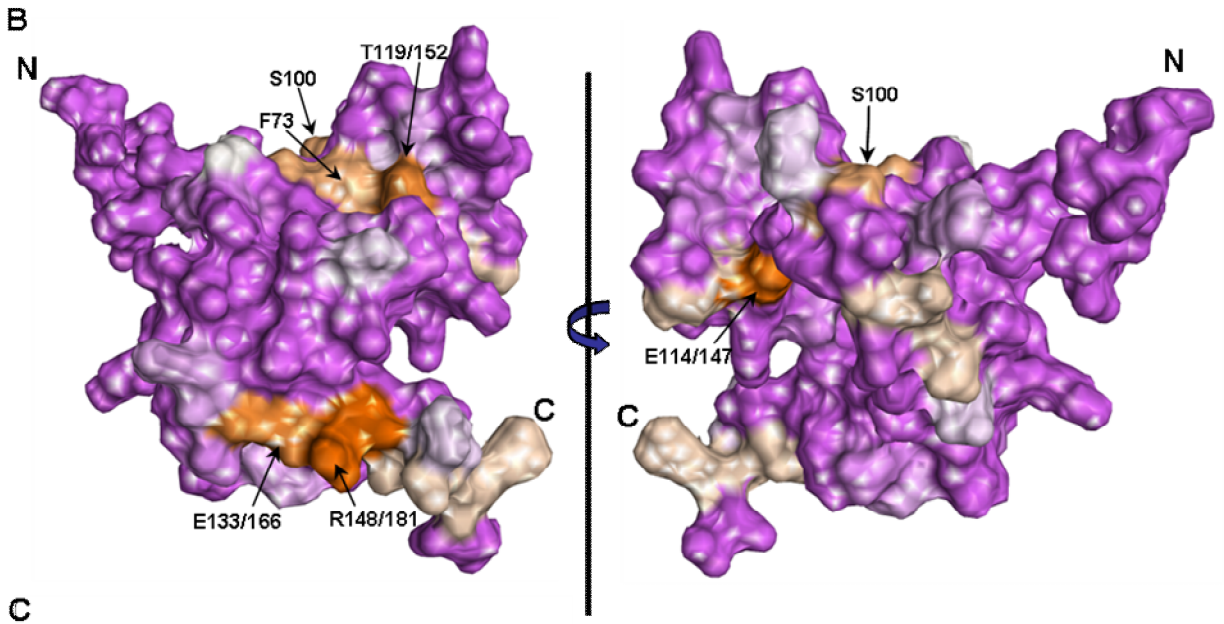
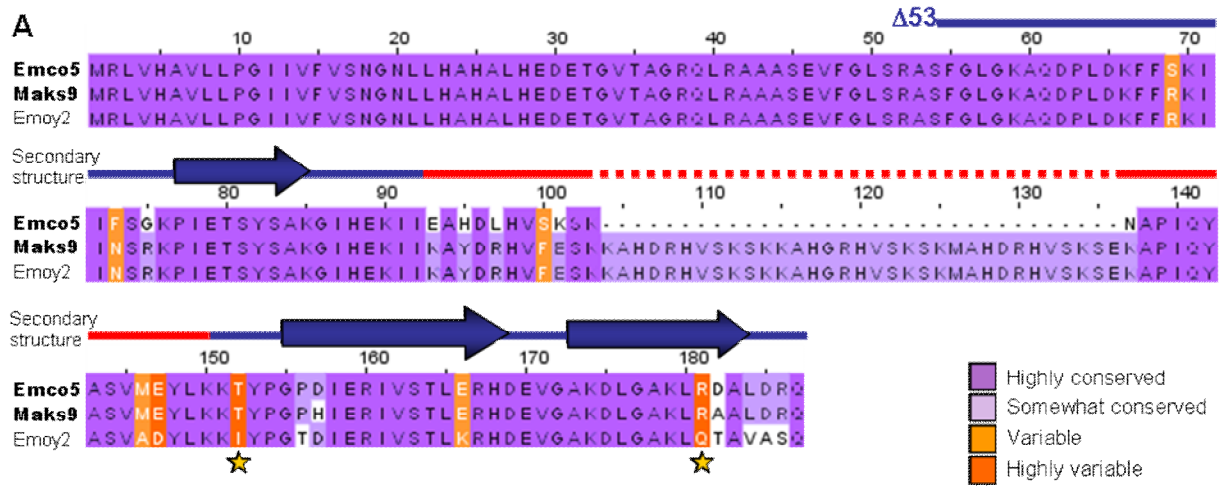


Figure 2-7. Naturally occurring polymorphisms of ATR13. **A.** A clustalX alignment of ATR13 variants colored by percent conservation calculated from 15 isolates in Jalview; three are shown. ATR13 alleles recognized by RPP13Nd are shown to the left in bold. Residues previously implicated in recognition are marked by yellow stars. Secondary structure is represented above corresponding residues; lines indicating coil whereas arrows denote alpha helices. The red portion of the secondary structure indicates disordered residues. **B.** Naturally occurring polymorphisms mapped onto a representative ATR13 structure rendered in Chimera. Polymorphic residues are shown in orange hues, while conserved residues are in purple. **C.** Ribbon diagram of ATR13 structure showing helices.

are missing. By process of elimination, we conclude that these missing signals correspond to residues in segment 97 – 115, as all other residues have backbone amide proton assignments. Of the residues with assigned HN resonances, approximately 88% of the side chain signals were also assigned. A summary of the NMR-derived restraints and structural statistics are presented in Table 2-1. The well-ordered region of the structure (76-88 and 120-150) is defined by 14 restraints per residue. These data yielded a well-defined backbone fold, but the sidechains are less well defined. The NOE, dihedral, residual dipolar coupling, and hydrogen bond restraint violations for ATR13 are good as are most of the structural quality factors (Table 2-1). The relatively high value obtained from Verify3D (Table 2-1) is due to the ill-defined state of the loop region (residues E89 – Y115) (see below). The portion of ATR13 elucidated by NMR consists of a central helix (residues 122- 135) that packs against a short helix and turn (P77-H88) on one side, and a long C-terminal helix (residues A140 – A150) on the other.

The N-terminal residues prior to the first helix (G54-P77) are not particularly well defined by the NOE data. As an alternative, the steady-state ^1H - ^{15}N NOE enhancement provides a qualitative measure of dynamics [59]. Rigid HN bonds typically have NOE enhancements of approximately 0.8. As the sub-nanosecond dynamics increases, the NOE enhancement decreases, and can even become negative. Heteronuclear NOE values for residues G56 through D62 increase slowly from -1.0 to 0.5, characteristic of a flexible N-terminus. However, there is some evidence that residues L64 through K76 are more ordered than could be defined. For example, the program TALOS [60], which compares measured CA, CB, CO, and HA chemical shifts to those from a database of known structures, predicts that the phi / psi angles for residues L64-K70 adopt a helical conformation, while in the later portions of the segment (S69-K76) several weak dNN NOEs and small $^3\text{J}_{\text{HNHA}}$ couplings (~ 5 Hz) suggest a turn or helical structure. These data give rise to the hint of structure for S69 through K76 (Figure 2-6B, C). Residues L64 through K76 also have fairly high heteronuclear NOE values (~ 0.7) which supports the premise that there is some order within this region that is not defined by the NMR data.

The most outstanding feature of the structure is an ill-defined loop that extends from E89 to Y115. In the segment 97 – 115, only N104 and A105 are assigned. N104 and A105 show reduced ^1H - ^{15}N heteronuclear NOE values (~ 0.5), also suggesting that at least a portion of the segment is flexible (Figure 2-6B). In attempts to solve the crystal structure, density for the single selenomethionine (M113), which is located in the loop region, was displaced from the remaining protein density, which is consistent with disorder in this region. As stated earlier, approximately 16 amide signals were missing from the ^1H - ^{15}N HSQC spectrum, and many must correspond to residues within this region. The absence of peaks suggests that this loop has flexibility on an intermediate time scale under the conditions studied.

Because of the large internal loop, the NMR structures are best defined at the C-terminus, as well as a smaller region at the N-terminus. Structural homology searches using the Dali server (http://ekhidna.biocenter.helsinki.fi/dali_server/start) yielded several candidate proteins with weak structural similarity (Table 2-2) indicating that ATR13 may possess similarities to GTP-binding nuclear protein RAN, Importin subunit beta-1, and a serine/threonine protein phosphatase 2A.

Loss of Recognition (LOR) by Site Directed Mutagenesis (SDM) of ATR13 Emco5

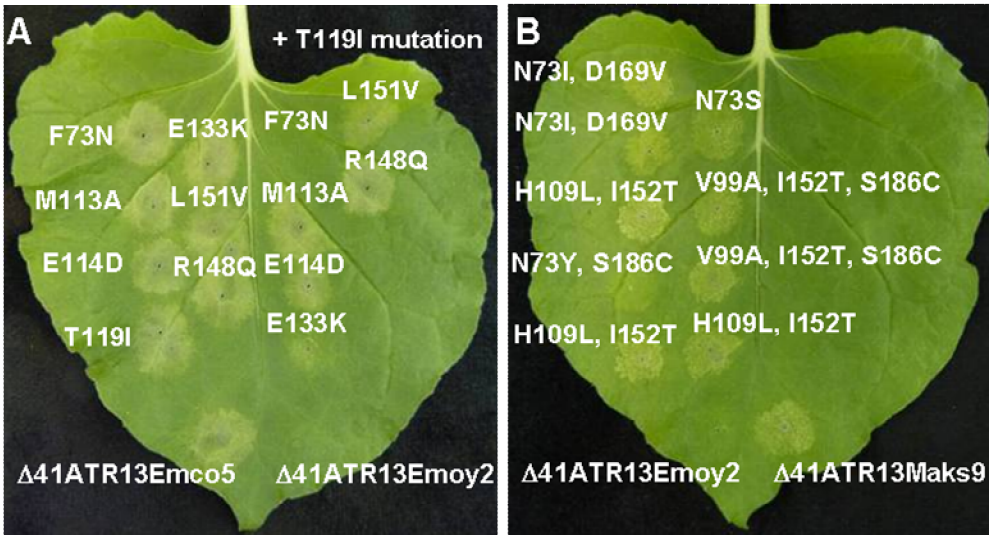
Exploiting natural variation occurring between recognized and unrecognized alleles of ATR13, Emco5 and Emoy2 respectively, we singly or doubly mutated polymorphic residues possessing vastly different chemical properties between alleles, or residues previously implicated in recognition (Figure 2-7B) [40]. Using the surrogate *Agrobacterium/N.benthamiana* system [41], we demonstrated that single amino acid changes of these residues have little to no effect on recognition of ATR13 Emco5 by RPP13Nd. However, in several cases, double mutations reduce the intensity of HR (E133(166)K, T119(152)I and T119(152)I, R148(181)Q) or eliminate it, as is the case with F73N, T119(152)I (Figure 2-8A). When mapped onto the structure, F73 and T119(152) appear to be surface-exposed and in close proximity (Figure 2-8C), implicating this specific region in avirulence determination.

Gain of Recognition (GOR) by Random Mutagenesis of ATR13 Emoy2

As a complement to the loss-of-recognition screen, we performed gain-of-recognition random mutagenesis on ATR13 Emoy2. After screening 800 mutant ATR13 Emoy2 alleles for altered recognition by RPP13-Nd on *N. benthamiana*, we identified nine clones that possessed an intermediate recognition phenotype (Figure 2-8B). All nine of these mutants had either the I(119)152T, or N73Y/S/I substitutions, lending support to the theory that these two residues are critical for RPP13-Nd mediated HR. In addition, like unrecognized alleles, the Maks9 variant of ATR13 has an asparagine at residue 73, however it is recognized by RPP13-Nd. In this allele, when N73 is substituted with a phenylalanine like that found in Emco5 and most recognized alleles, the resistance response by RPP13-Nd is more robust than that generated against wildtype Maks9 (data not shown) again implicating this residue position as crucial for full RPP13-Nd recognition.

Loss of Recognition (LOR) by Random Mutagenesis of ATR13 Emco5

To more thoroughly explore the avirulence role of ATR13 in conjunction with RPP13-Nd, we performed random mutagenesis to identify additional amino acids that play a role in ATR13 recognition. Of 1,200 colonies screened, 95 clones showed a loss-of-recognition phenotype. When sequenced, 50 of these clones had either frame shift mutations or early stop codons, while the remaining 45 had either single, double, or triple mutations (Figure 2-9C). We also sequenced 95 mutant clones showing intact HR signaling. These retention-of-recognition (ROR) mutants were used to eliminate background mutations that did not alter recognition (Table 2-3). When inoculated onto *N. benthamiana*, the 45 LOR mutants display varied timing and intensity of hypersensitive response, as well as a range of mutant protein stabilities relative to wildtype levels (Figure 2-9). Fourteen mutant alleles of ATR13 Emco5 appear to accumulate amounts of protein equaling or in excess of the wildtype level, and when analyzed in the context of the structure, these residues seem nested within its core, rather than surface-exposed (Figure 2-8C). Interestingly, most of the altered residues occur in regions that are conserved among natural ATR13 variants. When we mutate one of these conserved residues, Y(115)148N, from another recognized allele of ATR13, Maks9, we can again abolish recognition by RPP13Nd, showing that the altered phenotype is not specific to the mutant ATR13 Emco5 (data not shown).



C

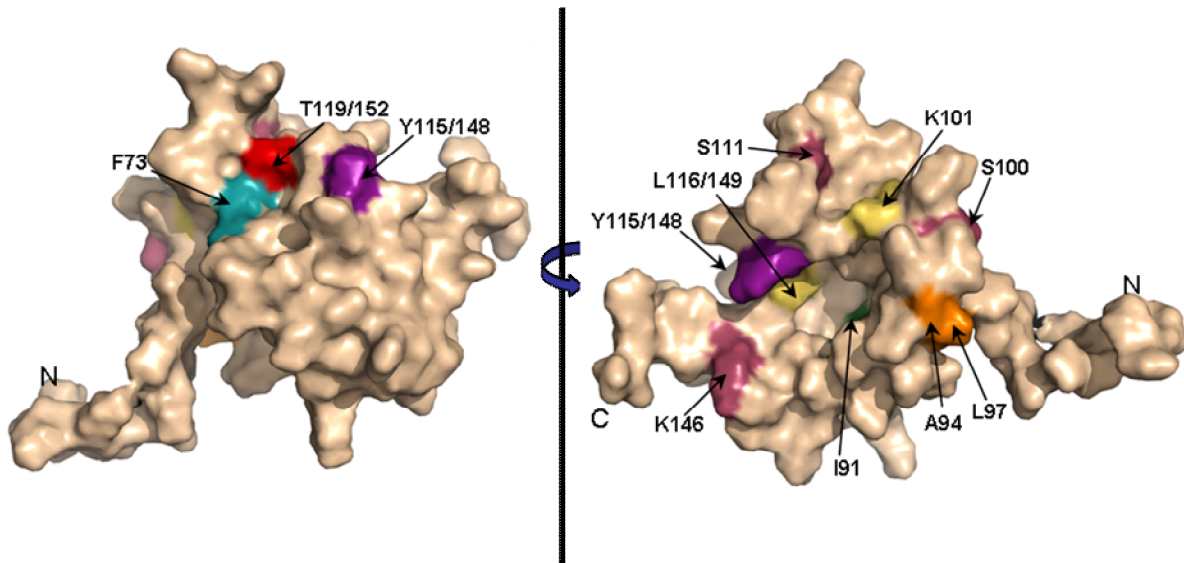
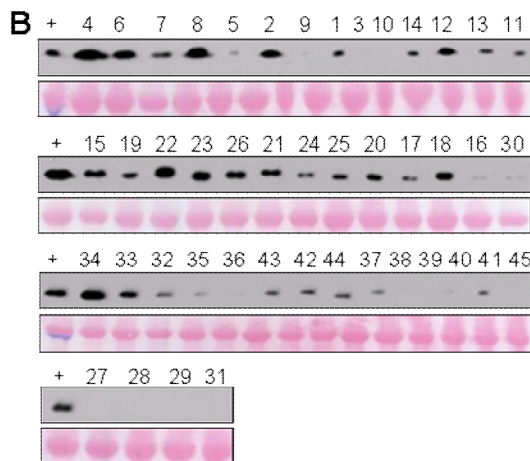
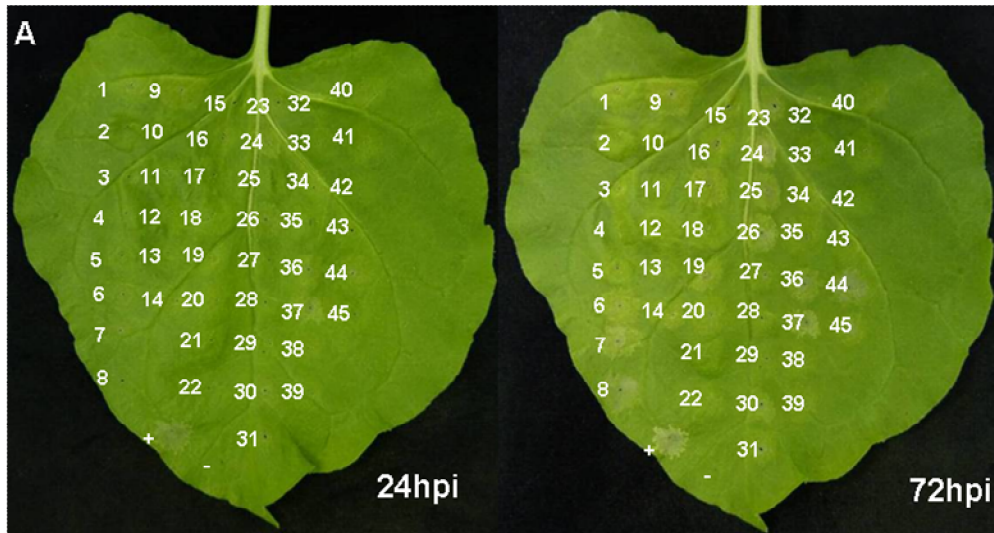


Figure 2-8. Site-directed loss-of-recognition (LOR) and random gain-of-recognition (GOR) mutagenesis of ATR13 scored for HR in RPP13 transgenic *N. benthamiana* plants. **A.** Site-directed mutation of residues from ATR13 in the Emco5 allele to those found in the unrecognized Emoy2 allele producing LOR by RPP13Nd. Inoculations on the right of the leaf are double mutants containing the T119I amino acid change. Note that residue numbers correspond to amino acid positions in Emco5. **B.** Residues mutated in the Emoy2 allele of ATR13 producing GOR by RPP13Nd. The numbering of these residues corresponds to amino acid positions in Emoy2, for example T119 Emco aligns structurally with I152 Emoy. **C.** F/N73 (teal) and T/I119(152) (red) residues mapped onto the ATR13 structure. Additionally, mutants generated from random loss-of-recognition mutagenesis that maintained ATR13 at the wildtype level are shown. Colors indicate mutations that occurred together to compromise RPP13 recognition. Where different, residue positions are listed relative to Emco5 position first and Emoy2 position after slash.



#	Mutations	#	Mutations	#	Mutations
1	L132P	16	I91S, D124G	31	S111C, L132H
2	T119P *	17	H95L,H 135P	32	K85N, L116P, K141N
3	H95P	18	A94E, L97P *	33	S100P, S111I, K146E *
4	Y115N *	19	F67S, H88L	34	I71M, K103T, Y115C
5	T131P	20	T80G, P123L	35	K66E, E79K, I87S
6	Y115H	21	I91S, I92T	36	L57P, I71M, K76R, S130P
7	L64P	22	K101E, L116P *	37	F73S, K85E, I87T, L151P
8	Y115C	23	L64P, K103M	38	E89G, S130P, E137K
9	V129D	24	I91N, K146E	39	Y115H, D124V, V129A
10	L132P	25	D65N, I78N	40	K59R, K103M, I128F, K141E
11	S111C	26	F55L, S83P	41	S69L, H98L, I128T
12	I91N *	27	I87F, H98L	42	L97P, I128T, E137G
13	L132P	28	A94V, S130T	43	S102P, Y109S, H135P
14	L116Q	29	I128N, Q154L	44	S81G, K101A, K141A
15	D65V, V112E	30	A84T, V129D	45	G122M, L132H, D149G

Figure 2-9. Random loss-of-recognition (LOR) mutagenesis of ATR13 Emco5 scored for HR in RPP13Nd transgenic *N. benthamiana* plants. **A.** Inoculations of various mutants generated by random pcr mutagenesis showing the varied timing and intensity of HR response after 24h and 72h. **B.** Western blot of various clones probed with α -ATR13 and ponceau for loading. **C.** A key to inoculation and expression data, consolidating complete lack of HR (red font), wildtype protein expression (yellow boxes), and residue alterations. Those clones marked with an asterisk had unique mutations not present in the retention-of-function mutational database or in other clones.

ATR13 localization and Identification of a Nucleolar Localization sequence (NoLS)

Upon review of the disordered residues in the Emco5 allele of ATR13, we noticed that these disordered residues flanked an insertion present in other alleles, namely Maks9 and Emoy2, both of which have been observed to localize to the nucleolus. To assess whether this 33 residue insertion was responsible for nucleolar targeting, we embedded this sequence at the analogous position in the Emco5 allele (Figure 2-10A),

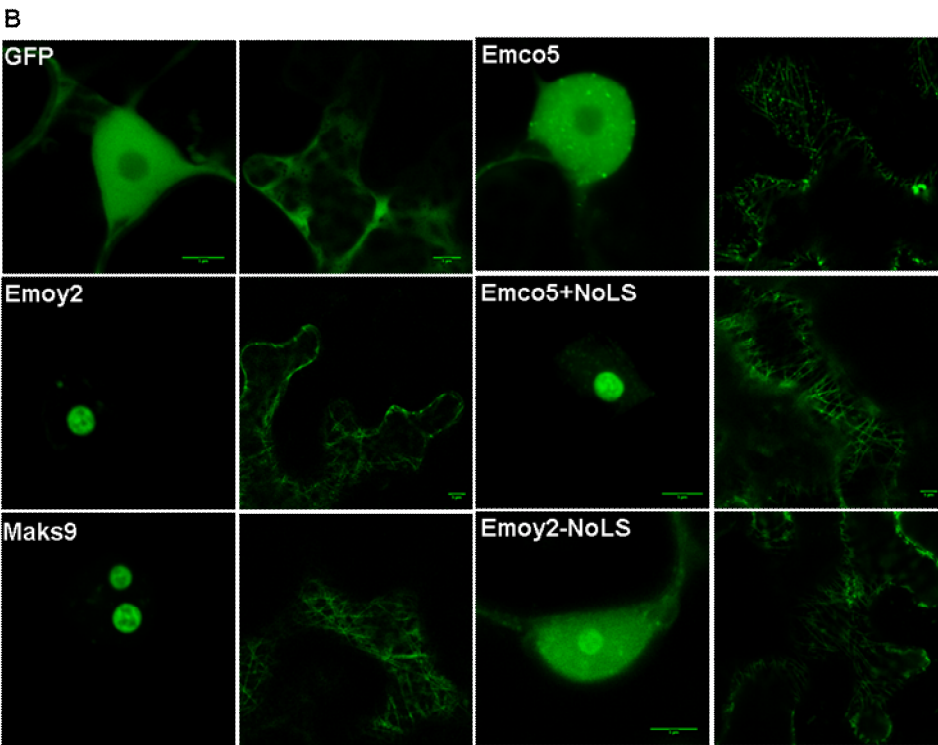
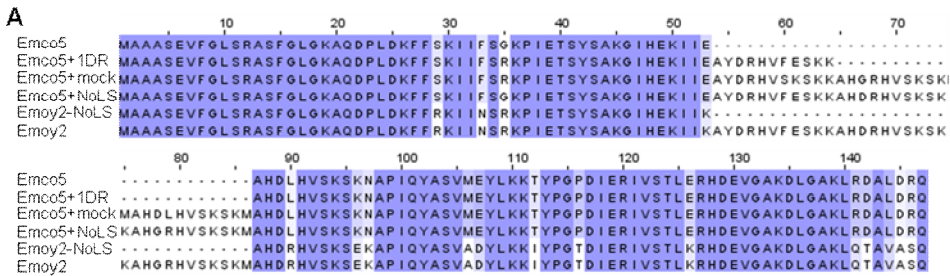
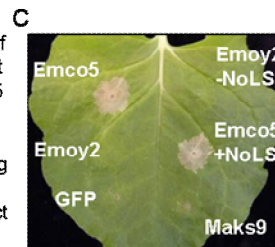


Figure 2-10. Nucleolar targeting signal of ATR13. **A.** An alignment of various ATR13 chimeras showing the naturally occurring insertion present in Maks9 and Emoy2 alleles of ATR13, the insertions added to the Emco5 allele, and the deletion from the Emoy2 allele. **B.** Localization of GFP-fused ATR13 chimeras expressed transiently in *N. benthamiana*. The left panels are focused on nuclei and nucleoli, whereas panels right of labeling are images of associated cytoplasm. Scale bars are 5µm. **C.** Expression of these constructs in *N. benthamiana* containing RPP13Nd showing intact recognition patterns despite altered localization.



usually excluded from the nucleolus and present in both nucleus and cytoplasm. We show that the addition of this 33 residue insertion results in a dramatic change in localization of the Emco5 allele—the chimeric form of ATR13 Emco5 becomes highly enriched in the nucleolus (Figure 2-10B). To check if the deletion of this insertion in the Emoy2 allele abrogated nucleolar localization, we removed these 33 amino acids and determined that while it was still present to a lesser degree in the nucleolus, Emoy2 was now present

throughout the cell, both in cytoplasm and nucleus, similar to wildtype Emco5 localization. Despite the change in localization of these two alleles, RPP13-Nd

recognition remained unaltered; Emco5+NoLS is still recognized and triggers HR, whereas Emoy2-NoLS remains unrecognized (Figure 2-10C).

It is also worth noting that in addition to nuclear or nucleolar localization, the cytoplasm appears to undergo dramatic changes when any of the three alleles of ATR13 are expressed *in planta*. Relative to GFP, ATR13 appears to localize to distinct cytoplasmic strands, possibly microtubules, as well as to punctate bodies throughout the cytoplasm.

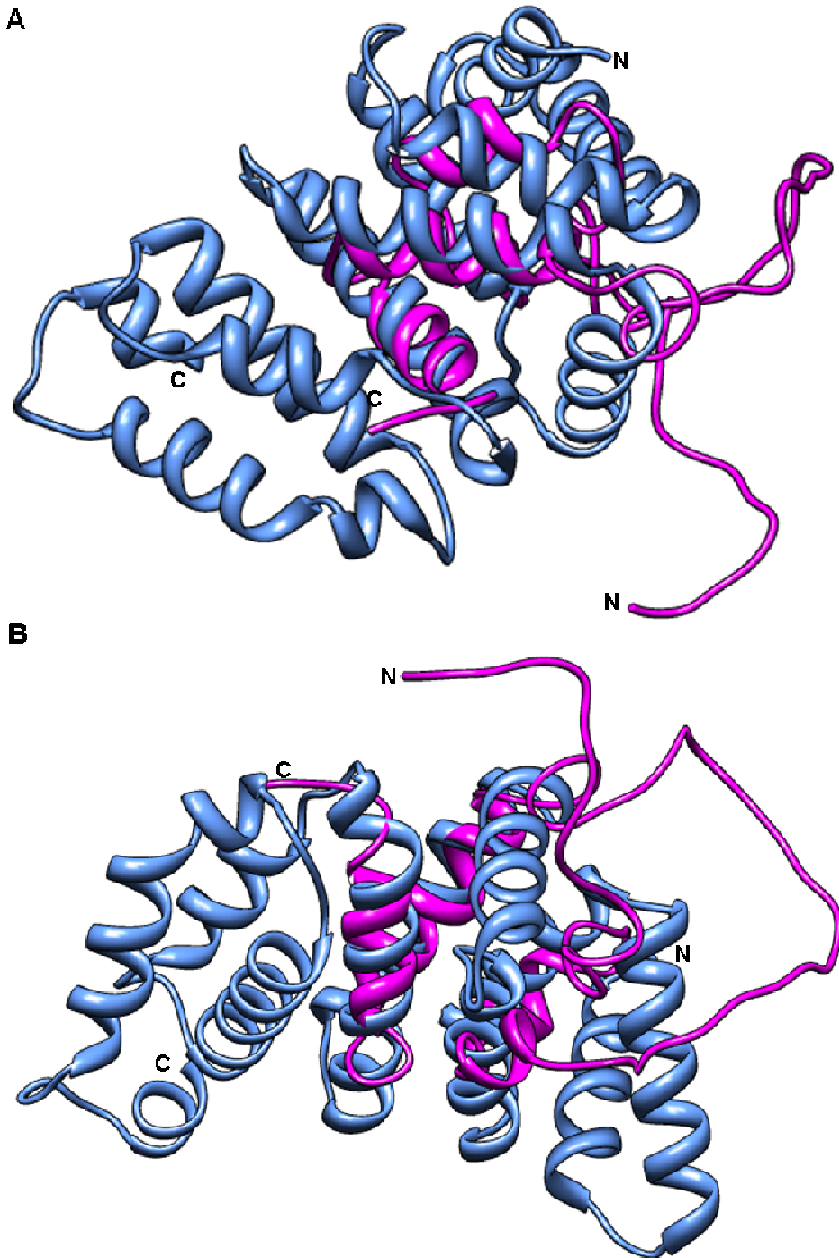


Figure 2-11. Structural overlay of ATR13 Emco5 with the first 200 amino acids of nuclear Ran-GTP subunit D. A-B. Two different views of the structural alignment of $\Delta 53$ ATR13 Emco5 with Ran-GTP subunit D (ATR13 shown in magenta and Ran-GTP shown in blue).

Discussion:

The structure of ATR13 from Emco5 was determined to moderate resolution using NOE, $^1J_{\text{HNHA}}$ coupling, hydrogen exchange, and residual dipolar coupling data. The presence of significant disordered regions, somewhat poor magnetization transfer, and in some cases peak overlap, hampered our efforts to obtain a structure of higher resolution. Nevertheless, the structure was of sufficient quality to permit comparison with other proteins in the protein data bank. The global fold of ATR13 from Emco5 weakly resembles that of several proteins including GTP-binding nuclear RAN (Figure 2-11A-B), Beta-1 subunit importin, and a serine/threonine phosphatase 2A, as well as several other proteins. While other labs have observed general virulence effects measured by bacterial proliferation in *Arabidopsis* due to ATR13 [42], in our hands we did not see enhanced bacterial growth on the susceptible ecotypes examined in this study or previously [27]. Perhaps this inconsistency is due to natural variation of ecotypes examined in our studies, or to the subtleties of bacterial strains, backbone vectors, or inoculation techniques. However, it is worth noting that eukaryotic obligate biotrophs have very different lifestyles than prokaryotic pathogens, and may therefore have different defense-suppression and nutritional requirements, making virulence difficult to assay in a surrogate system.

Regarding recognition by RPP13, it is interesting to note that despite the highly polymorphic nature of ATR13, only a small subset of these polymorphic residues appear to be involved in RPP13Nd-mediated recognition. While previous studies implicate E(114)147, T(119)152, and R(148)181 as being essential for full RPP13Nd recognition of the Wela3 and Maks9 alleles of ATR13 [40] here we show that ATR13 Emco5 recognition is mediated specifically by F/N73 and T/I(119)152 substitutions, as determined by both our LOR SDM and GOR mutagenesis screens. When mapped onto the structure of ATR13 Emco5, these two residues are in close proximity and are solvent exposed, suggesting a surface-exposed patch that is required for RPP13-Nd recognition. Several *Arabidopsis* accessions are known to contain R-genes other than RPP13 that function in ATR13 recognition [26]. These other R-genes, as well as other functional alleles of RPP13, may serve as a driving force behind the polymorphic patches created by other residues in ATR13. Additionally, it is noteworthy that many of the residue changes uncovered during the LOR random mutagenesis screen occurred in residues that are conserved in both recognized and unrecognized alleles of ATR13. There are distinct differences in timing and intensity of hypersensitive response, implicating these residues in proper folding or stability. However, several mutants appear to accumulate protein to the wildtype level, and at least one of these mutations, Y148N, also alters RPP13-Nd recognition of ATR13 Maks9. In several of the structure models this tyrosine is proximal to N73 or T152 (data not shown).

The disordered loop is one of the most interesting features of the ATR13 structure. This portion of ATR13 Emco5 flanks one of four 11 amino acid direct repeats found in other alleles of ATR13 [40]. These other alleles are shown to localize to the nucleolus when expressed *in planta*, whereas ATR13 Emco5 does not. When these three missing direct repeats are added to the ATR13 Emco5 allele, the chimera relocates to the plant nucleolus, suggesting that this region is involved in nucleolar localization. Nucleolar localization is difficult to predict, as little data is currently available

regarding how proteins are targeted to the nucleolus [61], however several hallmarks of nucleolar localization signals (NoLS) include surface exposed coiled coil domains containing an abundance of lysines or arginines [62]. In the 33 amino acid stretch that defines the nucleolar targeting sequence, lysines and arginines account for nearly one-third of residue content. Additionally, regions of disorder often require one or several ligands for stabilization [62]. This region of ATR13 could potentially bind rRNA, rDNA, or a protein involved in nucleolar trafficking. Thus far, this is the only described example of an oomycete protein localizing to the plant nucleolus. Moreover, it is functional in the host rather than in the originating pathogen, suggesting a signaling hierarchy; secretion and translocation across the host plasma membrane occurring prior to nucleolar targeting.

The nucleolus is best known for its role in ribosome biosynthesis, yet it is also essential for regulating the cell cycle and the cellular response to stress. In humans a mere 30% of known nucleolar proteins play a role in ribosome biosynthesis, whereas the remaining 70% play various roles in cell maintenance, apoptosis, DNA replication and repair, cell cycle control, and stress signaling [63]. In plants, the nucleolus has been shown to be a target of several pathogen classes, including a groundnut rosette virus that recruits RNA processing machinery to produce viral RNP (ribonucleoprotein) particles needed for systemic infection [64]. For the Picorna-like Potato virus A, the nucleolar localization of one of its proteins, NIa, is required for completion its infection cycle on *Nicotiana* [65]. *Globodera pallida*, a potato cyst nematode, has also been shown to target the nucleolus during various life stages presumably to suppress host defense [66]. With the varied roles the nucleolus plays in directing cellular activities, it seems an attractive target for an intercellular obligate biotroph requiring compromised host defense and a steady supply of nutrients.

In addition to its nuclear and nucleolar localization, ATR13 appears to localize to microtubules of the cytoplasmic scaffolding and to discrete punctate spots along these strands, possibly vesicles. As an obligate biotroph, nutrient acquisition is one of the key factors influencing survival and success of the invading pathogen. To that end, hijacking cellular transport machinery would be an effective strategy for funneling nutrients from plant host to obligate pathogen. The various localizations of ATR13 suggest it may possess multiple roles in pathogenesis, much like the EspF effector from *Escherichia coli* which has been shown to target the mitochondria, nucleolus, and cytoplasm of infected mammalian cells [67].

Summary and Future Directions:

In this study we solve the structure of ATR13, a structurally flexible and highly polymorphic effector protein from Hpa. We infer that its maintenance in Hpa, in spite of the drive to evade host recognition by RPP13, illustrates its importance in pathogen virulence—especially in the context of Hpa’s abbreviated effector repertoire [4]. Based on structural similarities, we show that ATR13 has similarity to RAN-GTP and other nuclear proteins involved in protein trafficking. Additionally, we identify two ATR13 residues essential for robust HR in the presence of RPP13Nd. We map these residues onto our structure and show that they localize to a single solvent-exposed patch which corresponds to an area under high diversifying selection. Lastly, we show that the highly flexible internal loop we identified base on our NMR data plays a role in nucleolar localization and can be added to a non-nucleolar protein to redirect that protein to the nucleolus.

While many obstacles exist in teasing out the precise virulence functions of ATR13, such as the inability to culture Hpa and the high levels of functional redundancy typically found in effectors [68], [69], much can be done to further characterize the role of ATR13 in pathogenesis. Exploring ATR13’s similarity to RAN-GTP is an exciting new area to focus our efforts. The fact that ATR13 has similarity to this protein and to various phosphatases begs the question: does ATR13 modify nuclear proteins or affect nuclear transport? Various assays can be done to answer these questions, and meanwhile looking for targets and interacting partners of ATR13 could help us understand the virulence mechanism of ATR13.

In light of our findings, examining the role of the nucleolus in pathogenesis is also an area that requires further exploration. Knowing that several alleles of ATR13 are localized to the nucleolus, a structure necessary for a variety of cellular processes including the cellular stress response, we might look more closely at its role during pathogenesis and determine if known stress responses are altered upon challenge with pathogen-delivered ATR13.

Lastly, we have shown two surface-exposed patches on the ATR13 structure that are highly polymorphic, yet only one of these regions appears relevant to RPP13Nd recognition. Hall et al. have shown that there is an additional R-gene present in several of the *A. thaliana* UK accessions [26]. It will be interesting to see if recognition conferred by these R-genes is affected when residues in either surface-exposed patch of ATR13 are mutated, or if the same LOR and GOR mutants identified in this study maintain their phenotype in the context of this other R-gene.

Table 2-1. NMR parameters, restraints, and statistics regarding the ATR13 structure.

<u>ATR13 Structural Restraints and Statistics A</u>			
NOE		448	
	Intra	i=j	155
	Sequential	i-j =1	142
	Medium	i-j < 5	80
	Long	i-j > 5	71
Dihedral			43
HN RDC			27
Hydrogen Bond B		28	
<u>Restraint RMSDs C</u>			
NOE (Å)			0.025 +/- 0.004
Phi Dihedral (deg)		0.2 +/- 0.2	
RDC (Hz), Qrdc		0.8 +/- 0.2, 7.4%	
Hydrogen Bond (Å)		0.029 +/- 0.006	
<u>Coordinate RMSDs D</u>			
Backbone			0.8 Å
Heavy atom			1.5 Å
Close contacts(per structure) E,F		0.2	
<u>Ramachandran analysis D,E</u>			
Most favored region (%)			83.2
Additionally allowed (%)			14.9
Generously allowed (%)			1.6
Disallowed (%)		0.3	
<u>Structure Quality Factors E,G</u>			
Verify3D			-5.14
ProsaII			-1.99
Procheck	(phi-psi)		-2.28
Procheck	(all)		-4.79
MolProbity			-1.36

- A) Parameters are for the 20 best of 200 structures.
- B) Two restraints per hydrogen bond for a total of 14 hydrogen bonds.
- C) For NOEs, on average, there was one NOE violation greater than 0.2 Å per structure, with the maximum violation equal to 0.5 Å. For phi dihedral restraints, on average, there were 0.4 violations greater than one degree, with the maximum violation of four degrees. For residual dipolar couplings, on average, there were 0.8 violations greater than 1.5 Hz, with the maximum violation equal to 3.4 Hz. For hydrogen bonds, on average, there were 0.4 violations greater than 0.1 Å, and all were less than 0.2 Å.
- D) Includes residues 76-88, and 120-150.
- E) Determined with the Protein Structure Validation Suite (PSVS) version 1.4.
- F) Close contacts are defined as within 1.6 Å for H atoms, 2.2 Å for heavy atoms.
- G) With respect to mean and standard deviation for a set of 252 X-ray structures < 500 residues, of resolution <= 1.80 Å, R-factor <= 0.25 and R-free <= 0.28; a positive value indicates a 'better' score
alpha helices: 123-135, 141-147, 149-152

Table 2-2. Proteins with structural homology to ATR13 Emco5 identified by the DALI server.

Z	rmsd	lali	nres	%idPDB	Description
2.6	4.2	71	584	7 PDB	MOLECULE: ADAPTOR-RELATED PROTEIN COMPLEX 2 ALPHA 2
2.6	4.8	77	854	9 PDB	MOLECULE: GTP-BINDING NUCLEAR PROTEIN RAN;
2.5	4.7	77	861	10PDB	MOLECULE: IMPORTIN SUBUNIT BETA-1;
2.3	5	75	871	3 PDB	MOLECULE: PROTEIN (IMPORTIN BETA SUBUNIT);
2.2	9.3	75	241	9 PDB	MOLECULE: LP04448P;
2.2	5.1	66	319	11PDB	MOLECULE: PROTEIN (CLATHRIN HEAVY CHAIN);
2.2	4.5	77	849	9 PDB	MOLECULE: GTP-BINDING NUCLEAR PROTEIN RAN;
2.2	4.7	78	857	9 PDB	MOLECULE: GTP-BINDING NUCLEAR PROTEIN RAN;
2.2	8.5	63	582	8 PDB	MOLECULE: SERINE/THREONINE-PROTEIN PHOSPHATASE 2A 65 KDA RE
2.1	4.6	72	845	3 PDB	MOLECULE: IMPORTIN BETA-1 SUBUNIT;
2.1	5.2	65	464	12PDB	MOLECULE: SMG-7 TRANSCRIPT VARIANT 2;
2.1	3.3	64	211	6 PDB	MOLECULE: EIF4G-LIKE PROTEIN;
2.1	8.8	64	228	6 PDB	MOLECULE: PP2A A SUBUNIT;
2.1	4.9	74	871	3 PDB	MOLECULE: IMPORTIN BETA-1 SUBUNIT;
2.1	4.8	78	859	9 PDB	MOLECULE: GTP-BINDING NUCLEAR PROTEIN RAN;
2.1	4.6	78	860	9 PDB	MOLECULE: IMPORTIN BETA-1 SUBUNIT;
2.1	8.6	63	581	6 PDB	MOLECULE: PROTEIN PHOSPHATASE 2, REGULATORY SUBUNIT A (PR 6
2.1	3.3	65	210	6 PDB	MOLECULE: EIF4G-LIKE PROTEIN;
2.1	3.6	61	588	8 PDB	MOLECULE: PROTEIN (PROTEIN PHOSPHATASE PP2A);
2.1	8.6	68	583	7 PDB	MOLECULE: SERINE/THREONINE-PROTEIN PHOSPHATASE 2A 65 KDA RE
2	7.3	70	550	4 PDB	MOLECULE: PHOSPHOTIDYLINOSITOL 3 KINASE 59F;
2	3.7	66	610	6 PDB	MOLECULE: LEUKOTRIENE A-4 HYDROLASE;
2	4.5	65	145	8 PDB	MOLECULE: ADP-RIBOSYLATION FACTOR BINDING PROTEIN GGA1;
2	4.9	75	876	3 PDB	MOLECULE: PROTEIN (IMPORTIN BETA SUBUNIT);
2	5.3	76	873	3 PDB	MOLECULE: IMPORTIN BETA-1 SUBUNIT;
2	5.3	66	458	12PDB	MOLECULE: SMG-7 TRANSCRIPT VARIANT 2;
2	8.3	64	575	9 PDB	MOLECULE: SERINE/THREONINE-PROTEIN PHOSPHATASE 2A 65 KDA

Table 2-3. Various amino acid changes in ATR13 Emco5 that disrupt RPP13 recognition. Wildtype residue identities are listed in bold next to their amino acid position. LOR mutants generated by PCR random mutagenesis are listed in red, orange, and blue, corresponding to whether those changes occurred as single, double, or triple mutations. Retention of recognition (ROR) mutants are listed in black next to the loss of function mutants and possess intact RPP13Nd recognition, illustrating that amino acid position's tolerance for change.

	LOR		ROR		LOR		ROR		LOR		ROR	
S	54	-	G	H	88	L	-	G	122	M	C	
F	55	L	-	E	89	G	G	P	123	L	-	single aa change
G	56	-	-	K	90	-	-	D	124	G,V	-	double aa change
L	57	P	P	I	91	N,S	F	I	125	-	-	triple+ aa change
G	58	T	-	I	92	T	-	E	126	-	G	
K	59	R	-	E	93	-	-	R	127	-	H	
A	60	-	-	A	94	E,V	-	I	128	T,N,F	-	
Q	61	-	-	H	95	P,L	L	V	129	D,A	-	
D	62	-	G	D	96	-	-	S	130	P,T	-	
P	63	-	L,T	L	97	P	H	T	131	P	-	
L	64	P	-	H	98	L	L	L	132	P,H	-	
D	65	V,N	V,G	V	99	-	I	E	133	-	V	
K	66	E	Q,R	S	100	P	-	R	134	-	A	
F	67	S	S,I	K	101	E,A	N	H	135	P	L	
F	68	-	S	S	102	P	P,T	D	136	-	G	
S	69	L	-	K	103	M,T	-	E	137	G,K	G	
K	70	-	M	N	104	D	S	V	138	-	A,L	
I	71	M	M,K,V	A	105	-	-	G	139	-	R,V	
I	72	-	-	P	106	-	-	A	140	-	T	
F	73	S	S	I	107	-	V	K	141	E,A,N	E	
S	74	-	-	Q	108	-	R	D	142	-	-	
G	75	-	-	Y	109	S	-	L	143	-	-	
K	76	R	R,M	A	110	-	-	G	144	-	-	
P	77	-	-	S	111	C,I	-	A	145	-	-	
I	78	N	V	V	112	E	E	K	146	E	E,R	
E	79	K	V,G	M	113	-	L	L	147	R	-	
T	80	G	A	E	114	-	V	R	148	-	-	
S	81	G	G	Y	115	C,N,H	-	D	149	G	E	
Y	82	-	F	L	116	P,Q	P	A	150	-	-	
S	83	P	-	K	117	-	E	L	151	P	P	
A	84	T	T	K	118	-	-	D	152	-	V,A	
K	85	N,E	I	T	119	P	-	R	153	-	L	
G	86	-	-	Y	120	-	H	Q	154	L	-	
I	87	F,S,T	N	P	121	-	L					

Chapter 3. ATR13 interactors and Co-immunoprecipitation experiments

Introduction:

After the discovery of ATR13 [23] and sequencing of the Hpa draft genome [4], molecular signatures associated with oomycete effectors were identified and used to train prediction programs to identify new potential effectors ([70], [34], [71]). Once identified, these predicted effectors must be characterized and verified by determining function, discovering effector targets, or identifying R-proteins that can recognize them. To this end, many laboratories have performed extensive surveys to identify virulence effects of predicted effectors [72], [71], tried various yeast two-hybrid and biochemical methods to isolate interactors [73], [74], or screened poorly characterized ecotypes for novel recognition specificities (personal communications). While the previous section addressed the virulence component of ATR13, here we discuss various methods used to identify proteins that interact with ATR13.

Identifying effector targets is a difficult task; several effectors need host modification for functionality [75], many are weakly expressed, and in the case of obligate biotrophs, isogenic delivery from the natural pathosystem and genetic transformation is (to date) impossible due to the genetic intractability of the pathogen. Yet, many groups have had success identifying interacting proteins by yeast two-hybrid screens. In 2009, Bos et al. identified several proteins that interacted with Avr3a, an effector from *Phytophthora infestans* involved in suppressing cell death in potato. One of these interacting proteins was the host E3 ligase CMPG1 which was shown to be stabilized in the presence of Avr3a^{K1}, thereby eliminating INF-triggered cell death [76]. Employing yeast two-hybrid screens, Domingues et al. have also identified functional classes of sweet orange proteins that interact with the bacterium *Xanthomonas citri* effector PthA family, implicating protein folding and nuclear targeting machinery as clear targets of pathogen effectors [77]. However, despite these promising examples, there are limitations to this technique including false positives due to mis-localized proteins, incomplete host expression libraries, or lack of interaction because of solubility requirements. In our hands, we were unable to verify any of the interactions we identified from our yeast two-hybrid screen (data not shown), and hence focused our attention on a biochemical approach.

Biochemical methods have been successfully used to identify and verify effector targets and members of protein complexes [78], [79], [80], [81]. Additionally, biochemical methods have also been used to identify modifications to host proteins involved in defense signaling [82], [83]. Such powerful and universally applicable tools have not gone unnoticed. In 2003, Shao from the Innes group showed that the plant protein PBS1 was the direct substrate of *P. syringae* effector AvrPphB and that the two interacted *in planta* as demonstrated by co-immunoprecipitation experiments [14]. In regards to identifying proteins found in a complex, immunoprecipitation experiments using epitope-tagged protein fusions or gene-specific polyclonal antibodies have opened up endless possibilities for isolation strategies to identify interacting proteins. RIN4, an *Arabidopsis* protein essential in the negative regulation of defense signaling, is a target of multiple *Pseudomonas* TTSS effectors [84], [85]. Its discovery as a common target for these unrelated effectors underscores its importance in plant immunity. To

further explore the role of RIN4 in defense signaling, Liu et al (2009) [86] pulled down proteins involved in resistance complexes associated with RIN4 using an affinity-purified RIN4 antibody, identifying a plasma membrane H⁺ ATPase involved in regulating stomatal aperture.

In addition to identifying targets of effectors, interactions of effector and cognate R-gene pairs can be explored using biochemistry. Several examples of effectors and their R-genes have been shown to interact directly [87], [88], [89], [90]. Biochemical strategies have been instrumental in showing the direct interaction between several of these effectors and the cognate R-genes that recognize them. Direct association between the tobacco mosaic virus helicase domain, p50, and the NBS-LRR region of the N factor from *Nicotiana tabacum* has been shown by co-IP *in planta* [90]. Another example of biochemical characterization of an effector interacting with its R-protein is the case of RPP1^{Wsb} and ATR1. Krasileva et al. showed a correlation between recognition specificity and interaction between R-gene and effector. Additionally, using co-immunoprecipitation experiments, the minimal domain necessary for interaction with ATR1 was identified as the LRR domain of RPP1 [91].

Here we develop tools necessary to implement these techniques with ATR13, an effector from the oomycete *Hyaloperonospora arabidopsidis* that is recognized by the *Arabidopsis* resistance gene RPP13. Additionally, we set out to characterize the interaction between ATR13 and its cognate R-gene, RPP13. Several examples of direct interaction between host resistance gene and corresponding pathogen effector have been described above, and the highly polymorphic C-terminus of both ATR13 and RPP13 is suggestive of a balancing selection driven by a direct physical interaction. Derived from an obligate biotroph, ATR13 can only be delivered as a single effector by a surrogate system, in our case *Pseudomonas syringae* or *P. fluorescens*. ATR13 can also be expressed *in planta* through transient assays with *Agrobacterium tumefaciens* or by the creation of stable transgenic *A. thaliana* plants. With the aim of identifying targets of ATR13 virulence, as well as characterizing the dynamics of ATR13/RPP13 recognition, this study employs all of these methods, as well as the use of exogenously expressed ATR13 protein associated with, or covalently attached to, resin and fashioned into affinity columns. Using the aforementioned approaches, we identify two potential interactors of ATR13: PRP39-1 and RCC1, and show interaction between the ATR13 and RPP13 proteins. Identifying ATR13 interactors and determining the nature of the interaction between ATR13 and RPP13 will provide a basis for elucidating the molecular events that control plant innate immunity and may lead to the design of novel methods for engineering durable resistance to this destructive class of pathogen.

Materials and Methods:

3.1 GST-ATR13 glutathione column with plant extract

ATR13 Emco5 without its signal peptide ($\Delta 19$) was cloned into pGEX and expressed in fusion with an N-terminal Glutathione-S-Transferase (GST) tag in ER2566 *E. coli*. 500ml cultures of OD 0.5 were induced with 500uM IPTG for 6 hours at 28C and spun down at 3,000rpm to collect cells. Cells were resuspended in buffer A (20mM Tris-HCl pH8.0, 0.5mM NaCl, 30mM Imidazole, 5% glycerol, 2mM β -mercaptoethanol) and lysed for 30 minutes on ice with 10ug/ml lysozyme followed by sonication (3x 30 seconds, 30% duty cycle and output). Cell debris was pelleted at 20,000rpm for 20 minutes and supernatant was filtered through a Millipore vacuum filtering unit (.45um pore). 50ul of pre-washed glutathione-sepharose slurry was added to the bacterial lysate and incubated end over end at 4C overnight. The following morning, resins were collected by 5 minutes of centrifugation at 3,000rpm and washed three times in buffer A. These resins were then incubated with lysates from various *Arabidopsis* lines to pull down targets of ATR13.

Plant lysates were prepared by grinding 1g of 3 week old *Arabidopsis* seedlings in liquid nitrogen and then suspending the powdered plant material in buffer A. The *Arabidopsis* lines assayed in this experiment included the Columbia-5 ecotype as well as the Columbia-5 ecotype containing an RPP13-Nd transgene obtained from Dr. Jim Beynon's lab. Plant debris was pelleted by centrifugation at 20,000 rpm for 15 minutes, after which the supernatant, or lysate, was collected. After 2 hours of end-over-end incubation with resin at 4C, the lysate-resin mixtures were packed into columns and washed 3 times with 5x column volumes of extraction buffer. Interacting proteins were eluted from each column in fractions by the addition of elution buffer containing reduced glutathione. Fractions were analyzed by SDS-PAGE, followed by silver stain, and colloidal coomassie stain. Bands that appeared unique to ATR13-containing samples relative to the GST control sample were excised and prepared for analysis by mass spectrometry.

3.2 CNBr-Sepharose ATR13 with plant extract

Purified ATR13 protein was covalently bound to activated CNBr-sepharose. In hopes of showing interaction between ATR13 and RPP13 as well as identifying targets of ATR13 action, ATR13 Emco5 was cloned into the pET-DUET1 vector and expressed as described in the previous section in fusion with an N-terminal His tag. Pelleted bacterial cells were resuspended in buffer B (50mM Tris-HCl pH7.5, 150mM NaCl, 0.1% Triton-X, 0.2% NP-40, 6mM β -mercaptoethanol, and 1 tablet complete protease inhibitor cocktail (Roche)) and cells were lysed by 30 minute incubation on ice with 10ug/ul lysozyme and 3x 30 seconds sonication at 30% duty cycle and output. Cell debris was pelleted by 15 minutes of centrifugation at 20,000rpm. Supernatant was filtered using a Millipore unit (0.45um pore) and loaded onto a 5ml nickel column (GE healthcare) with an FPLC pump. Bound protein was washed on the column with 20 column volumes of buffer B and eluted in 2ml fractions using an imidazole gradient. Purified protein was dialyzed into coupling buffer (0.1M NaHCO₃, 0.5M NaCl, pH8.3) for conjugation to CNBr activated sepharose (manufacturer's protocol). RIN4 resin was also prepared using the

above protocol with the exception of the use of expression vector (pRSET in lieu of pET-DUET1) as a control for the following experiment. Separate columns were constructed using ATR13 Emco5 resin and RIN4 resin for a total of four 1ml columns, two for ATR13 and two for RIN4. Arabidopsis lysate prepared as described above was run over these columns twice from either the Columbia ecotype containing an RPP13-Nd::HA transgene or a Columbia mutant with compromised rps2 signaling complemented with an RPS2::HA transgene. Resin was washed with 20 column volumes of plant extraction buffer and bound proteins were eluted using pH disruption.

Samples were run on SDS-PAGE gels and blotted onto nitrocellulose. Membranes were probed with HA-HRP antibody in hopes of detecting RPS2::HA in RIN4 samples and RPP13Nd::HA in ATR13 Emco5 samples and not vice versa. Unfortunately the controls (RIN4 and RPS2 association) did not work, and no unique bands were identified in the ATR13 column samples as determined by SDS-PAGE stained with colloidal coomassie.

3.3 Generation of transgenic Arabidopsis lines

ATR13 Emco5 and Emoy2 alleles both with and without signal peptide were PCR amplified with Sal1 and Nde1 restriction sites included in the primer pairs. The PCR products were digested with appropriate restriction enzymes and ligated into the dex-inducible pTA vector. These constructs were then transformed into electro-competent *Agrobacterium tumefaciens* strain GV3101. The following flowering Arabidopsis ecotypes were dipped into a bacterial suspension of OD1 in a 10mM MgCl₂, 5% sucrose, 0.025% silwet solution: Col5, Col5 containing an RPP13Nd transgene, and an *eds1/ndr1* double mutant containing an RPP13Nd transgene. Several weeks later, seeds were collected from individual lines, sterilized with 50% bleach, and plated on MS with hygromycin (100ug/ml) selection. Individuals that grew successfully were transplanted to soil and allowed to produce seed. This seed (T2) was then collected and germination ratios were measured for each plant. Individuals with a 75% germination frequency, suggesting a single gene insertion, were transplanted onto soil and allowed to produce seed. This seed (T3) was plated on MS hygromycin and produced the T3 generation. Lines that gave rise to 100% germination efficiency suggested they arose from homozygous individuals and were propagated for further studies. CFP was cloned into pTA in a manner comparable to that described above.

Emco5 and Emoy2 ATR13 alleles with and without signal peptide were cloned into a version of the pTA vector with an N-terminal CFP tag in a fashion similar to that described in the above paragraph. *Arabidopsis* ecotypes selected for transformation included Col5 and Col5:RPP13Nd. Identification of homozygous, single-insertion lines was performed as described above. ATR13 expression was induced with dexamethasone and protein expression levels were determined for all constructs listed above.

Lastly, Col5 *Arabidopsis* lines containing native promoter driven RPP13Nd tagged with HA were generated. The Arabidopsis line originally obtained from Dr. Jim Beynon's laboratory had a 5.4kb BAC clone insertion containing RPP13Nd without tag and with additional genomic information from the Niederzanz ecotype [23]. RPP13Nd native promoter with coding region and RPP13Nd 3'UTR were PCR amplified from isolated Niederzanz genomic DNA using various primer pairs. While the 3' UTR was

relatively simple to clone into the pENTR vector, the native promoter and coding region fragment proved more difficult, possibly due to a certain level of toxicity to the bacteria. The promoter with coding region and additional HA tag added by PCR was cloned into pBLUNT in the reverse orientation and the 3'UTR was added to this construct using Xho1 and Nde1 restriction sites. The intact promoter, coding region, and 3'UTR fragment was removed from pBLUNT using a partial digest with BamH1 and Xho1 and ligated into the p4541 binary vector. This construct was then transformed into *Agrobacterium* strain GV3101 and flowering Col5 Arabidopsis plants were transformed as described above. Transgenic propagation was performed as already described with the exception that kanamycin (100ug/ml) was used as selection instead of hygromycin. RPP13Nd::HA transgenic lines were tested for recognition capabilities by growth curves with *Pseudomonas syringae* DC3000 delivering ATR13 or empty vector.

3.4 Co-immunoprecipitations from Arabidopsis plants expressing ATR13

Col5 transgenic plants containing dex inducible ATR13 Emco5 or CFP transgenes were sprayed with a 30uM dexamethasone, 0.05% silwet solution and allowed to express protein for 24 hours. 5g of tissue was collected from each plant lineage and prepared by grinding tissue in liquid nitrogen and adding 2:1 v/w extraction buffer (50mM Tris-HCl pH7.5, 15mM EGTA, 100mM NaCl, 0.1% Triton-X, protease inhibitors). Plant debris was pelleted and supernatant was incubated end over end with affinity purified ATR13 or ATR1 antibodies DMP cross-linked to protein G beads. After 2 hours at 4C, beads were spun down at 3,000rpm and washed 3 times in 1ml extraction buffer. Bound proteins were eluted using 1M glycine pH 3.0, and then mixed with 3x Laemmli buffer and run on SDS-PAGE gels for silver staining or western blots. This experiment was repeated several times with an additional 30 minute DSP or DTSP crosslinking step and 30 minute Tris quenching step prior to tissue collection.

For transgenic lines containing dexCFP and dexATR13Emco5+CFP, tissue was prepared by the method described above and plant lysates were incubated with anti GFP-dynabeads for 2 hours at 4C. Beads were collected using a magnetic platform and three 1ml washes were performed at room temperature. Samples were resuspended in 25ul 3x laemmli buffer and boiled for 5 minutes. These samples were then loaded onto an SDS-PAGE gel and stained with colloidal coomassie to visualize proteins uniquely associated with ATR13 expressed *in planta* compared to proteins present in CFP samples. Additionally, above experiments were also conducted using *Arabidopsis* plants containing the ATR13-CFP fusion with CFP as a negative control. These plant extracts were incubated with polyclonal CFP for both sample sets, and treated as just described.

3.5 ATR13 non-protein targets

Because we could not find association with other proteins, we focused our attention on strategies that might reveal small molecules as potential interactors of ATR13. Arabidopsis plants containing dex-inducible CFP or ATR13Emco5+CFP were sprayed with dexamethasone and induced for 24 hours. 0.5 grams of tissue were collected, powdered in liquid nitrogen, and transferred to a 12 ml glass tube. Three milliliters of 90% methanol was added to the samples and vortexed on low speed. Samples were incubated in a water bath sonicator for 20 minutes and centrifuged at 5000rpm, 4C to pellet debris. Supernatant was collected and 2 milliliters of 90%

methanol was added to the pellet for a second extraction, repeating above steps. Supernatants were pooled and evaporated over night under a vacuum of 5 torr. Samples were resuspended in 20% HPLC grade methanol, vortexed, sonicated for 5 minutes, and filtered through a 0.20um syringe filter prior to loading on the reverse phase column.

3.6 Co-immunoprecipitations in *Nicotiana benthamiana*

ATR13 alleles Emco5, Emoy2, and Maks9 were cloned into pEarleygate 103 and transformed into *Agrobacterium tumefaciens* GV3101. Strains were inoculated at OD 0.5 onto *Nicotiana benthamiana* leaves either with or without GV3101 delivering pMD-RPP13Nd::HA at OD 0.3. ATR1 and RPP1 constructs were used as controls for co-immunoprecipitation experiments. When leaves that had been co-inoculated with incompatible R-gene/effector pairs began to show the first signs of hypersensitive response, usually between 18-24 hours, 1-2g of tissue was collected and processed in liquid nitrogen, followed by extraction buffer (50mM Tris-HCl pH7.5, 150mM NaCl, 0.1% Triton-X, 0.2% NP-40, 6mM β -mercaptoethanol, 0.3uM Apronin, 10uM Leupeptin, 1uM Pepstatin A). Plant debris was spun down at 20,000 rpm for 20 minutes, and supernatant was collected. Polyclonal GFP antibodies were added to each sample and incubated at 4C for 2 hours, after which 50ul pre-washed protein G beads were added to the samples and incubated for an additional 2 hours at 4C. Samples were spun at 3,000 rpm, 4C to pellet beads and washed 3 times in 1ml extraction buffer. Beads were boiled in 25ul 3x laemmli buffer and samples were loaded onto SDS-PAGE gels for either coomassie stain or Western blotting. Blots were probed with α -HA-HRP.

3.7 Pulldowns in *N. benthamiana* with Flag and COIPs

ATR13 alleles were PCR amplified in frame with a GFP tag and inserted into pENTR-D with the TOPO reaction. These GFP-tagged ATR13 genes were then inserted into pEarleygate 202 using the LR reaction to be expressed in fusion with an N-terminal flag tag. Electrocompetent *Agrobacterium tumefaciens* GV3101 were transformed and inoculated onto *Nicotiana benthamiana* at an OD of 0.5 and allowed to express for 24 hours, or between 18-24 hours depending on the appearance of first HR symptoms in the case of co-inoculations with pMD-RPP13Nd::HA or pMD-RPP13Col::HA. One gram of tissue was collected from each inoculation, or combination thereof, and ground in liquid nitrogen. Plant proteins were extracted in 1:2 (w/v) of WEB buffer (50mM Tris-HCl pH7.5, 150mM NaCl, 0.1% Triton-X, 0.2% NP-40, 6mM β -mercaptoethanol, 0.3uM Apronin, 10uM Leupeptin, 1uM Pepstatin A), centrifuged at 20,000 rpm to pellet debris, and incubated with 10ul of pre-washed \square -flag conjugated resin (Sigma) for 2 hours, end over end, at 4C. Resin was collected by centrifugation, 3,000 rpm for 5 minutes, and washed 4x 1 ml WEB buffer with additional protease inhibitors (Roche complete cocktail). Bound proteins were eluted twice with 20ul of flag elution buffer (50mM Tris-HCl pH7.5, flag peptide (500ug/ml), 5% glycerol) at room temperature for 10 minutes with agitation from a rotary platform at setting level 4. Elutions were pooled, 20ul of 3x Laemmli buffer were added, and samples were loaded on SDS-PAGE gels for either Western blotting, silver staining, or colloidal coomassie stain. Experiments were repeated three times.

3.8 Preparing samples for Mass Spectrometry

Protein bands unique to ATR13 samples were cut from coomassie or silver stained gels and processed for mass spectrometry analysis. Gel slices were cut into 1mm³ pieces and immersed in a solution of 25mM ammonium bicarbonate in 1:1 acetonitrile/water and vortexed for 10 minutes. Supernatant was removed and these steps were repeated three times. Gel pieces were vacuum-centrifuged to complete dryness and rehydrated in a 12.5ng/ul trypsin solution and incubated at 37C overnight. Peptides were recovered with an initial water extraction, followed by three rounds of 45% water/50% acetonitrile/5% formic acid extractions involving 10 minute vortex and 5 minute sonication steps. Extractions were pooled and reduced in volume to approximately 10ul before submitting to the mass spectrometry facility.

Results and Discussion:

Despite the information we have gleaned from the structure of ATR13, we still have limited insight into what role it plays during pathogenesis. To understand the function of a protein, it is helpful to identify interactors of that protein, and to this end, we have performed various experiments in order to determine potential targets of ATR13. After optimizing ATR13 expression conditions, we generated large amounts (30mg/ml) of GST-ATR13Emco5 fusion protein in order to use its binding capacity to glutathione-sepharose to create an affinity column. Leaf extracts from *Arabidopsis* ecotype Col5 and Col5:RPP13Nd were run over this column, as well as a GST control column, and after washing, GST-ATR13Emco5 and GST were eluted off the column with the addition of reduced glutathione. Relative to GST controls, GST-ATR13Emco5 samples looked promising, containing several protein bands that appeared specific to ATR13 (Figure 3-1). However, when these samples were analyzed by tandem MS/MS, the higher molecular weight bands were found to contain GST, while lower molecular

A

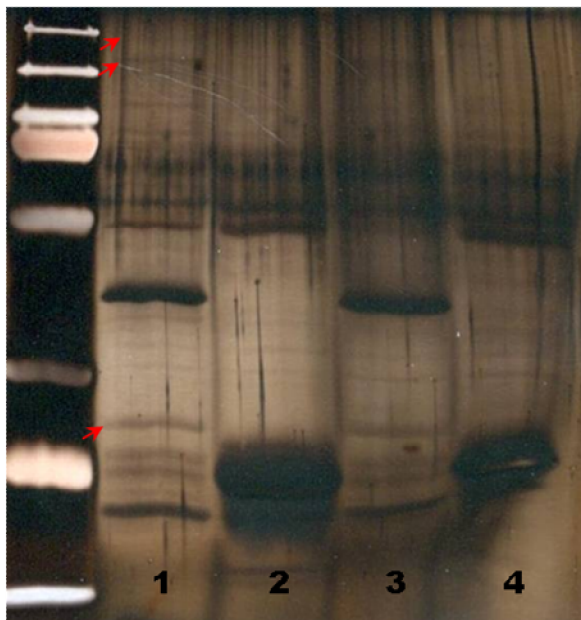
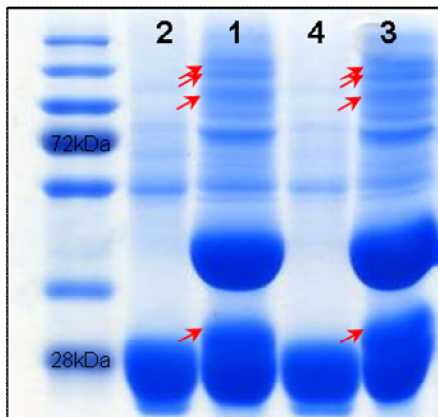


Figure 3-1. Pulldowns with GST-ATR13Emco5 and plant lysates from *Arabidopsis thaliana* ecotypes Col5 and Col5:RPP13Nd.

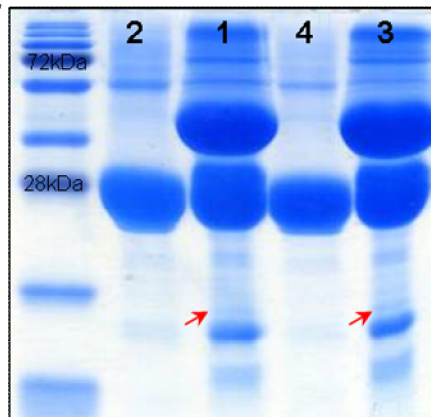
A. Silver stain of 10% SDS-PAGE gel showing unique bands associated with GST-ATR13 samples relative to GST controls. **B-C.** Scale up of pulldowns run on 10% and 15% SDS-PAGE gels stained with colloidal coomassie showing unique bands associated with GST-ATR13Emco5 samples. Unique bands are highlighted with red arrows.

1. GST-ATR13+Col5
2. GST +Col5
3. GST-ATR13+Col5:RPP13Nd
4. GST +Col5:RPP13Nd

B



C



weight bands were either bacterial proteins from the expression host, or ATR13 degradation products.

Because the abundance of GST seemed to mask possible protein targets of ATR13, purified His6-ATR13Emco5 protein was conjugated to activated CNBr-sepharose with the dual goals of identifying targets of ATR13 and to show interaction between ATR13 and RPP13. For the latter goal to be addressed, transgenic *Arabidopsis thaliana* plants containing an HA-tagged RPP13Nd transgene were made. The ability of these plants to trigger defense responses in the presence of ATR13Emco5 was verified by growth curves of *Pseudomonas syringae* DC3000, where growth of strains delivering ATR13Emco5 was restricted on plants containing functional RPP13Nd:HA (Figure 3-2). The transgenic line that appeared to possess the most clear restriction of bacterial growth while retaining a wildtype phenotype was the Col5-

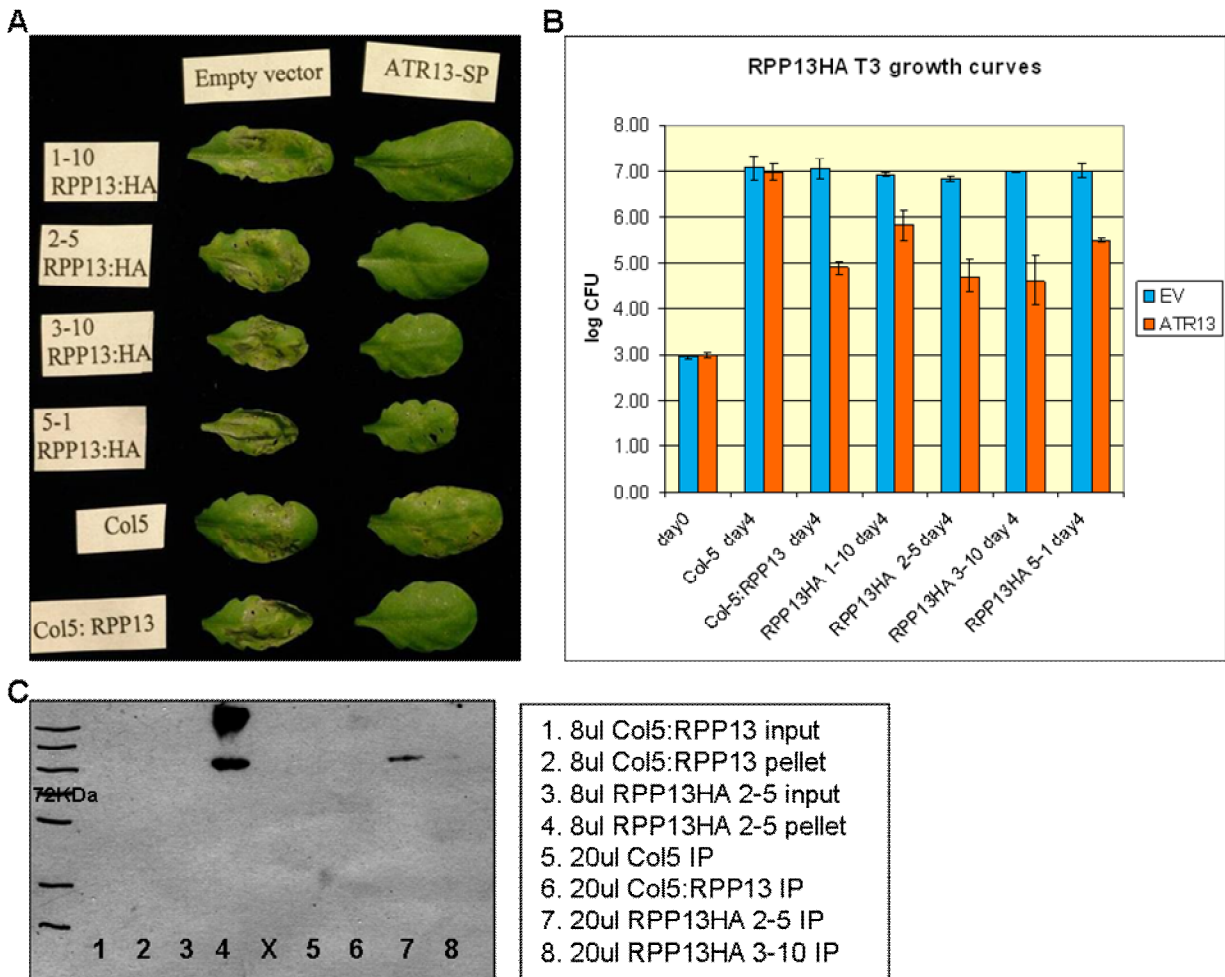


Figure 3-2. Stable transgenic Col5 plants containing an HA-tagged version of RPP13Nd.
A. Leaves from various transgenic lines pictured three days after inoculation with 10^4 CFU/ml of DC3000 delivering ATR13 Emco5 or empty vector. **B.** Growth curves of transgenic Col5:RPP13Nd:HA. **C.** Western blot of stable transgenics after IP with α -HA beads (Roche) using α -HA-HRP antibody.

RPP13Nd:HA 2-5 line (Figure 3-2B), henceforth referred to as RPP13Nd:HA. Additionally, protein from this line was detected after IP from 0.2 grams of tissue, confirming that not only is the protein functional, but it is made in amounts detectable on a Western (Figure 3-2C). With this stable transgenic line of RPP13Nd:HA and another line with RPS2:HA, we performed pull-downs using the His6-ATR13Emco sepharose and RIN4 sepharose (Figure 3-3). Included as both a positive and negative control, RIN4 is known to associate with RPS2 in vivo and presumably not RPP13 [92]. When incubated with plant lysate from either RPS2:HA or RPP13Nd:HA, RIN4 sepharose did not appear to interact with either tagged protein (Figure 3-3A). ATR13 sepharose also did not associate with its intended RPP13Nd:HA target, however this is not surprising considering the positive control also failed. Regardless of this outcome, we looked at other proteins that did associate with either ATR13 or RIN4 resin using silver stain (Figure 3-3B). While both resins appear to pull down a large number of proteins within

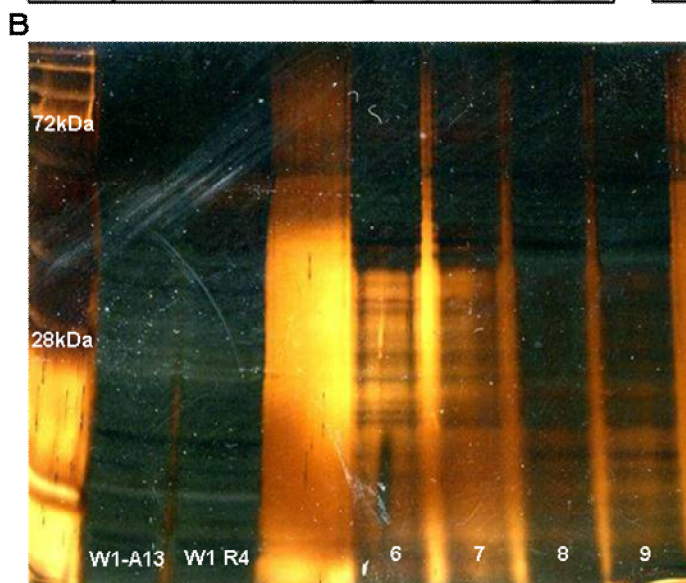
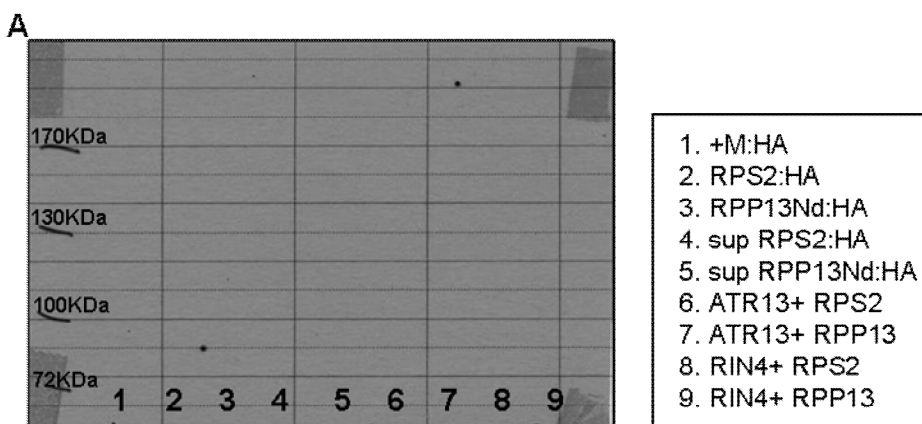


Figure 3-3. ATR13 and RIN4 CNBr-activated sepharose pull-downs of Col5:RPP13Nd-HA and Col0:RPS2-HA. **A.** Western blot of reciprocal pull-downs of RPP13HA and RPS2HA from *Arabidopsis* plant lysate using ATR13 Emco5 sepharose and RIN4 sepharose. Blot is probed with α -HA-HRP and exposed overnight. **B.** Silver stain of proteins associated with ATR13 sepharose and RIN4 sepharose. First two lanes are low salt washes of ATR13 and RIN4 resins, followed by an empty lane, then samples described in figure legend.

detection limits, none of these proteins appear specific to ATR13. This could be due to protein orientation, which would also explain why RIN4 and RPS2 did not appear to associate. When binding proteins to activated CNBr sepharose, primary amines from the protein backbone are covalently linked to the surface of the sepharose in a variety of random orientations, limiting the availability of interaction surfaces. With these non-

exposed surfaces hidden from protein targets, there are potentially not enough protein molecules in a favorable orientation to pull down detectable amounts of interacting proteins.

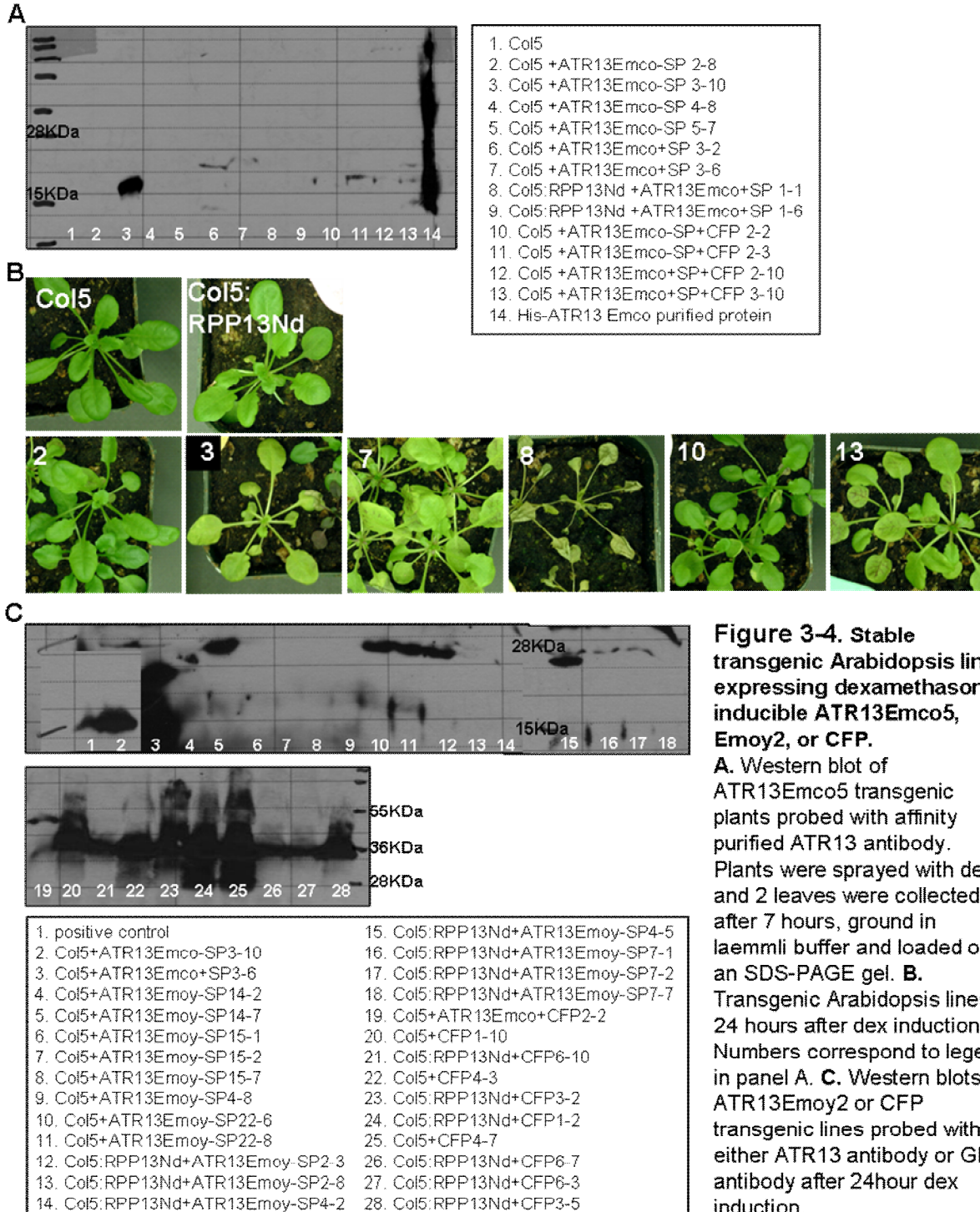


Figure 3-4. Stable transgenic Arabidopsis lines expressing dexamethasone inducible ATR13Emco5, Emoy2, or CFP.

A. Western blot of ATR13Emco5 transgenic plants probed with affinity purified ATR13 antibody. Plants were sprayed with dex and 2 leaves were collected after 7 hours, ground in laemmli buffer and loaded onto an SDS-PAGE gel. **B.** Transgenic Arabidopsis lines 24 hours after dex induction. Numbers correspond to legend in panel A. **C.** Western blots of ATR13Emoy2 or CFP transgenic lines probed with either ATR13 antibody or GFP antibody after 24hour dex induction.

To address this pitfall of using resin-bound protein as a probe, we generated transgenic *Arabidopsis* lines expressing ATR13 driven by a dexamethasone-inducible promoter that could be used in pulldowns with affinity purified ATR13 antibodies [93].

Arabidopsis Col5 and Col5:RPP13Nd lines were transformed with dex-inducible ATR13 alleles Emco5 and Emoy2 as well as a CFP control and an ATR13Emco5+CFP fusion (Table 3-1). Plant lines were tested for protein expression (Figure 3-4A, C) and whole plant phenotypes after dex induction (Figure 3-4B). Plants containing both RPP13Nd and ATR13Emco5 collapsed between 4-8 hours after spraying with dex. Col5 plants containing only ATR13 became chlorotic and displayed anthocyanin production along venation patterns of leaves. Also, when germinated on medium containing even 1/1000th the typical working concentration of dexamethazone, seeds containing functional dex machinery failed to germinate or aborted growth soon after germination (Figure 3-5).

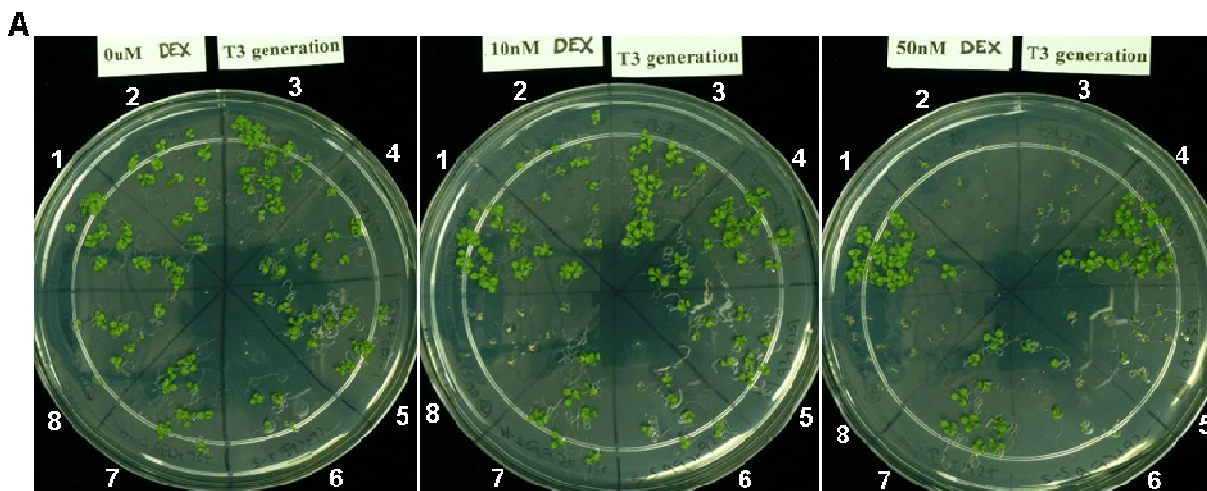


Figure 3-5. Dexamethasone toleration of stable transgenics grown on plates.

A. Various transgenic lines containing ATR13 growing on different concentrations of dexamethasone, typically used at 30uM. 1. Col5:RPP13Nd, 2. Col5+ATR13Emco-SP3-10, 3. Col5+ATR13Emco+SP3-5, 4. Col5:RPP13Nd+ATR13Emco-SP1-1, 5. Col5:RPP13Nd+ATR13Emco+SP1-1, 6. Col5+ATR13Emco-SP+CFP2-2, 7. Col5+ATR13Emco+SP+CFP2-10, 8. Col0+AvrRpt2

Whether this lethal phenotype was due to the toxicity of intact dex signaling machinery on early plant development [94] or due to the function of ATR13 remains unresolved. Regardless, three week old Col5:dexATR13Emco5-SP 3-10 seedlings were grown on soil and sprayed with 30uM dex in 0.05% silwet and induced for 24 hours. Five grams of above ground material was collected for immunoprecipitation experiments and plant lysate was split into two aliquots and incubated with either anti-ATR13 sepharose or anti-ATR1 sepharose as a negative control. Figure 3-6A shows a strong enrichment of ATR13 protein in samples eluted off of anti-ATR13 resin, whereas anti-ATR1 resin does not bind any ATR13. When these same samples were silver stained, however, we did not see unique bands (other than ATR13) in the anti-ATR13 sample relative to the anti-ATR1 sample (Figure 3-6B, C). Worried that the interaction between ATR13 and its target might be weak or transitory, we experimented with various cleavable crosslinking reagents such as DSP and DTSP to stabilize the interaction, yet we were still unable to detect proteins in the anti-ATR13 sample that were not present in the anti-ATR1 sample (Figure 3-6D, E).

Again concerned that our polyclonal ATR13 antibody was only interacting with unbound ATR13 protein due to steric inhibitions of target-bound ATR13, we opted to

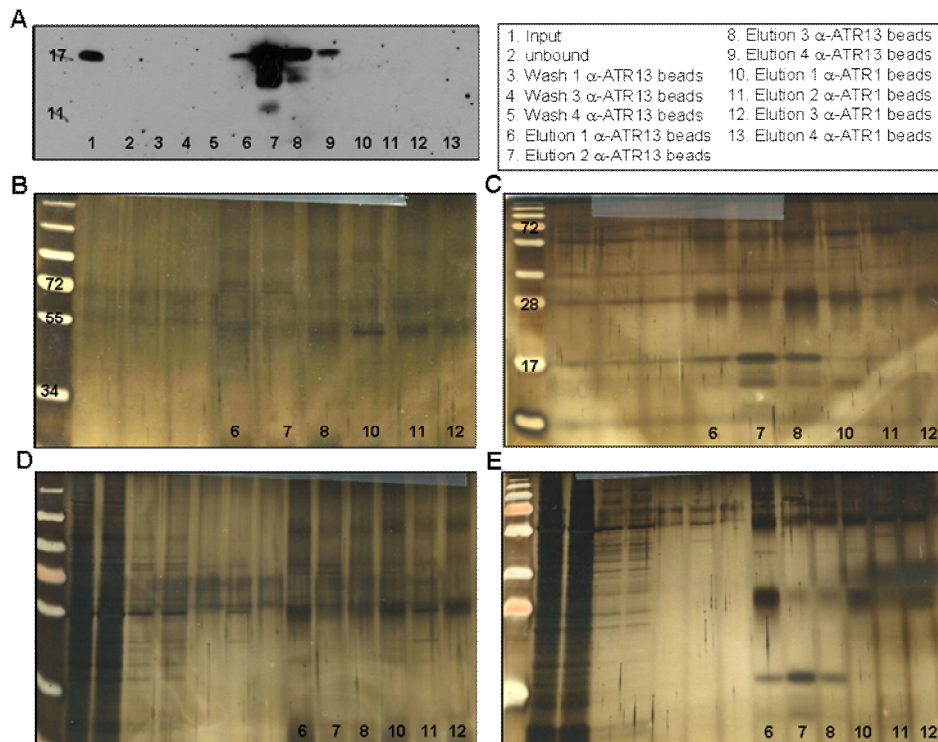


Figure 3-6. Immunoprecipitation of ATR13 and interacting proteins. **A.** Western blot of ATR13 fractions after elution from protein G beads. **B-C.** Silver stain of proteins associated with ATR13 elutions. **D-E.** Silver stain of proteins associated with ATR13 elutions that have been stabilized with DSP.

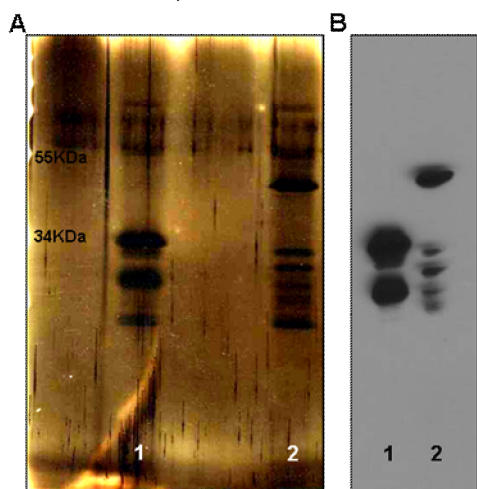


Figure 3-7. Pulldown of dex-induced ATR13Emco5+CFP expressed in stable transgenic *Arabidopsis* using α -GFP dynabeads. **A.** Silver stain of SDS-PAGE gel of bead elutions showing protein bands associated with ATR13Emco5+CFP and CFP controls. **B.** Western blot of SDS-PAGE with elution samples from ATR13Emco5+CFP and CFP probed with α -GFP. Sample 1 is the elution from α -GFP dynabeads incubated with Col5:CFP1-10, and sample 2 is the elution from α -GFP dynabeads incubated with Col5:ATR13Emco5+CFP2-2.

use dex-inducible CFP and ATR13Emco5+CFP lines with anti-GFP resin. While at first glance the silver stained gel appeared to give a clean and promising result (Figure 3-7A), when these same samples were probed on a Western blot with anti-GFP, bands that had seemed unique to the ATR13Emco5+CFP samples reacted with anti-GFP

antibody, indicating that they were probably degradation products of the ATR13Emco5 +CFP fusion protein (Figure 3-7B).

After numerous unsuccessful attempts at pulling out protein interactors of ATR13, we decided to explore small molecules as possible ATR13 targets. To do this, we looked for changes between the chemical profiles of transgenic lines expressing CFP or ATR13 Emco5+CFP under the assumption that any perturbation of a small signaling compound, such as a hormone, would have visible effects on the overall metabolite composition of the plant [95]. Organic compounds were extracted in methanol from 0.5 grams of dex-induced CFP and ATR13Emco5+CFP *Arabidopsis* tissue and separated using HPLC reverse phase chromatography. Figure 3-8A shows the profile of methanol soluble compounds from plants expressing CFP after dex induction, while figure 3-8B shows the compound profile of plants expressing ATR13Emco5+CFP. A comparison of these profiles shows little variation between compositions of both samples, with only

subtle differences between the levels of certain compounds. This consistency between treatments suggests that ATR13Emco5 does not affect methanol-soluble metabolite composition, and therefore is unlikely to target small molecules.

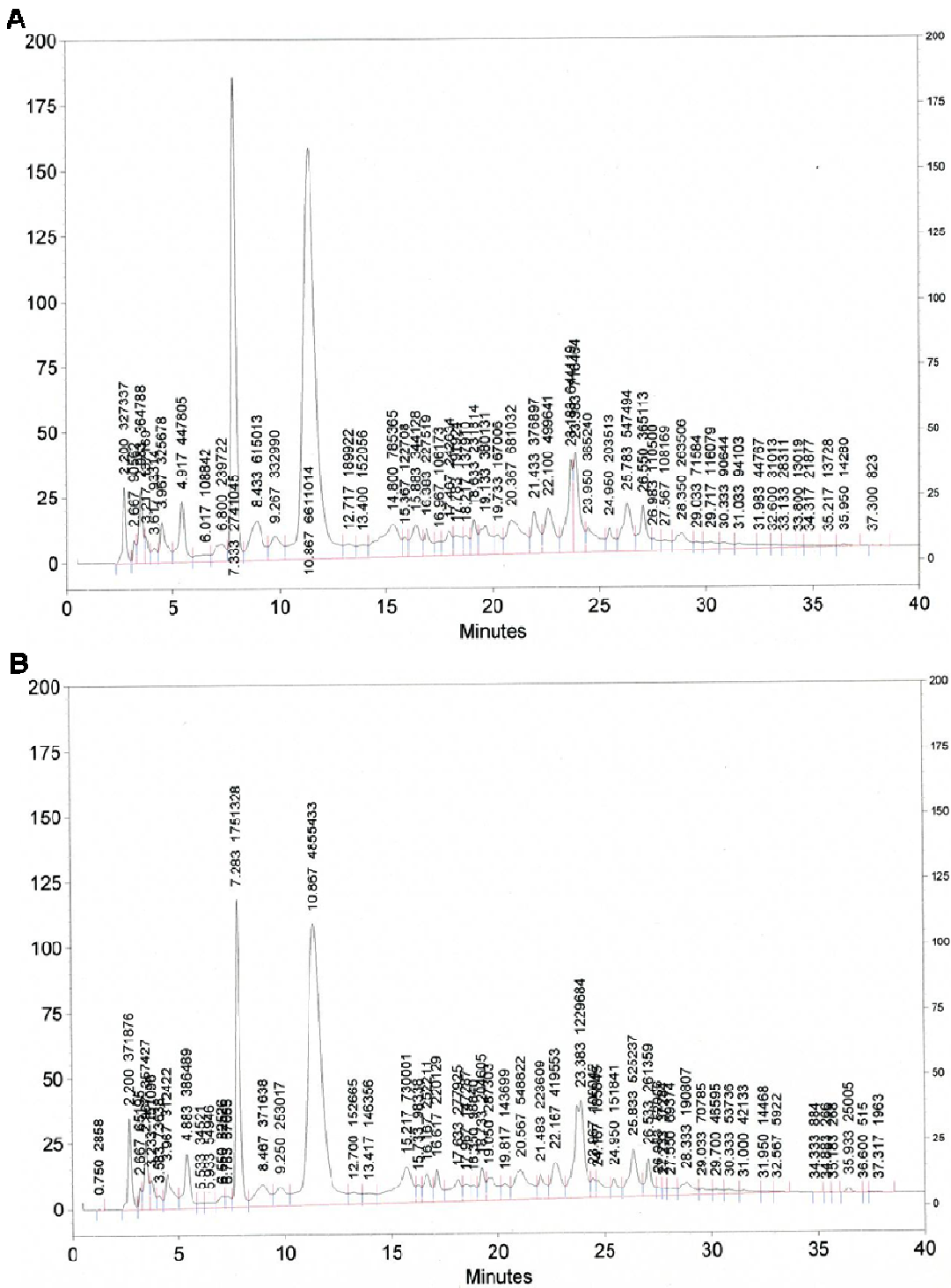


Figure 3-8. Methanol soluble organic compounds isolated from *A. thaliana*.
A. Metabolite composition of dex-induced *A. thaliana* plants expressing CFP. **B.** Metabolite composition of dex-induced *A. thaliana* plants expressing ATR13 Emco5+CFP.

Continuing to search for interactors using biochemical methods, we turned back to *in planta* expression and took advantage of the *Agrobacterium tumefaciens*/*Nicotiana benthamiana* transient expression system. Initially, we used constitutively expressed ATR13 Emoy2 and Maks9 GFP fusions, as well as ATR1 Emoy2 and Cala2 GFP fusions as controls. With co-expressed cognate R-genes RPP13Nd-HA and RPP1Ws-HA included as positive controls, we were able to show association of the recognized ATR1 Emoy2 allele with its cognate R-gene, however RPP13Nd did not associate with the recognized GFP-ATR13 Maks9 allele (data not shown). Regardless, we ran samples and visualized with silver stain, revealing no unique bands in ATR13 samples (data not shown).

Undeterred, we tagged ATR13-GFP fusions and GFP alone with an additional N-terminal flag tag and repeated pull down attempts using anti-flag agarose. This time we were able to show association of ATR13 alleles with RPP13Nd-HA *in planta*, yet recognition specificity did not correlate with this association (Figure 3-9A). ATR13

Emoy2 and Maks9 both pulled down RPP13Nd-HA, as did the GFP negative control, however in the sample containing Maks9, a single higher molecular weight band was visible in addition to a lower molecular weight derivative. In the ATR13 Emoy2 and GFP samples a higher molecular weight doublet was present in the co-immunoprecipitation experiments. The non-specific interaction between RPP13Nd-HA and GFP was probably due to the over-expression of GFP.

Stoichiometrically, the amount of RPP13Nd-HA that associated with GFP was equal to that of ATR13 Emoy2, despite the fact that GFP expression levels that were at least twice that of ATR13 Emoy2 (Figure 3-9B). Regardless, there was a clear differential between RPP13Nd-HA species that associated with ATR13 Maks9 versus ATR13 Emoy2. It is possible that the single band we see in Maks9 samples is the activated form of RPP13, whereas in Emoy2 and GFP samples, the doublet is suspended in an inactive form of the R-protein. These experiments require further exploration, such as biochemical characterization of RPP13Nd in the presence of recognized versus unrecognized alleles of ATR13, or truncation studies of RPP13Nd to identify the region of RPP13Nd that actually associates with ATR13. RPP13Col:HA samples were unstable or did not express to a comparable level to RPP13Nd, therefore not much can be concluded from the absence of *in planta* association between RPP13Col and ATR13.

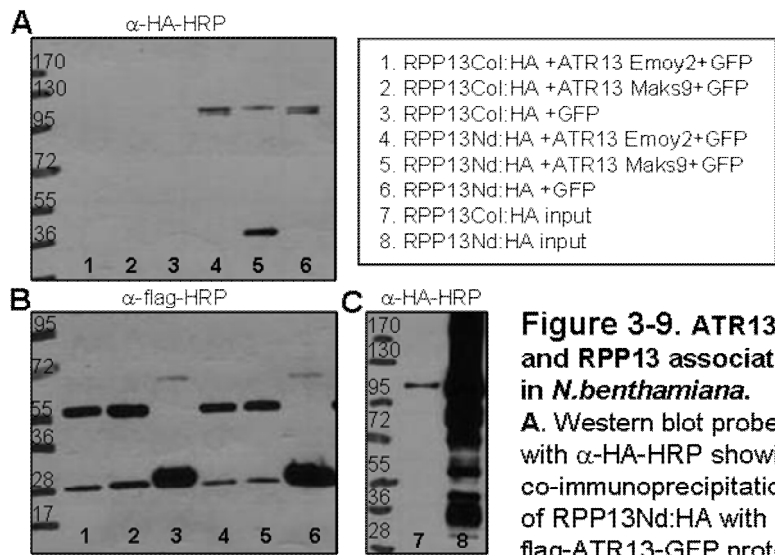


Figure 3-9. ATR13 and RPP13 association in *N. benthamiana*.

A. Western blot probed with α -HA-HRP showing co-immunoprecipitation of RPP13Nd:HA with flag-ATR13-GFP protein.

B. Blot from panel A stripped and reprobed to show levels of ATR13 and GFP pulled down with a-flag resin. **C.** RPP13 input levels based on western blot of IP using a-HA resin.

Encouraged by the association of ATR13 with its cognate R-gene, we separated co-immunoprecipitation samples on an SDS-PAGE gel and silver stained to look for bands unique to ATR13 samples relative to GFP (Figure 3-10). In lanes 2 and 3 there

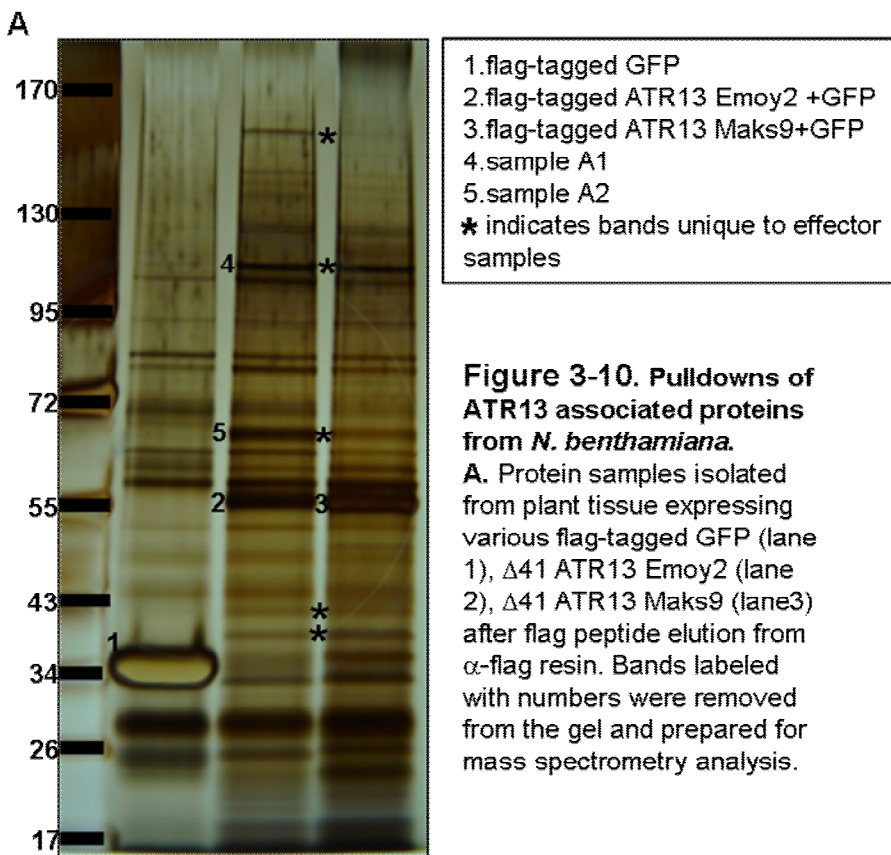


Figure 3-10. Pull-downs of ATR13 associated proteins from *N. benthamiana*.

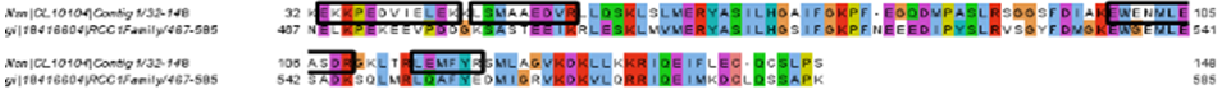
A. Protein samples isolated from plant tissue expressing various flag-tagged GFP (lane 1), $\Delta 41$ ATR13 Emoy2 (lane 2), $\Delta 41$ ATR13 Maks9 (lane 3) after flag peptide elution from α -flag resin. Bands labeled with numbers were removed from the gel and prepared for mass spectrometry analysis.

are clearly unique bands present in both ATR13 samples, the most distinct being a high molecular weight band near 115kDa and another around 65kDa. These bands were analyzed using LC/MS/MS and found to contain 6 peptides from a Prp39-like family of proteins and 3 peptides from a Regulator of Chromatin Condensation 1 family (Table 3-2). Since these peptides were pulled out of a *Nicotiana* database (courtesy of Dinesh-Kumar laboratory,

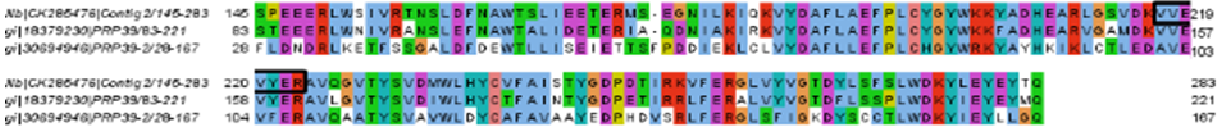
UC Davis), the contigs associated with each peptide fragment were blasted against the *Arabidopsis thaliana* database and alignments were made from the top hits of from each *Nicotiana* contig (Figure 3-11). Though definitive claims cannot be made as to the actual protein target of ATR13 in *Arabidopsis*, the peptide identities help to narrow the focus of future pursuits. Table 3-3 shows the best hits for each contig blasted against NCBI's non-redundant protein database. In light of the localization experiments with ATR13 discussed in the previous chapter, interaction with the nuclear-localized Prp39-like family and RCC1 family, as well as with tubulin, is consistent with localization patterns of ATR13 alleles (previous chapter).

The *Arabidopsis thaliana* *PRP39-1* gene is believed to be involved in the autonomous pathway's regulation of flowering time under all conditions, encoding a protein that possesses two tetratricopeptide repeat superhelical domains [96]. Tetratricopeptide repeat domains (TPRs) are typically involved in mediating protein:protein interactions and assembly of multi-protein complexes [97], [98], [99]. These domains are often found in RNA processing enzymes, including Prp39p, a yeast protein found to have high similarity to AT PRP39-1 that is required for assembly of splicing complexes and involved in pre-mRNA 3' end processing [100]. Mutants in AT *PRP39-1* transition more slowly from vegetative to reproductive stages, showing delayed flowering-- a developmental process that is

A



B



C



Figure 3-11. Alignments generated from BLAST hits of contigs associated with peptides pulled down with flag-ATR13 protein expressed in *N. benthamiana*.
A. Sample A2 contig partially aligned with an *Arabidopsis thaliana* RCC1 family protein. **B.** One of the contigs from sample A1 aligned to members of the PRP39 family of *A. thaliana*. **C.** The other contig associated with sample A1 aligned to the same PRP39 family in *A. thaliana*. Peptides recovered from mass spectrometry are outlined with back boxes.

dependent on functional mRNA processing machinery and proper splicing [101]. Several possibilities exist that make altering the function of AT PRP39-1 an attractive target for Hpa:1) by delaying flowering time, senescence is also delayed, thereby prolonging a hospitable environment in which the obligate biotroph might thrive, and 2) by altering proper splicing mechanisms, cellular defense responses at the transcriptional level can be blocked, preventing proteins involved in the defense response from being properly translated, thereby allowing enhanced pathogen growth [102]. Upon examination of SALK lines containing insertions in coding regions of both *AT-PRP39-1* and *AT-PRP39-2*, the growth of Hpa isolate Maks9 appeared comparable to growth on wildtype Columbia plants (data not shown). Lines were not verified as homozygous at the mutant locus, so it is possible that despite claims of homozygosity, we were dealing with heterozygous individuals.

The other interactor of ATR13 identified during pulldown experiments is a member of the RCC1 or RCC1-like family of proteins. The Regulation of Chromatin Condensation 1 (RCC1) protein is conserved in yeasts, plants, and animals, and is essential for maintaining nuclear transport [103]. Loss of RCC1 leads to suppression of nuclear protein import in cells and arrest of cell cycle progression [104]. In addition to its

role in nuclear transport, RCC1 is involved in the formation of nucleus initiation, termination of transcription, pre-mRNA splicing and 3' end formation, mRNA export, and DNA replication [105]. RCC1 contains a seven blade propeller domain that binds to the H2A and H2B components of nucleosomes [106], [107], stimulating its catalytic activity to exchange guanine nucleotides associated with Ran (*ras*-related nuclear protein) to GTP [108]. This creates a Ran-GTP gradient that drives nuclear envelope assembly and nuclear transport [107]. Ran-GTP is nuclear-specific and has the dual role of dissociating cargo from import carriers and loading cargo onto export machinery [109]. Interestingly, as mentioned in the previous chapter, the ATR13 structure loosely resembles a Ran GTPase and other proteins involved in nuclear trafficking. Since RCC1 domains are known to bind Ran GTPases present in nucleoporins, it is possible that ATR13 mimics Ran-GTP and competitively binds to RCC1, preventing RCC1 from catalyzing the exchange of GDP for GTP on Ran proteins. This would alter the balance of Ran-GTP and RAN-GDP, thereby blocking nuclear trafficking. This could be beneficial to the pathogen by preventing resistance-related transcripts from being exported to translational machinery [110]. Many questions remain, however we now have an idea of where to start looking for answers.

Summary and Future Directions:

In this study we identified two *Arabidopsis* protein families that may be targeted by the Hpa effector, ATR13: PRP39-like and RCC1-like protein families. The trend of multiple effector targets has been observed for several effectors including the *E. coli* effector EspF [67]. Taking into account the localization patterns of ATR13 discussed in the previous chapter, it is not surprising that this effector has multiple functions and targets in the plant cell. We also show a weak *in planta* association of ATR13 with its cognate R-gene, RPP13. Lastly, we show that the *in planta* expression of ATR13 has no effect on methanol-soluble metabolites extracted from plant cells.

Much more can be done to authenticate and characterize the interaction between ATR13 and its suspected targets. Firstly, more complete peptide coverage of these putative ATR13 targets in mass spectrometry experiments would help identify the exact proteins that seem to be involved in interactions with ATR13. Once single targets from these protein families are identified, interactions between ATR13 and its targets can be verified by co-IP *in planta* and through yeast 2 hybrid assays. ATR13 GTP binding can also be tested to see if RCC1 recognizes ATR13 as a substrate, and chromatin condensation from plant cells expressing ATR13 can be assayed by micrococcal nuclease digest to determine if global changes in chromatin state are observed.

Additionally, considering that ATR13 may alter a cell's ability to process mRNA, RNA seq experiments are in queue and will provide information about levels of mRNA transcripts present in cells that have been exposed to ATR13. Also, it is possible that ATR13 targets a defense-related compound or protein triggered by native pathogen delivery. Though pulldowns of ATR13 from Hpa-infected tissue were unsuccessful in detecting even a small amount of ATR13, perhaps a scale up of this experiment would provide us with enough ATR13 to pulldown and probe for interacting proteins.

Table 3-1. List of stable transgenic *Arabidopsis thaliana* plants generated during my dissertation.

<u>Ecotype / background</u>	<u>Promoter</u>	<u>Transgene</u>
Columbia 5 (Col5)	Dex-inducible	ATR13Emco5 +SP
Col5	Dex-inducible	ATR13Emco5 -SP
Col5	Dex-inducible	ATR13Emco5 +SP +CFP
Col5	Dex-inducible	ATR13Emco5 -SP +CFP
Col5	Dex-inducible	ATR13Emoy2 -SP
Col5	Dex-inducible	ATR13Emoy2 -SP+CFP
Col5	Dex-inducible	CFP
Col5	Native	RPP13Nd:HA
Col5:RPP13Nd	Dex-inducible	ATR13Emco5 +SP
Col5:RPP13Nd	Dex-inducible	ATR13Emoy2 -SP
Col5:RPP13Nd	Dex-inducible	ATR13Emoy2 -SP+CFP
Col5:RPP13Nd	Dex-inducible	CFP
<i>eds1/ndr1</i> :RPP13Nd	Dex-inducible	ATR13Emco5 +SP
<i>eds1/ndr1</i> :RPP13Nd	Dex-inducible	ATR13Emco5 -SP

Table 3-2. List of peptides identified in each *N. benthamiana* flag-ATR13 pulldown sample and the *Nicotiana* contigs associated with them.

<u>Sample</u>	<u><i>Nicotiana</i> Contigs</u>	<u>Number of hits</u>	<u>Peptide sequences</u>
A1	Nt TC24466	2	FLYLVSGK, RIDLLDSLVDK
	Nb CK285476	1	VVEVYER
A2	Nsn CL10104Contig1	6	2x EKKPEDVIELEK, LSMAAEDVR 2x EWENMLEASDR, LEMFYR
Maks	Nt AM835490	1	DVNAAVATIK
	Nt EB447852	1	LAVNLIPFPR

Table 3-3. Best BLAST hit alignments with contigs identified from peptide fragments found in samples A1 (A) and A2 (B) pulled down from *N. benthamiana* with flag-tagged ATR13.

A

Sequences producing significant alignments: Nb CK285476					
Accession	Description	Max score	Total score	Query coverage	E value
XP_002272685.1	PREDICTED: hypothetical protein [Vitis vinifera]	342	342	99%	3.00E-92
CAN60852.1	hypothetical protein [Vitis vinifera]	334	334	99%	9.00E-90
XP_002526546.1	Pre-mRNA-processing protein prp39, putative [Ricinus communis] >gb	286	286	98%	1.00E-75
XP_002889490.1	hypothetical protein ARALYDRAFT_333729 [Arabidopsis lyrata subsp.	268	268	75%	4.00E-70
NP_563700.1	PRP39; binding [Arabidopsis thaliana] >gb AAL07170.1 unknown pro	264	264	65%	1.00E-68
AAC16751.1	Contains similarity to pre-mRNA processing protein PRP39 gb L29224	262	262	75%	3.00E-68
CBI37183.3	unnamed protein product [Vitis vinifera]	256	256	63%	2.00E-66
XP_002303113.1	predicted protein [Populus trichocarpa] >gb EEE82386.1 predicted pr	243	243	48%	1.00E-62
ACJ86238.1	unknown [Medicago truncatula]	241	241	92%	6.00E-62
XP_002320608.1	predicted protein [Populus trichocarpa] >gb EEE98923.1 predicted pr	240	240	48%	2.00E-61
NP_001049340.1	Os03g0210400 [Oryza sativa Japonica Group] >gb ABF94590.1 Pre-r	230	230	56%	1.00E-58
EEC74741.1	hypothetical protein OsI_10482 [Oryza sativa Indica Group]	230	230	56%	1.00E-58
XP_002465661.1	hypothetical protein SORBIDRAFT_01g043300 [Sorghum bicolor] >gb	227	227	56%	1.00E-57
EEE58564.1	hypothetical protein OsJ_09874 [Oryza sativa Japonica Group]	225	225	56%	4.00E-57
XP_001763214.1	predicted protein [Physcomitrella patens subsp. patens] >gb EDQ720	211	211	56%	6.00E-53
XP_001773580.1	predicted protein [Physcomitrella patens subsp. patens] >gb EDQ616	211	211	49%	8.00E-53
XP_001758020.1	predicted protein [Physcomitrella patens subsp. patens] >gb EDQ772	210	210	49%	2.00E-52
ABR17775.1	unknown [Picea sitchensis]	197	197	46%	1.00E-48
EFJ34954.1	hypothetical protein SELMODRAFT_61333 [Selaginella moellendorffii]	189	189	48%	2.00E-46
EFJ09397.1	hypothetical protein SELMODRAFT_129910 [Selaginella moellendorffii]	189	189	48%	3.00E-46

B

Sequences producing significant alignments: Nsn CL10104					
Accession	Description	Max score	Total score	Query coverage	E value
XP_002283782.1	PREDICTED: hypothetical protein [Vitis vinifera]	182	182	85%	2.00E-44
XP_002516507.1	Protein pim1, putative [Ricinus communis] >gb EEF45848.1	160	160	89%	6.00E-38
XP_002324218.1	predicted protein [Populus trichocarpa] >gb EEF02783.1 p	157	157	92%	4.00E-37
CBI20846.3	unnamed protein product [Vitis vinifera]	149	149	86%	1.00E-34
CAK22423.1	regulator of chromosome condensation family protein [Bet.	145	145	92%	2.00E-33
EEE56319.1	hypothetical protein OsJ_03316 [Oryza sativa Japonica Gro	142	142	89%	9.00E-33
NP_001130888.1	hypothetical protein LOC100191992 [Zea mays] >gb ACF7	142	142	90%	1.00E-32
NP_001044114.1	Os01g0725600 [Oryza sativa Japonica Group] >dbj BAB90	142	142	89%	1.00E-32
EEC71410.1	hypothetical protein OsI_03583 [Oryza sativa Indica Group	142	142	89%	1.00E-32
XP_002456275.1	hypothetical protein SORBIDRAFT_03g033330 [Sorghum bi	140	140	89%	4.00E-32
ACL53116.1	unknown [Zea mays] >gb ACN36328.1 unknown [Zea ma	136	136	91%	1.00E-30
XP_002871480.1	hypothetical protein ARALYDRAFT_487995 [Arabidopsis lyr.	124	124	74%	5.00E-27
NP_568250.1	UVB-resistance protein-related / regulator of chromosome	123	123	74%	6.00E-27
CAB87718.1	putative protein [Arabidopsis thaliana]	122	122	74%	1.00E-26
AAM63715.1	unknown [Arabidopsis thaliana]	122	122	74%	1.00E-26

Chapter 4. The Search for Members of the RPP13 Signaling Pathway

Introduction:

Plant immunity is a complex web of signaling cascades, resistance genes, and cellular reprogramming. Pathogens are detected when surface-exposed pathogen associated molecular patterns (PAMPs) are detected by pathogen recognition receptors (PRRs) or receptor-like kinases (RLKs) on the surface of the plant cell plasma membrane [111]. This recognition event triggers a MAP Kinase signaling cascade that results in the mounting of a defense response called PAMP-triggered immunity (PTI) resulting in the hypersensitive response (HR) and restriction of pathogen spread. PTI can be suppressed, however, by pathogen-derived proteins known as effectors that are delivered into the host and act to disrupt PTI signaling. As a counter measure, plants have evolved a second line of defense—R-gene mediated resistance known as effector-triggered immunity, or ETI. In ETI, specialized resistance proteins (R-genes) recognize the presence or activity of an effector and trigger defense responses such as release of antimicrobial compounds or proteins and HR to limit the spread of the pathogen [17].

R-gene products fall into two major classes: proteins that contain an N-terminal coiled-coil domain followed by a nucleotide binding sequence and a leucine-rich repeat domain (CC-NBS-LRRs) and proteins that contain an N-terminal toll-like interleukin receptor domain followed by a nucleotide binding sequence and leucine-rich repeats (TIR-NBS-LRRs) [112]. Though few of the ~150 resistance genes identified in *Arabidopsis thaliana* have been well characterized [113], most have common dependencies on SGT1a, STG1b, RAR1, PAD4, or SA accumulation for full functionality [114]. In addition to these functional requirements, most CC-NBS-LRR and TIR-NBS-LRR resistance pathways depend on the downstream function of NDR1 or EDS1, respectively, to mount a defense response to pathogen challenge [115]. However, there are a few examples of R-genes that function independently of the additional protein components and typical pathways listed above. *A. thaliana*'s ZAR1 is a member of the CC-NBS-LRR class of resistance proteins that recognizes the HopZ1a effector delivered by *Pseudomonas syringae* during the course of plant infection with none of the additional requirements previously mentioned [116]. Additionally, the *A. thaliana* CC-NBS-LRR resistance gene RPP13, the focus of this study, also functions independently of all known resistance-related proteins and pathways [28].

During infection, the oomycete *Hyaloperonospora arabidopsidis* delivers a number of effectors, including the effector ATR13, whose presence is detected in the cytoplasm by RPP13 in a race-specific manner, triggering a localized cell death and resistance response [23]. *A. thaliana* Columbia ecotypes (Col5) containing the RPP13Col5 allele are susceptible to oomycete isolates carrying the ATR13 Emco5 allele, however transgenic Col5 lines containing the RPP13 allele from the Neiderzenz ecotype (RPP13Nd) recognize ATR13 Emco5 and trigger a resistance response [117]. Both *ATR13* and *RPP13* are highly polymorphic genes, implying that the alleles have undergone diversifying selection at their respective loci, perhaps suggestive of a direct interaction between R-gene and effector serving to drive this evolution [40]. Interestingly, while RPP13 is one of the most polymorphic *Arabidopsis* genes described to date [118], only three different alleles of *RPP13* function in ATR13 recognition [26].

To dissect this seemingly novel resistance pathway exploited by RPP13 after recognition of ATR13, we employed a forward genetics strategy and used EMS mutagenesis to generate an *Arabidopsis* population no longer able to recognize ATR13. Since *H. arabidopsidis* is an obligate biotroph, it is difficult to culture and genetically manipulate, therefore no isogenic strains differing in a single effector are available for experimentation. By exploiting the type III secretion system of *P. syringae* [119], we were able to deliver ATR13 Emco5 via *P. syringae* and observe the expected resistance response using HR or a bacterial growth assay [27].

In addition, it has been shown that certain R-gene products, such as MLA10 of barley and the N receptor of tobacco, are required in the nucleus for an effective defense response [120], [88], [121]. This implies that these R-gene products, typically found in the cytoplasm, serve as molecular switches that are targeted to the nucleus upon activation by recognition of their effectors [122]. In this chapter, in addition to attempting to identify components of RPP13-mediated defense signaling, I will determine the localization of RPP13 and discuss the dynamics of its activation. If RPP13 relocates to the nucleus upon activation by ATR13 recognition, we would expect to identify only proteins involved in an RPP13-resistance complex or the downstream nuclear targets of RPP13.

Materials and Methods:

4.1 Generating EMS populations

EMS (Sigma) was added at concentrations of 0.1%, 0.2%, and 0.3% to 0.38 grams of *Arabidopsis thaliana* seed (approximately 20,000 seeds) ecotype Col5 containing an RPP13Nd transgene and incubated end over end at room temperature for 16 hours. M1 seeds were washed and immediately germinated on soil in seventy-two 3 inch pots at a seed density of 100 seeds per pot for each EMS concentration. Seeds from 5 single siliques from plants treated with each EMS concentration were counted to determine which gave optimal levels of mutagenesis, indicated by 25% embryo lethality. M1 seed from the 0.2% EMS treatment best fit this criterion and M2 seed was collected from the 72 pools and planted out in 3 inch pots at a seed density of 100 seeds per pot for screening. Additionally, another *Arabidopsis thaliana* line, Col5 containing the RPP13Nd transgene with an additional dex-inducible full length ATR13 Emco5 transgene, was also mutagenized following the aforementioned protocol with 0.2% EMS. This M1 seed was grown on soil in 3 inch pots at 100 plants per pot and collected into 72 pools for M2 screening.

4.2 Screening mutant *Arabidopsis* populations with *Pseudomonas syringae* DC3000 delivery of ATR13 Emco5

Eight flats of *Arabidopsis thaliana* M2 seed totaling 14,400 seeds from EMS mutagenized Col5-RPP13Nd were planted at a density of 100 seeds per 3 inch pot. After the first set of true leaves emerged, two week old seedlings were sprayed with a suspension of 0.05% silwet and DC3000 OD 0.05 delivering ATR13 Emco5. Plants were allowed to dry and flats were capped for 24 hours to encourage disease symptoms to develop. Four days after inoculation, plants were scored for disease based on the appearance of chlorotic halos. Infected plants were transplanted and affected leaves were removed. Plants were allowed to recover for several weeks and were then screened for compromised RPP13Nd mediated resistance by growth assay.

4.3 Screening mutant *Arabidopsis* populations with *Pseudomonas fluorescens* delivery of ATR13 Emco5

7,200 M2 seed from the EMS mutagenized pools of Col5-RPP13Nd seed were planted in netted pots at a density of 50 plants per 3 inch pot. Once two sets of true leaves had emerged, *Pseudomonas fluorescens* (OD 1) delivering ATR13 Emco5 was vacuum infiltrated into the leaves. Plants possessing intact RPP13Nd signaling triggered HR, leaving plants with compromised RPP13Nd signaling as the only survivors. Original infected leaves were removed from surviving plants prior to several weeks recovery in 16 hour light cycles. RPP13Nd recognition was further verified or debunked by growth assay.

4.4 Identifying mutants by selection in Col5-RPP13Nd containing a dex-inducible ATR13 Emco5

More than 167,500 seeds (2327 from each pool) of the M2 mutant population of Col5:RPP13Nd containing the dex-inducible ATR13 Emco5 transgene were sterilized in 50% bleach and resuspended in 0.1% agarose. Seed suspensions were spread on MS

plates containing (20ug/ul) basta selection and placed in 24 hour light. After ten days, a sterile 30uM dexamethasone solution was flooded onto the plates following which plates were resealed and returned to 24 hour light. After four days, plates were collected and surviving individuals were transplanted onto soil and propagated to the M3 generation. M3 individuals were rescreened on MS plates with both hygromycin and basta to ensure both transgenes were still present, as well as with dexamethasone to confirm compromised RPP13Nd recognition of ATR13 Emco5. Additionally, these lines were assayed for HR by *P. fluorescens* delivered ATR13 Emco5 and growth assay by *P. syringae* DC3000 ATR13 delivery. Putative mutant lines were also grown on soil and sprayed with *Hyaloperonospora arabidopsidis* isolates Maks9 and Emco5 (1×10^6 spores/ml). Plants were scored for pathogen growth by eye and by lactophenol trypan blue staining. To stain, whole plants were boiled in lactophenol trypan blue [21] for 5 minutes and allowed to cool to room temperature for 3-5 hours. Excess stain was collected, and plant tissue was destained in 15mM chloral hydrate.

4.5 Identifying mutants in RPP13Nd signaling by compromised Hpa recognition

60,000 M2 seeds of EMS mutagenized Col5:RPP13Nd *Arabidopsis* were sown at a density of 100 seeds per 3 inch pot. Ten day old seedlings were sprayed with Hpa Maks9 conidia (1×10^6 spores/ml) and placed in a 15°C chamber maintaining 16 hour light cycles in high humidity. After seven days, plants were examined with a dissecting scope and scored visually for presence or absence of conidiophores. Plants that appeared to allow pathogen growth were transplanted to separate pots and rescued by placing individuals in a 24°C chamber with 16 hour light cycles. Infected leaves were removed and stained with lactophenol trypan blue. Chloral hydrate was used as destain. Plants that appeared to have compromised RPP13Nd mediated resistance were checked for the presence of RPP13Nd by PCR with the following RPP13 Nd specific primers: 5' gaacacgaagacttcttaa 3' and 5' agagtcacatcactaca 3'. Expression levels of RPP13Nd, as well as other well known genes involved in resistance, were examined by semi quantitative RT-PCR. RNA was extracted from potential mutants using the Trizol reagent and normalized by nanodrop measurements after clean up. cDNA was generated by superscript reverse transcriptase II (Invitrogen), and subsequent PCR was performed using RED-Extract N'Amp Taq (Sigma) with Actin as a loading control. Other genes tested in each mutant used in the study, include: Sgt1a, Sgt1b, and RAR1.

4.6 Mapping of mutants in RPP13Nd signaling

Verified RPP13Nd signaling mutants were crossed to the Landsberg ecotype as well as backcrossed to the Col5:RPP13Nd parent. Because of male sterility issues, mutant plants were typically recipients in these crosses, and wildtype parents were used as pollen donors. Crosses were propagated to the F2 generation for mapping. Genomic DNA was extracted from ninety-three F2 individuals that showed susceptibility to Hpa Maks9, and ten primer sets representing each chromosome arm were used for rough mapping.

Results and Discussion:

In order to dissect this seemingly novel resistance pathway, we performed EMS mutagenesis on *Arabidopsis* transgenic lines containing the RPP13 Neiderzenz allele in a Columbia 5 background. Original attempts to screen the mutant population with the

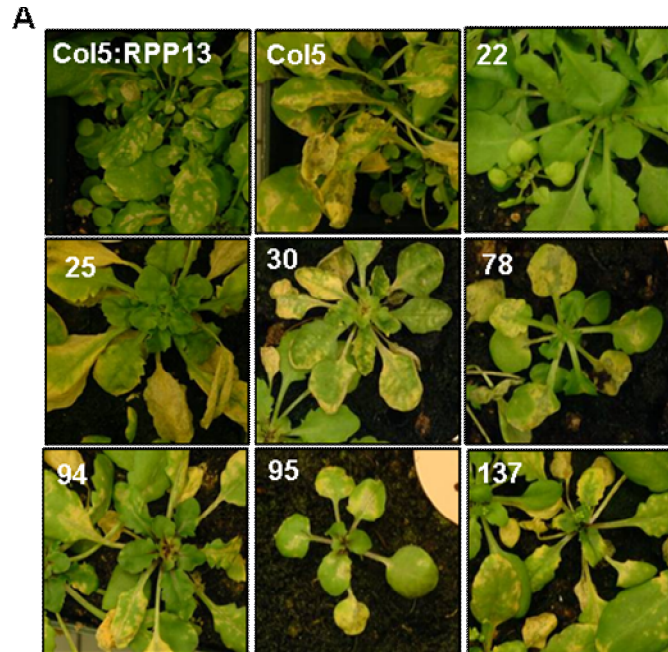


Figure 4-1. Mutant Col5:RPP13 plants screened with *Pseudomonas syringae* DC3000 delivering ATR13Emco5.

A. Representative array of promising diseased individuals unable to mount a resistance response to DC3000 delivering ATR13Emco5.

surrogate pathogen *Pseudomonas syringae* DC3000 delivering ATR13Emco5-SP proved difficult. Though spray inoculation conditions were supposedly optimized in pilot experiments using Col5 and Col5:RPP13Nd plants (data not shown), both mutants and controls showed a range of susceptibilities depending presumably on chamber microenvironments (Figure 4-1). Regardless of this variability, we selected mutants with the most dramatic chlorosis phenotypes and rescued them by removing infected leaves and returning them to a 16h light cycle chamber. The pool of potential mutants dwindled as not all mutants recovered from initial infection, plants that survived did not always set seed, and some seeds did not germinate on soil or on MS medium. Mutants that did give rise to an M3 population were screened with both *Pseudomonas fluorescens* delivering ATR13Emco5 for the absence of HR (data not shown) and with *Pseudomonas syringae* DC3000 delivering ATR13Emco5 in growth assay for development of disease (Figure 4-2). Of the 97 mutants originally rescued, only 31 gave rise to an M3 population. Of these 31 individuals, nearly half appeared to have altered RPP13 recognition phenotypes. When these individuals were checked for the presence of RPP13Nd by PCR, they did not possess the R-gene, yet most had mutant phenotypes, indicating that they were probably contaminants introduced before the mutagenesis process.

Learning from our difficulties with the previous screening method, we turned to the non-pathogenic *Pseudomonas fluorescens* as a screening agent. *P. fluorescens* does not cause disease or elicit a hypersensitive response on *Arabidopsis* in the absence of a recognized effector or intact plant recognition machinery, allowing us to create a screen for survivors *in lieu* of a disease screen. Since we lost a number of mutants in the DC3000 screen due to their inability to recover after infection, we felt hopeful that this approach would eliminate losses due to that hurdle. We added ATR13Emco5 to the *P. fluorescens* repertoire and vacuum infiltrated several flats

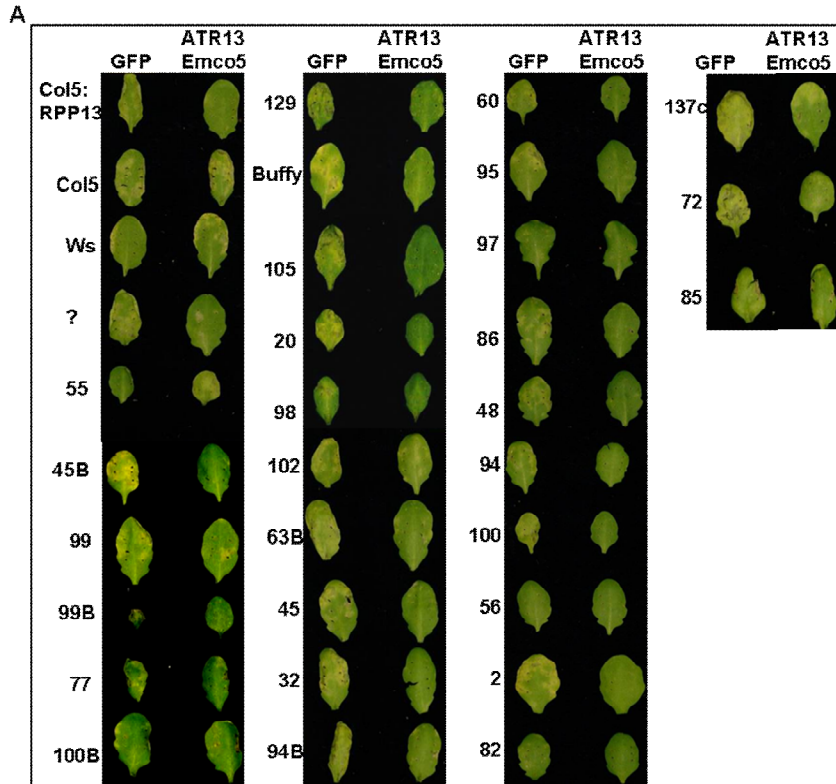
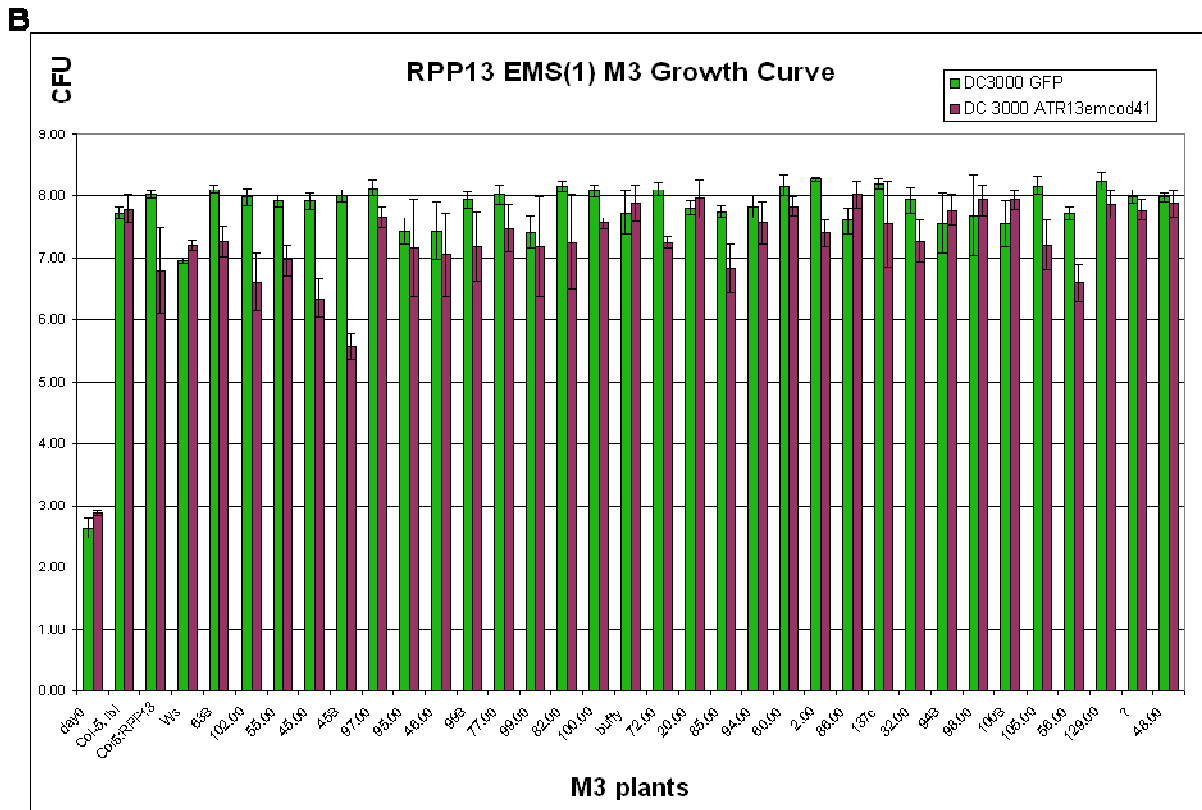


Figure 4-2. Disease assay on potential Col5:RPP13Nd mutants.
A. *Arabidopsis* leaves four days after inoculation with DC3000 1×10^4 delivering GFP or ATR13 Emco5.
B. Corresponding growth curve of leaves pictured in panel A.



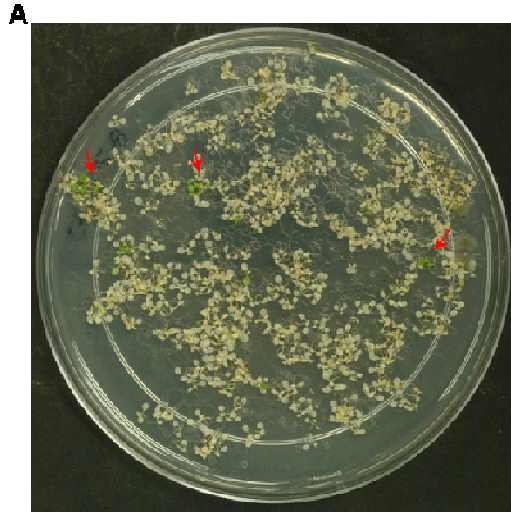


Figure 4-3. Selection for Col5:RPP13Nd +dexATR13Emco5 mutants unable to mount a defense response after dex induction.
A. Representative MS plate with basta selection of a single mutant pool five days after flooding with 30uM dexamethasone. Red arrows indicate individuals that were transplanted after surviving dex induction.

of EMS-mutagenized Col5:RPP13Nd seed with *P. fluorescens* at OD 1.0. We learned unfortunately that when ATR13Emco5 is delivered by *P. fluorescens* the HR response is not quite strong enough to kill an entire plant and our vacuum infiltration had no effect on plant growth (data not shown). Alternatively, vacuum efficiency may not have been as high as would be required for an effective screen.

Despite our difficulties with *P. fluorescens* as a screening agent, we remained convinced that a screen for survivors would give better yields than scoring for disease. To this end, we mutagenized our stable transgenic Col5:RPP13Nd containing a dex-inducible version of ATR13Emco5 with EMS. M2 seed from these individuals was grown on MS medium and mutants were selected by dex induction of ATR13Emco5 (Figure 4-3). Survivors were transplanted onto soil and allowed to recover for four weeks before ATR13Emco5 delivery by *P. fluorescens* in an HR assay (Figure 4-4). In total, from this selection we recovered 134 candidate mutants, 78 of which produced seed. The M3



Figure 4-4. HR assay using *P. fluorescens* delivering various effectors on Col5:RPP13+dexATR13 Emco5 mutant plants.

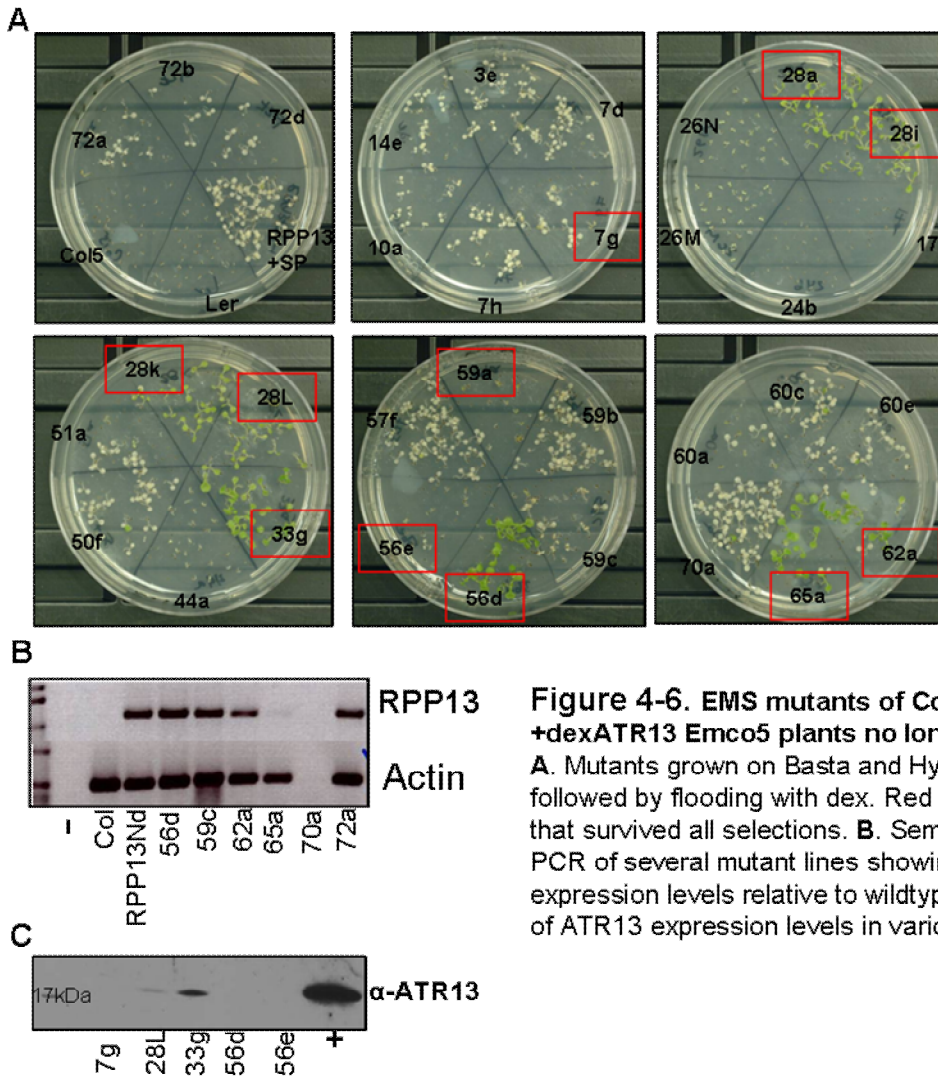


Figure 4-6. EMS mutants of Col5:RPP13Nd +dexATR13 Emco5 plants no longer producing HR.
A. Mutants grown on Basta and Hygromycin selection, followed by flooding with dex. Red boxes indicate plants that survived all selections. **B.** Semi-quantitative RT-PCR of several mutant lines showing RPP13 expression levels relative to wildtype. **C.** Western blot of ATR13 expression levels in various mutants.

Plants surviving after dex induction would be either mutants in RPP13Nd, its promoter, the GVG transcription factor activated by dexamethasone, ATR13, the promoter driving ATR13 expression, or the RPP13 resistance pathway. The M3 seed from promising mutants were plated on MS medium containing both basta and hygromycin to ensure the presence of both transgenes, and again flooded with dex to further eliminate possible contaminants (Figure 4-6A). Additionally, these mutants were screened for the presence of wildtype RPP13Nd by PCR and for expression levels of RPP13Nd by semi-quantitative RT-PCR (Figure 4-6B). ATR13 Emco5 was also sequenced and checked for expression by western blot in mutants that possessed and expressed RPP13Nd to wildtype levels (Figure 4-6C). Around this time, our lab obtained *Hyaloperonospora arabidopsidis* (Hpa) isolate Emco5, allowing us to screen these potential mutants by delivery of ATR13 via its natural pathogen. Putative mutants were sown on soil and sprayed with a suspension of Hpa conidia at (1×10^6 spores/ml (Figure 4-7). Interestingly, when mutants that fit the above criteria were inoculated with Hpa and

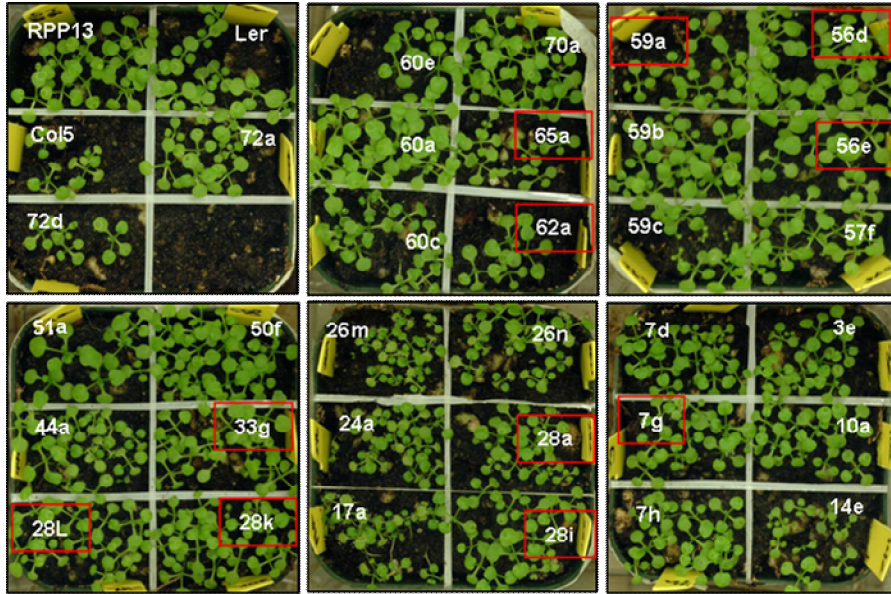


Figure 4-7. Hpa inoculations on Col5:RPP13Nd +dexATR13 Emco5 mutant plants. Red boxes indicate mutants that contain RPP13Nd.

stained with lactophenol trypan blue, the two most promising mutants, 28L and 33g, continued to restrict pathogen growth despite their inability to cause HR after dex induction on selective medium (Figure 4-8). Initially, we presumed these mutants might be illustrative of the bifurcation of resistance and the hypersensitive response [123]

[124], [125], however, when reviewing these mutants' responses to other effectors delivered by *P. fluorescens*, we noted that HR signaling was intact as other effectors were fully recognized in these background (Figure 4-4). It is possible that the RPP13Nd mutants have an independent signaling pathway that results in resistance *and* triggers HR independently of other R-genes, however, we opted to alter our strategy and revert to a more traditional screening method to identify mutants in the RPP13 resistance response.

Having obtained strains of Hpa, we decided to use the natural pathogen to screen EMS mutant populations of Col5:RPP13Nd, reasoning that if we could isolate mutants with wildtype RPP13Nd expression levels and sequence, those mutants would have to be in the RPP13Nd

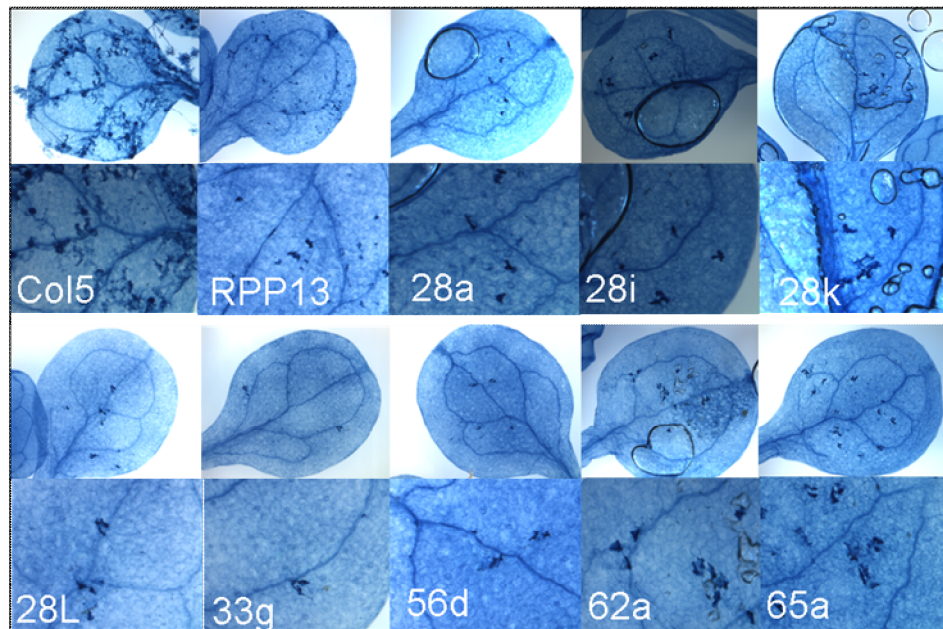


Figure 4-8. Lactophenol trypan blue staining of potential mutants identified in an EMS mutagenesis screen using Col5:RPP13Nd +dexATR13 Emco5 transgenic plants, none of which appear to restrict the growth of Hpa.

signaling pathway and would already be confirmed to be deficient in Hpa recognition and resistance. We screened over 60,000 plants in pools using the avirulent Maks9 Hpa isolate (capable of growing on true leaves unlike Emco5) and were able to recover seven individuals that were no longer resistant to this strain of Hpa: three from pool 65, two from pool 30, and two from pool 48. Cotyledons from each of these mutants were stained with lactophenol trypan blue (Figure 4-9A). Using sequence analysis and semi-quantitative RT-PCR, we showed that all these mutants contained non-mutated RPP13Nd. Mutant family 65 expressed RPP13Nd at the wildtype level (Figure 4-9B), while both individuals from pool 30 and pool 48 expressed at a much lower level, possibly due to a gene product acting in trans to regulate RPP13 expression. These results suggest our mutants contain mutations in additional genes that are essential for RPP13-mediated resistance. We also explored the possibility that genes previously implicated in resistance may have been affected by the mutagenesis. To address this possibility, we sequenced Sgt1a, Sgt1b, and Rar1, and determined expression levels in the mutants we recovered, showing genes were still intact and functional (Figure 4-9C).

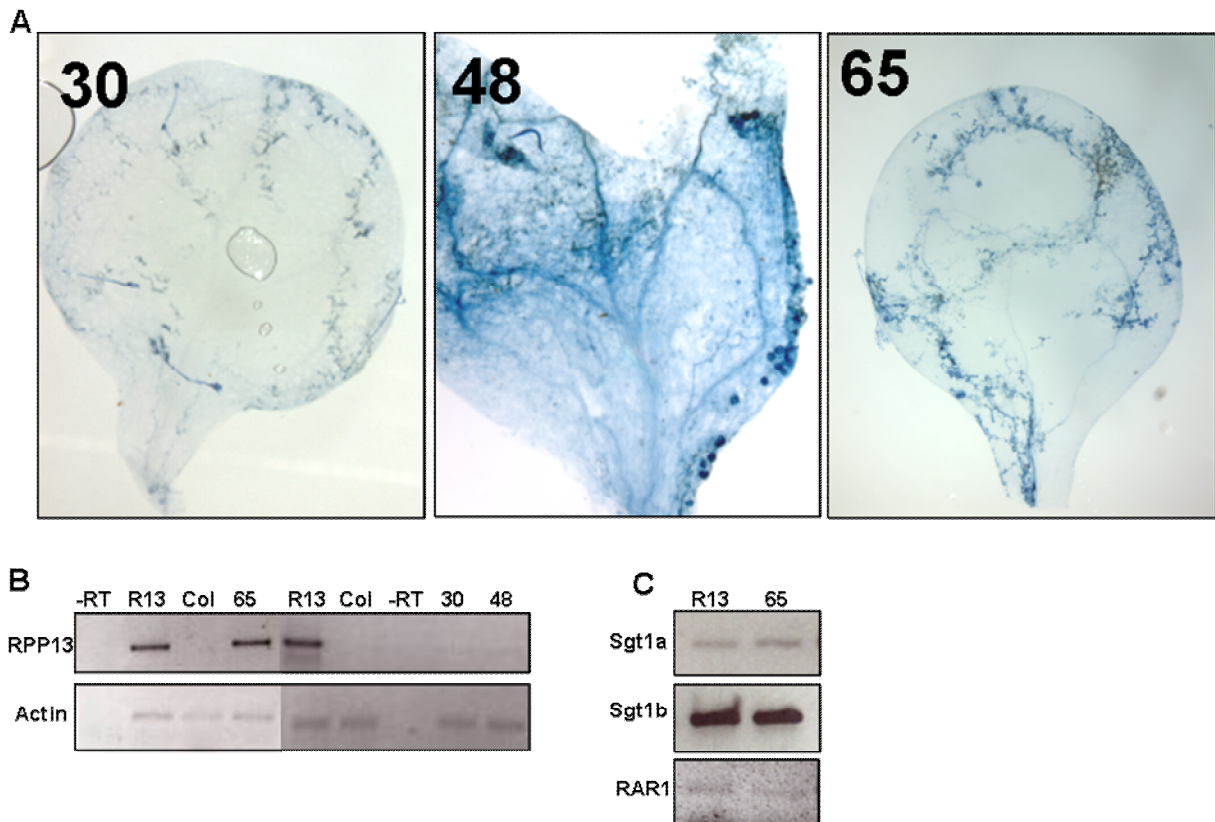


Figure 4-9. EMS Col5:RPP13Nd mutants no longer able to restrict Hpa Maks9 growth.

A. Lactophenol trypan blue staining of infected mutant cotyledons showing spread of Hpa. **B.** Semi-quantitative RT-PCR showing expression levels of RPP13 in various mutants. **C.** Mutant 65 expression analysis of genes known to play a role in the resistance response.

In hopes of generating mapping populations, we waited for mutants to bolt so we could perform crosses with both the Landsberg (Ler) ecotype and the Col5:RPP13Nd parent. Mutants from pools 65 and 38 bolted but could not self-fertilize, later determined

to be the result of male sterility. These lines were used as females and Ler and Col5:RPP13Nd pollen was used as male donors, eventually yielding siliques filled with F1 seed. We were unable to generate M3 individuals from these plants, so further characterization was not possible until backcrosses had given rise to F1 individuals that could be selfed to produce F2 plants that would segregate for the susceptibility phenotype. Mutants derived from pool 48, originally thought to be delayed in flowering, would not bolt. We sprayed these plants with giberellic acid, which induced bolting after several days but did not stimulate flower maturation. Mutants from pool 48 could not be propagated and were therefore lost from our pool of mutants.

Once we had generated segregating F2 mapping populations between our Columbia-derived mutants and the Landsberg ecotype, we scored the population for susceptibility to Hpa Maks9 and Emco5. The Landsberg ecotype also possesses two R-genes, RPP21 and RPP8, capable of mounting a defense response to Hpa Maks9 and Hpa Emco5 respectively. If our mutation affected only RPP13-mediated resistance, segregation ratios of 7:64 susceptible to resistant should emerge, four of those seven

RRPP LL	RRPP LI	RRPp LI	RRPp LL	RrPP LL	RrPP LI	RrPp LL	RrPp LI
RRPP LI	RRPP II	RRPp II	RRPp LI	RrPP LI	RrPP II	RrPp LI	RrPp II
RRPp LI	RRPp II	RRpp II	RRpp LI	RrPp LI	RrPp II	Rrpp LI	Rrpp II
RRPp LL	RRPp LI	RRpp LI	RRpp LL	RrPp LL	RrPp LI	Rrpp LL	Rrpp LI
RrPP LL	RrPP LI	RrPp LI	RrPp LL	rrPP LL	rrPP LI	rrPp LL	rrPp LI
RrPP LI	RrPP II	RrPp II	RrPp LI	rrPP LI	rrPP II	rrPp LI	rrPp II
RrPp LL	RrPp LI	Rrpp LI	Rrpp LL	rrPp LL	rrPP LI	rrpp LL	rrpp LI
RrPp LI	RrPp II	Rrpp II	Rrpp LI	rrPp LI	rrPp II	rrpp LI	rrpp II

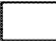


-  Susceptible plants if mutation only effects RPP13-mediated resistance
-  Additional susceptible plants if mutation effects both RPP8/21 and RPP13-mediated resistance
-  Resistant plants

Figure 4-10. Punnett square illustrating expected segregation ratios for various scenarios of mutant phenotype, where “P” is the wildtype allele of our mutant locus, “R” is the wildtype allele of RPP13Nd, and “L” is the wildtype allele of either RPP8 or RPP21 depending on the Hpa isolate used for screening. Lowercase letters denote non-functional alleles of gene.

susceptibles also containing RPP13Nd (Figure 4-10). Initially we grew plants on soil, sprayed with Maks9 and rescued susceptible individuals for 4 days before spraying with Basta to eliminate non-RPP13 containing plants. However, none of these infected plants survived the Basta treatment. Assuming that infection followed by the application of herbicide over-stressed the plants, we grew plants on soil, infected with Hpa, rescued susceptible individuals and screened these individuals by PCR for the presence or absence of RPP13 and RPP21. Surprisingly, with only 80% infection efficiency, we recovered 168 out of 543 F2 plants that permitted Hpa Maks9 growth, and with 66% infection efficiency 26 out of 562 permitted Hpa Emco5 growth. Corrected for infection efficiency, we found 38.6% susceptibility to Maks9 and 7% susceptibility to Emco5, leading us to believe that RPP21, and not RPP8, might also be dependent on a functional copy of our mutant gene, altering expected ratios to 7/16 or 43.75% susceptibility. We selected 72 susceptible plants from the Maks9 pool and found 59 to contain RPP13Nd (82% instead of the expected 57%), a ratio that seemed skewed towards possessing the RPP13Nd locus. Chromosomal markers from these plants were amplified by PCR, yet we could not determine a correlation between the susceptibility phenotype and Col5 versus Ler identity at any marker positions. Additionally, when we examined individuals that were susceptible to Emco5, none contained RPP13Nd.

Concerned with the lack of single locus segregation and our inability to isolate mutants containing RPP13Nd with compromised recognition of ATR13 Emco5, we germinated a subset of F2 Ler x 65 individuals on MS medium containing Basta to pre-select for plants containing RPP13Nd. Plants that germinated (the expected 75%) were transplanted to soil and sprayed with Hpa Maks9. 25% of the rescued individuals were susceptible to Hpa Maks9, a ratio consistent with both compromised RPP21 and RPP13 recognition. If our mutant was compromised only in RPP13 recognition, we would expect to see only 6.25% susceptibility in the screening population. When these mutants were screened by PCR to determine marker segregation, we were unable to identify any chromosomal region that associated with the susceptibility phenotype. Reasons for this could include: some kind of linkage, Hpa Maks9 spore contamination with another virulent strain of Hpa (though Hpa Maks9 did not grow on Col5:RPP13Nd negative controls), cross-pollination with some unidentified ecotype of *A. thaliana* that happened to amplify the right size markers for Ler, or a mutant with a dominant negative phenotype (though F1 plants were resistant). Resistance to Hpa, and in general, has been linked to plant development phenotypes [126], [127], so perhaps our segregation ratios are skewed because of pleiotropic effects of the mutant allele, if it plays a role in development.

In the interest of further characterizing RPP13, we decided to resolve its localization. We performed subcellular fractionation using two-phase partitioning, percoll gradients, and various size exclusion filters and determined that RPP13 associates most strongly with the plasma membrane, though to a lesser degree with the cytoplasmic fraction (Figure 4-11). This is especially interesting, as RPP13 has no predicted membrane localization motifs or modifications as determined using a series of prediction programs on the EXPASY server and was therefore thought to be cytoplasmic. Because other R-genes associated with the plasma membrane dynamically relocate to the nucleus once activated by effector detection [122], we checked if nuclei of RPP13Nd:HA transgenic *Arabidopsis* plants became enriched in

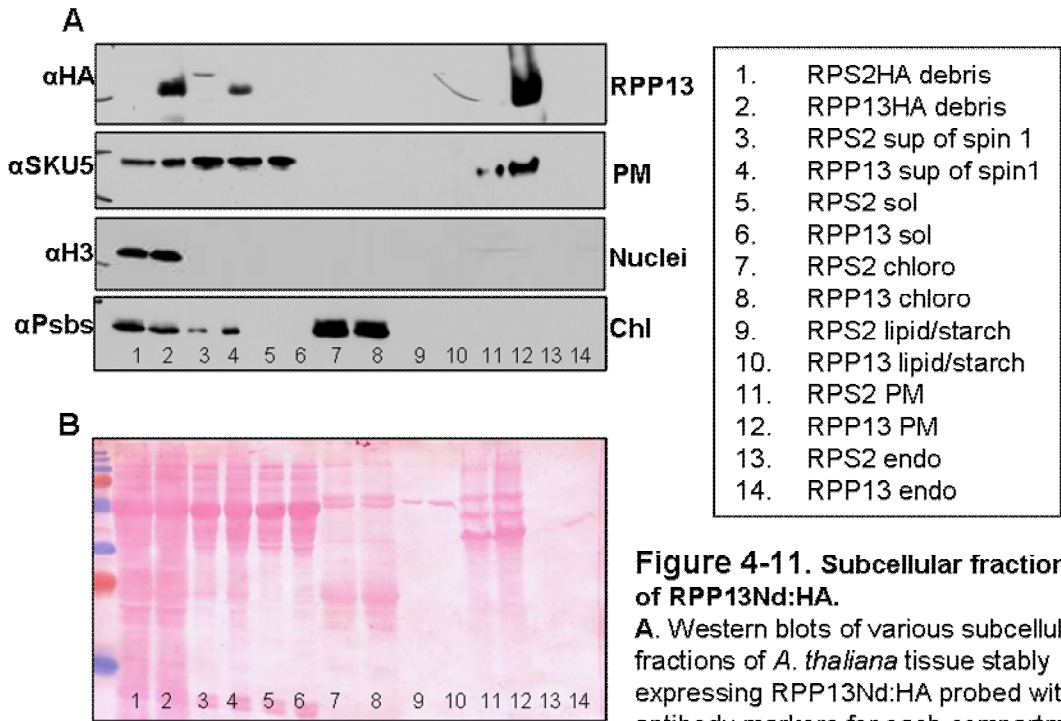


Figure 4-11. Subcellular fractionation of RPP13Nd:HA.

A. Western blots of various subcellular fractions of *A. thaliana* tissue stably expressing RPP13Nd:HA probed with antibody markers for each compartment. SKU5 is the plasma membrane marker, H3 is the nuclear marker, and Psbs is the chloroplast marker. **B.** Ponceau stained loading control of membrane.

RPP13 protein after delivery of ATR13 Emco5 or GFP by *P. fluorescens*. In the case of RPP13, we did not detect a change in nuclear RPP13 accumulation upon treatment, suggesting that perhaps there are intermediates in the signaling pathway that serve to relay signals for defense response activation.

Summary and Future Directions:

During this study we generated mutant populations in the Col5:RPP13Nd and Col5:RPP13Nd +dex ATR13 Emco5 +SP transgenic lines. From the dex-inducible mutant pools we identified several mutants that no longer caused cell death when incubated with dex. These mutants fall into the following categories: mutants with altered RPP13Nd sequence, mutants that no longer expressed RPP13, mutants that no longer produced ATR13 Emco5, and mutants that continued to show resistance to Hpa but did not cause cell death. This last class of mutants can be further characterized by examining the HR response and potentially mapping the loci responsible for this phenotype.

From the Col5:RPP13Nd mutant screen with Hpa, we identified three groups of mutants in RPP13 signaling: two that compromised RPP13 expression, mutants 30 and 48, and one that expressed RPP13 to the wildtype level, mutant 65. While other genes involved in resistance, such as RAR1 and Stg1a/1b, remained intact, these mutants no longer mounted a defense against Hpa. All mutants recovered were either male-sterile or otherwise unable to produce mature reproductive structures, limiting our ability to further characterize M3 mutants. The two mutants capable of producing fertile carpels, 30 and 65, were crossed to Ler plants and mapping populations were generated. Although these mapping populations segregated for susceptibility to Hpa Maks9, a single corresponding genetic locus could not be identified. Perhaps screening more rigorously with Hpa Emco5 would lead to reduced background infection rates and implicate a single locus that compromises RPP13Nd resistance.

Finally, using biochemical fractionation, we showed that RPP13 associates with the plasma membrane, despite the absence of known targeting motifs or modifications. We also conclude that this protein does not dynamically relocalize to the nucleus upon effector detection, indicating that there are likely other proteins or signaling molecules involved in relaying RPP13 defense signaling. Future work characterizing the nature of RPP13's association with the membrane could lead to the identification of interacting membrane proteins or peripheral proteins that play a role in defense signaling. Perhaps using a biochemical approach to identify these RPP13 interactors would allow for the identification of proteins that produce pleiotropic or lethal phenotypes when mutated, explaining why these genes were not identified in our EMS-mutagenesis screens.

References:

1. Helga Forster, M.D.C., Hille Elwood, Mitchell L. Sogin, *Sequence analysis of the small subunit ribosomal RNAs of three zoosporic fungi and implications for fungal evolution.* *Mycologia*, 1990. **82**(3): p. 306-312.
2. Mims, C., et al., *Ultrastructure of the host-pathogen interface in Arabidopsis thaliana leaves infected by the downy mildew Hyaloperonospora parasitica (vol 82, pg 1001, 2004).* *Can J Bot*, 2004. **82**(10): p. 1545-1545.
3. Kamoun, S., *Molecular genetics of pathogenic oomycetes.* *Eukaryot Cell*, 2003. **2**(2): p. 191-9.
4. Baxter, L., et al., *Signatures of adaptation to obligate biotrophy in the Hyaloperonospora arabidopsidis genome.* *Science*, 2010. **330**(6010): p. 1549-51.
5. Tyler, B.M., et al., *Phytophthora genome sequences uncover evolutionary origins and mechanisms of pathogenesis.* *Science*, 2006. **313**(5791): p. 1261-6.
6. Haas, B.J., et al., *Genome sequence and analysis of the Irish potato famine pathogen Phytophthora infestans.* *Nature*, 2009. **461**(7262): p. 393-8.
7. Jiang, R.H., et al., *RXL effector reservoir in two Phytophthora species is dominated by a single rapidly evolving superfamily with more than 700 members.* *Proc Natl Acad Sci U S A*, 2008. **105**(12): p. 4874-9.
8. Win, J., et al., *Computational and comparative analyses of 150 full-length cDNA sequences from the oomycete plant pathogen Phytophthora infestans.* *Fungal Genet Biol*, 2006. **43**(1): p. 20-33.
9. Whisson, S.C., et al., *A translocation signal for delivery of oomycete effector proteins into host plant cells.* *Nature*, 2007. **450**(7166): p. 115-8.
10. Postel, S. and B. Kemmerling, *Plant systems for recognition of pathogen-associated molecular patterns.* *Semin Cell Dev Biol*, 2009.
11. Nurnberger, T., et al., *Innate immunity in plants and animals: striking similarities and obvious differences.* *Immunol Rev*, 2004. **198**: p. 249-66.
12. Block, A. and J.R. Alfano, *Plant targets for Pseudomonas syringae type III effectors: virulence targets or guarded decoys?* *Curr Opin Microbiol*, 2011. **14**(1): p. 39-46.
13. Mackey, D., et al., *RIN4 Interacts with Pseudomonas syringae Type III Effector Molecules and Is Required for RPM1-Mediated Resistance in Arabidopsis.* *Cell*, 2002. **108**(6): p. 743-54.
14. Shao, F., et al., *Cleavage of Arabidopsis PBS1 by a bacterial type III effector.* *Science*, 2003. **301**(5637): p. 1230-3.
15. Mudgett, M.B., *New insights to the function of phytopathogenic bacterial type III effectors in plants.* *Annu Rev Plant Biol*, 2005. **56**: p. 509-31.
16. Kamoun, S., *A catalogue of the effector secretome of plant pathogenic oomycetes.* *Annu Rev Phytopathol*, 2006. **44**: p. 41-60.
17. Chisholm, S.T., et al., *Host-microbe interactions: shaping the evolution of the plant immune response.* *Cell*, 2006. **124**(4): p. 803-14.
18. van Loon, L.C., M. Rep, and C.M. Pieterse, *Significance of inducible defense-related proteins in infected plants.* *Annu Rev Phytopathol*, 2006. **44**: p. 135-62.
19. Flor, H.H., *Inheritance of pathogenicity in Melampsora lini.* *Phytopathology*, 1942. **32**: p. 653-69.

20. Martin, G.B., et al., *Map-based cloning of a protein kinase gene conferring disease resistance in tomato*. Science, 1993. **262**(1432-36).
21. Koch, E. and A. Slusarenko, *Arabidopsis is susceptible to infection by a downy mildew fungus*. Plant Cell, 1990. **2**(5): p. 437-45.
22. Bittner-Eddy, P., et al., *Genetic and physical mapping of the RPP13 locus, in Arabidopsis, responsible for specific recognition of several Peronospora parasitica (downy mildew) isolates*. Mol Plant Microbe Interact, 1999. **12**(9): p. 792-802.
23. Allen, R.L., et al., *Host-parasite coevolutionary conflict between Arabidopsis and downy mildew*. Science, 2004. **306**(5703): p. 1957-60.
24. Rose, L.E., et al., *The maintenance of extreme amino acid diversity at the disease resistance gene, RPP13, in Arabidopsis thaliana*. Genetics, 2004. **166**(3): p. 1517-27.
25. Bittner-Eddy, P.D., et al., *RPP13 is a simple locus in Arabidopsis thaliana for alleles that specify downy mildew resistance to different avirulence determinants in Peronospora parasitica*. Plant Journal, 2000. **21**(2): p. 177-188.
26. Hall, S.A., et al., *Maintenance of genetic variation in plants and pathogens involves complex networks of gene-for-gene interactions*. Mol Plant Pathol, 2009. **10**(4): p. 449-57.
27. Rentel, M.C., et al., *Recognition of the Hyaloperonospora parasitica effector ATR13 triggers resistance against oomycete, bacterial, and viral pathogens*. Proc Natl Acad Sci USA, 2008. **105**(3): p. 1091-6.
28. Bittner-Eddy, P.D. and J.L. Beynon, *The Arabidopsis downy mildew resistance gene, RPP13-Nd, functions independently of NDR1 and EDS1 and does not require the accumulation of salicylic acid*. Mol Plant Microbe Interact, 2001. **14**(3): p. 416-21.
29. Gaastra, W. and L.J. Lipman, *Capnocytophaga canimorsus*. Vet Microbiol, 2010. **140**(3-4): p. 339-46.
30. Alexander, J. and C.A. Lee, *Lessons learned from a decade of Sudden Oak Death in California: evaluating local management*. Environ Manage, 2010. **46**(3): p. 315-28.
31. Madden, L.V. and M. Wheelis, *The threat of plant pathogens as weapons against U.S. crops*. Annu Rev Phytopathol, 2003. **41**: p. 155-76.
32. Hogenhout, S.A., et al., *Emerging concepts in effector biology of plant-associated organisms*. Mol Plant Microbe Interact, 2009. **22**(2): p. 115-22.
33. Bhattacharjee, S., et al., *The malarial host-targeting signal is conserved in the Irish potato famine pathogen*. PLoS Pathog, 2006. **2**(5): p. e50.
34. Jiang, R.H., et al., *RXLR effector reservoir in two Phytophthora species is dominated by a single rapidly evolving superfamily with more than 700 members*. Proc Natl Acad Sci USA, 2008. **105**(12): p. 4874-9.
35. Wang, C.I., et al., *Crystal structures of flax rust avirulence proteins AvrL567-A and -D reveal details of the structural basis for flax disease resistance specificity*. Plant Cell, 2007. **19**(9): p. 2898-912.
36. Ciuffetti, L.M., et al., *Host-selective toxins, Ptr ToxA and Ptr ToxB, as necrotrophic effectors in the Pyrenophora tritici-repentis-wheat interaction*. New Phytol, 2010. **187**(4): p. 911-9.
37. Ottmann, C., et al., *A common toxin fold mediates microbial attack and plant defense*. Proc Natl Acad Sci U S A, 2009. **106**(25): p. 10359-64.
38. Xing, W., et al., *The structural basis for activation of plant immunity by bacterial effector protein AvrPto*. Nature, 2007. **449**(7159): p. 243-7.

39. Allen, R.L., et al., *Host-parasite coevolutionary conflict between Arabidopsis and downy mildew*, in *Science*. 2004. p. 1957-60.
40. Allen, R.L., et al., *Natural variation reveals key amino acids in a downy mildew effector that alters recognition specificity by an Arabidopsis resistance gene*. *Mol Plant Pathol*, 2008. **9**(4): p. 511-23.
41. Tai, T.H., et al., *Expression of the Bs2 pepper gene confers resistance to bacterial spot disease in tomato*. *Proc Natl Acad Sci U S A*, 1999. **96**(24): p. 14153-14158.
42. Sohn, K.H., et al., *The downy mildew effector proteins ATR1 and ATR13 promote disease susceptibility in Arabidopsis thaliana*, in *Plant Cell*. 2007. p. 4077-90.
43. Delaglio, F., et al., *NMRPipe: a multidimensional spectral processing system based on UNIX pipes*. *J Biomol NMR*, 1995. **6**(3): p. 277-93.
44. Keller, R.a.W., K., *Computer-Aided Resonance Assignment (CARA)*.
45. Kay, L.E., *Field gradient techniques in NMR spectroscopy*. *Curr Opin Struct Biol*, 1995. **5**(5): p. 674-81.
46. Sattler, M., J. Schleucher, et al., *Heteronuclear multidimensional NMR experiments for the structure determination of proteins in solution employing pulsed field gradients*. *Prog. NMR Spectrosc*, 1999. **34**: p. 93-158.
47. Kuboniwa, H., et al., *Measurement of HN-H alpha J couplings in calcium-free calmodulin using new 2D and 3D water-flip-back methods*. *J Biomol NMR*, 1994. **4**(6): p. 871-8.
48. Szyperski, T., et al., *Support of 1H NMR assignments in proteins by biosynthetically directed fractional 13C-labeling*. *J Biomol NMR*, 1992. **2**(4): p. 323-34.
49. Ottiger, M., F. Delaglio, and A. Bax, *Measurement of J and dipolar couplings from simplified two-dimensional NMR spectra*. *J Magn Reson*, 1998. **131**(2): p. 373-8.
50. Clore, G.M., A.M. Gronenborn, and A. Bax, *A robust method for determining the magnitude of the fully asymmetric alignment tensor of oriented macromolecules in the absence of structural information*. *J Magn Reson*, 1998. **133**(1): p. 216-21.
51. Farrow, N.A., et al., *Backbone dynamics of a free and phosphopeptide-complexed Src homology 2 domain studied by 15N NMR relaxation*. *Biochemistry*, 1994. **33**(19): p. 5984-6003.
52. Guntert, P., *Automated NMR structure calculation with CYANA*. *Methods Mol Biol*, 2004. **278**: p. 353-78.
53. Brunger, A.T., et al., *Crystallography & NMR system: A new software suite for macromolecular structure determination*. *Acta Crystallogr D Biol Crystallogr*, 1998. **54**(Pt 5): p. 905-21.
54. Koradi, R., M. Billeter, and K. Wuthrich, *MOLMOL: a program for display and analysis of macromolecular structures*. *J Mol Graph*, 1996. **14**(1): p. 51-5, 29-32.
55. Bai, Y., et al., *Primary structure effects on peptide group hydrogen exchange*. *Proteins*, 1993. **17**(1): p. 75-86.
56. Abramoff, M.D., Magelhaes, P.J., Ram, S.J., *Image Processing with ImageJ*. *Biophotonics International*, 2004. **11**(7): p. 36-42.
57. Dong, A., et al., *In situ proteolysis for protein crystallization and structure determination*. *Nat Methods*, 2007. **4**(12): p. 1019-21.
58. Earley, K., Jeremy R. Haag, Olga Pontes, Kristen Opper, Tom Juehne, Keming Song, and Craig S. Pikaard, *Gateway-compatible vectors for plant functional genomics and proteomics*. *The Plant Journal*, 2006. **45**: p. 616-629.

59. Peng, J.W.a.G.W., *Investigation of protein motions via relaxation measurements*. Methods Enzymol, 1994. **239**: p. 563-593.
60. Cornilescu, G., F. Delaglio, and A. Bax, *Protein backbone angle restraints from searching a database for chemical shift and sequence homology*. J Biomol NMR, 1999. **13**(3): p. 289-302.
61. Michelle S. Scott, F.-M.B., Mark D. McDowall, Angus I. Lamond, Geoffrey J. Barton, *Characterization and prediction of protein nucleolar localization sequences*. Nucleic Acids Research, 2010. **38**(21): p. 7388-7399.
62. Emmott, E. and J.A. Hiscox, *Nucleolar targeting: the hub of the matter*. EMBO Rep, 2009. **10**(3): p. 231-8.
63. Boulon, S., et al., *The nucleolus under stress*. Mol Cell, 2010. **40**(2): p. 216-27.
64. Kim, S.H., et al., *Interaction of a plant virus-encoded protein with the major nucleolar protein fibrillarin is required for systemic virus infection*. Proc Natl Acad Sci U S A, 2007. **104**(26): p. 11115-20.
65. Rajamaki, M.L. and J.P. Valkonen, *Control of nuclear and nucleolar localization of nuclear inclusion protein a of picorna-like Potato virus A in Nicotiana species*. Plant Cell, 2009. **21**(8): p. 2485-502.
66. Jones, J.T., et al., *Identification and functional characterization of effectors in expressed sequence tags from various life cycle stages of the potato cyst nematode Globodera pallida*. Mol Plant Pathol, 2009. **10**(6): p. 815-28.
67. Holmes, A., et al., *The EspF effector, a bacterial pathogen's Swiss army knife*. Infect Immun, 2010. **78**(11): p. 4445-53.
68. Kvitko, B.H., et al., *Deletions in the repertoire of Pseudomonas syringae pv. tomato DC3000 type III secretion effector genes reveal functional overlap among effectors*. PLoS Pathog, 2009. **5**(4): p. e1000388.
69. Dean, P. and B. Kenny, *The effector repertoire of enteropathogenic E. coli: ganging up on the host cell*. Curr Opin Microbiol, 2009. **12**(1): p. 101-9.
70. Win, J., et al., *Adaptive evolution has targeted the C-terminal domain of the RXLR effectors of plant pathogenic oomycetes*. Plant Cell, 2007. **19**(8): p. 2349-69.
71. Oh, S.K., et al., *In planta expression screens of Phytophthora infestans RXLR effectors reveal diverse phenotypes, including activation of the Solanum bulbocastanum disease resistance protein Rpi-blb2*. Plant Cell, 2009. **21**(9): p. 2928-47.
72. Vleeshouwers, V.G., et al., *Effector genomics accelerates discovery and functional profiling of potato disease resistance and phytophthora infestans avirulence genes*. PLoS ONE, 2008. **3**(8): p. e2875.
73. Abramovitch, R.B., et al., *Type III effector AvrPtoB requires intrinsic E3 ubiquitin ligase activity to suppress plant cell death and immunity*. Proc Natl Acad Sci USA, 2006. **103**(8): p. 2851-6.
74. Wakeel, A., J.A. Kuriakose, and J.W. McBride, *An Ehrlichia chaffeensis tandem repeat protein interacts with multiple host targets involved in cell signaling, transcriptional regulation, and vesicle trafficking*. Infect Immun, 2009. **77**(5): p. 1734-45.
75. Coaker, G., A. Falick, and B. Staskawicz, *Activation of a phytopathogenic bacterial effector protein by a eukaryotic cyclophilin*. Science, 2005. **308**(5721): p. 548-50.
76. Bos, J.I., et al., *Phytophthora infestans effector AVR3a is essential for virulence and manipulates plant immunity by stabilizing host E3 ligase CMPG1*. Proc Natl Acad Sci U S A, 2010. **107**(21): p. 9909-14.

77. Domingues, M.N., et al., *The Xanthomonas citri effector protein PthA interacts with citrus proteins involved in nuclear transport, protein folding and ubiquitination associated with DNA repair*. Molecular Plant Pathology, 2010. **11**(5): p. 663-675.
78. Gavin, A.C., et al., *Functional organization of the yeast proteome by systematic analysis of protein complexes*. Nature, 2002. **415**(6868): p. 141-7.
79. Forler, D., et al., *An efficient protein complex purification method for functional proteomics in higher eukaryotes*. Nat Biotechnol, 2003. **21**(1): p. 89-92.
80. Gully, D., et al., *New partners of acyl carrier protein detected in Escherichia coli by tandem affinity purification*. FEBS Lett, 2003. **548**(1-3): p. 90-6.
81. Knuesel, M., et al., *Identification of novel protein-protein interactions using a versatile mammalian tandem affinity purification expression system*. Mol Cell Proteomics, 2003. **2**(11): p. 1225-33.
82. Mukherjee, S., Y.H. Hao, and K. Orth, *A newly discovered post-translational modification--the acetylation of serine and threonine residues*. Trends Biochem Sci, 2007. **32**(5): p. 210-6.
83. Stulemeijer, I.J. and M.H. Joosten, *Post-translational modification of host proteins in pathogen-triggered defence signalling in plants*. Mol Plant Pathol, 2008. **9**(4): p. 545-60.
84. Wilton, M., et al., *The type III effector HopF2Pto targets Arabidopsis RIN4 protein to promote Pseudomonas syringae virulence*. Proc Natl Acad Sci U S A, 2010. **107**(5): p. 2349-54.
85. Kim, M.G., et al., *Two Pseudomonas syringae type III effectors inhibit RIN4-regulated basal defense in Arabidopsis*. Cell, 2005. **121**(5): p. 749-59.
86. Liu, J., J. Elmore, and G. Coaker, *Investigating the functions of the RIN4 protein complex during plant innate immune responses*. Plant Signal Behav, 2009. **4**(12).
87. Jia, Y., et al., *Direct interaction of resistance gene and avirulence gene products confers rice blast resistance*. EMBO (European Molecular Biology Organization) Journal, 2000. **19**(15): p. 4004-4014.
88. Deslandes, L., et al., *Physical interaction between RRS1-R, a protein conferring resistance to bacterial wilt, and PopP2, a type III effector targeted to the plant nucleus*. Proc Natl Acad Sci U S A, 2003. **100**(13): p. 8024-9.
89. Dodds, P.N., et al., *Direct protein interaction underlies gene-for-gene specificity and coevolution of the flax resistance genes and flax rust avirulence genes*. Proc Natl Acad Sci U S A, 2006. **103**(23): p. 8888-93.
90. Ueda, H., Y. Yamaguchi, and H. Sano, *Direct interaction between the tobacco mosaic virus helicase domain and the ATP-bound resistance protein, N factor during the hypersensitive response in tobacco plants*. Plant Mol Biol, 2006. **61**(1-2): p. 31-45.
91. Krasileva, K.V., D. Dahlbeck, and B.J. Staskawicz, *Activation of an Arabidopsis Resistance Protein Is Specified by the in Planta Association of Its Leucine-Rich Repeat Domain with the Cognate Oomycete Effector*. Plant Cell, 2010.
92. Axtell, M.J. and B.J. Staskawicz, *Initiation of RPS2-specified disease resistance in Arabidopsis is coupled to the AvrRpt2-directed elimination of RIN4*. Cell, 2003. **112**(3): p. 369-77.
93. Aoyama, T. and N.-H. Chua, *A glucocorticoid-mediated transcriptional induction system in transgenic plants*. The Plant Journal, 1997. **11**(3): p. 605-612.

94. Andersen, S.U., et al., *The glucocorticoid-inducible GVG system causes severe growth defects in both root and shoot of the model legume Lotus japonicus*. Mol Plant Microbe Interact, 2003. **16**(12): p. 1069-76.
95. Foyer, C.H., M. Parry, and G. Noctor, *Markers and signals associated with nitrogen assimilation in higher plants*. J Exp Bot, 2003. **54**(382): p. 585-93.
96. Wang, C., et al., *The Arabidopsis thaliana AT PRP39-1 gene, encoding a tetratricopeptide repeat protein with similarity to the yeast pre-mRNA processing protein PRP39, affects flowering time*. Plant Cell Rep, 2007. **26**(8): p. 1357-66.
97. Blatch, G.L. and M. Lassle, *The tetratricopeptide repeat: a structural motif mediating protein-protein interactions*. Bioessays, 1999. **21**(11): p. 932-9.
98. Blom, E., et al., *Multiple TPR motifs characterize the Fanconi anemia FANCG protein*. DNA Repair (Amst), 2004. **3**(1): p. 77-84.
99. Boudreau, E., et al., *The Nac2 gene of Chlamydomonas encodes a chloroplast TPR-like protein involved in psbD mRNA stability*. EMBO J, 2000. **19**(13): p. 3366-76.
100. Lockhart, S.R. and B.C. Rymond, *Commitment of yeast pre-mRNA to the splicing pathway requires a novel U1 small nuclear ribonucleoprotein polypeptide, Prp39p*. Mol Cell Biol, 1994. **14**(6): p. 3623-33.
101. Zheng, J., et al., *Ratio-based analysis of differential mRNA processing and expression of a polyadenylation factor mutant pcfs4 using arabidopsis tiling microarray*. PLoS One, 2011. **6**(2): p. e14719.
102. Gassmann, W., *Alternative splicing in plant defense*. Curr Top Microbiol Immunol, 2008. **326**: p. 219-33.
103. Frankel, M.B., D.G. Mordue, and L.J. Knoll, *Discovery of parasite virulence genes reveals a unique regulator of chromosome condensation 1 ortholog critical for efficient nuclear trafficking*. Proc Natl Acad Sci U S A, 2007. **104**(24): p. 10181-6.
104. Tachibana, T., et al., *Loss of RCC1 leads to suppression of nuclear protein import in living cells*. J Biol Chem, 1994. **269**(40): p. 24542-5.
105. Dasso, M., *RCC1 in the cell cycle: the regulator of chromosome condensation takes on new roles*. Trends in Biochemical Sciences, 1993. **18**(3): p. 96-101.
106. Renault, L., et al., *The 1.7 Å crystal structure of the regulator of chromosome condensation (RCC1) reveals a seven-bladed propeller*. Nature, 1998. **392**(6671): p. 97-101.
107. Nemergut, M.E., et al., *Chromatin Docking and Exchange Activity Enhancement of RCC1 by Histones H2A and H2B*. Science, 2001. **292**(5521): p. 1540-1543.
108. Bischoff, F.R. and H. Ponstingl, *Mitotic regulator protein RCC1 is complexed with a nuclear ras-related polypeptide*. Proceedings of the National Academy of Sciences, 1991. **88**(23): p. 10830-10834.
109. Macara, I.G., *Transport into and out of the nucleus*. Microbiol Mol Biol Rev, 2001. **65**(4): p. 570-94, table of contents.
110. Tameling, W.I., et al., *RanGAP2 mediates nucleocytoplasmic partitioning of the NB-LRR immune receptor Rx in the Solanaceae, thereby dictating Rx function*. Plant Cell, 2010. **22**(12): p. 4176-94.
111. Zipfel, C., *Early molecular events in PAMP-triggered immunity*. Curr Opin Plant Biol, 2009. **12**(4): p. 414-20.
112. van Ooijen, G., et al., *Structure and function of resistance proteins in solanaceous plants*. Annual review of phytopathology, 2007. **45**: p. 43-72.

113. Ding, J., et al., *Unique pattern of R-gene variation within populations in Arabidopsis*. Mol Genet Genomics, 2007. **277**(6): p. 619-29.
114. Austin, M.J., et al., *Regulatory role of SGT1 in early R gene-mediated plant defenses*. Science, 2002. **295**(5562): p. 2077-80.
115. Parker, J.E., et al., *Unravelling R gene-mediated disease resistance pathways in Arabidopsis*. Molecular Plant Pathology, 2000. **1**(1): p. 17-24.
116. Lewis, J.D., et al., *Allele-specific virulence attenuation of the Pseudomonas syringae HopZ1a type III effector via the Arabidopsis ZAR1 resistance protein*. PLoS Genet, 2010. **6**(4): p. e1000894.
117. Bittner-Eddy, P.D., et al., *RPP13 is a simple locus in Arabidopsis thaliana for alleles that specify downy mildew resistance to different avirulence determinants in Peronospora parasitica [In Process Citation]*. Plant J, 2000. **21**(2): p. 177-88.
118. Ding, J., et al., *Contrasting patterns of evolution between allelic groups at a single locus in Arabidopsis*. Genetica, 2007. **129**(3): p. 235-42.
119. Galan, J.E. and H. Wolf-Watz, *Protein delivery into eukaryotic cells by type III secretion machines*. Nature, 2006. **444**(7119): p. 567-73.
120. Sheen, J. and P. He, *Nuclear actions in innate immune signaling*. Cell, 2007. **128**(5): p. 821-3.
121. Burch-Smith, T.M., et al., *A Novel Role for the TIR Domain in Association with Pathogen-Derived Elicitors*. PLoS Biol, 2007. **5**(3): p. e68.
122. McHale, L., et al., *Plant NBS-LRR proteins: adaptable guards*. Genome Biol, 2006. **7**(4): p. 212.
123. Komatsu, K., et al., *Viral-induced systemic necrosis in plants involves both programmed cell death and the inhibition of viral multiplication, which are regulated by independent pathways*. Mol Plant Microbe Interact, 2010. **23**(3): p. 283-93.
124. Liu, P.P., et al., *Systemic acquired resistance is induced by R gene-mediated responses independent of cell death*. Mol Plant Pathol, 2010. **11**(1): p. 155-60.
125. Stewart, S.A., et al., *The RAPI gene confers effective, race-specific resistance to the pea aphid in Medicago truncatula independent of the hypersensitive reaction*. Mol Plant Microbe Interact, 2009. **22**(12): p. 1645-55.
126. McDowell, J.M., et al., *Genetic analysis of developmentally regulated resistance to downy mildew (Hyaloperonospora parasitica) in Arabidopsis thaliana*. Mol Plant Microbe Interact, 2005. **18**(11): p. 1226-34.
127. Panter, S.N., et al., *Developmental control of promoter activity is not responsible for mature onset of Cf-9B-mediated resistance to leaf mold in tomato*. Mol Plant Microbe Interact, 2002. **15**(11): p. 1099-107.